UNIVERSITY OF OKLAHOMA

GRADUATE COLLEGE

EVALUATION OF SPECIALIZED CONCRETES FOR THE REPAIR OF DAMAGED CONTINUITY JOINTS IN PRESTRESSED GIRDER BRIDGES

A THESIS
SUBMITTED TO THE GRADUATE FACULTY
in partial fulfillment of the requirements for the
Degree of
MASTER OF SCIENCE

By

MICHAEL D. MESIGH
Norman, Oklahoma
2021

EVALUATION OF SPECIALIZED CONCRETES FOR THE REPAIR OF DAMAGED CONTINUITY JOINTS IN PRESTRESSED GIRDER BRIDGES

A THESIS APPROVED FOR THE SCHOOL OF CIVIL ENGINEERING AND ENVIRONMENTAL SCIENCE

BY THE COMMITTEE CONSISTING OF

Dr. Jeffery S. Volz, Chair

Dr. Royce W. Floyd

Dr. Christopher C. E. Ramseyer

Acknowledgements

I would like to begin by giving my advisor and mentor, Dr. Jeffery Volz, an enormous thank you for the opportunity to learn and grow as an engineer while researching beneath him. His vast knowledge, guidance, and support both as an advisor and professor were essential in completing my graduate studies.

This accomplishment could not have been achieved without the overwhelming support of my fiancé, Sela. The confidence she shows in me is second to none and is something that never goes unnoticed or unappreciated. Although not an engineer herself, her continuous encouragement of my studies helped make life just that much easier and I thank her for that.

I would also like to thank all the help I received at Fear's Laboratory. The knowledge and ability of our lab technician, Mike Schmitz, helped make possible the fabrication of anything you could dream up. I am forever indebted to Trevor and Jake for their hours upon hours of assistance in building, casting, moving, and finally destroying all of my specimens. None of this would have been made possible without you two. In addition, a big thanks to Steve and all the undergraduate helping hands for various loose ends around the lab.

An extended thank you to my thesis committee members Dr. Royce Floyd and Dr. Christopher Ramseyer for investing their time to help me in class, the lab, and reviewing this final document.

Last but not least I would like to thank my family. Their support system based on an expectation to always live to my full potential played a vital roll in reaching this milestone.

Table of Contents

List of Tables

List of Figures

Abstract

Precast, prestressed concrete simple span girder bridges made continuous through the use of continuity joints exhibit a great, structural advantage when dealing with additional dead and live loading across the deck. Unfortunately, time-dependent effects such as temperature, creep, and shrinkage may cause the girders to camber upward and the continuity joint to crack. The crack in the joint can cause a loss of continuity and leaves the reinforcement within prone to corrosion damage. A potential solution to this problem is to repair the damaged continuity joint using specialized concretes such as ultra-high-performance concrete (UHPC), fiber-reinforced self-consolidating concrete (FR-SCC), and a magnesium aluminum liquid phosphate concrete (MALP), called Phoscrete®. These specialized concretes have been shown to perform better than traditional concrete. An extensive literature review of previous research has been done to gain an understanding of what the current state of continuity joint repair is in and where it should be heading. The main objective of this study was to provide an adequate continuity joint repair solution for in-service bridges showing deterioration from time dependent effects.

This research began by constructing and combining twenty-four half-scale, half-length AASHTO Type II bridge girders resulting in twelve girder-joint-girder specimens. Steel reinforcement within the continuity joint was based on previous research and adapted to the specific sizing of the specimens for this research. The specimens were tested under two different load cases – positive and negative moment bending. Three of the twelve girder-joint-girder specimens acted as the control group and tested to negative moment flexural failure. Observations and data for the load at failure, strain, and deflection were collected. The remaining nine specimens were initially loaded in positive moment bending until a crack began to propagate upward within the continuity joint. This crack simulated girder-joint-girder damage found in the field. Repairs using additional reinforcement and specialized concretes were constructed and tested. Six repair specimens' moment capacities (two from each repair material) were determined in negative moment bending and three moment capacities (one from each repair material) were determined in positive moment bending. Once again observations and data for the load at failure, strain, and deflection were collected. The results from the tests were

compared to the data from the control group and each other. These results indicated viable options for girder-joint-girder repairs in the field.

1.0 Introduction

1.1 Background

Precast, prestressed concrete simple span girder bridges made continuous through the use of continuity joints exhibit a great, structural advantage when dealing with additional dead and live loading across the deck. A continuity joint in a girder bridge is initially two simply supported span girders set in place. After setting these spans in place, a cast-in-place deck and continuity joint are then poured across the girders. Once the deck is poured, the initial camber of the girder is reduced due to the weight of the wet concrete. The space between the two girder ends is referred to as the continuity joint. After the deck and joint have cured, they allow the girders and composite deck to act as a continuous beam for any additional dead and live loads which is very advantageous for bridge construction (Miller, et al. 2004).

The continuity gained from the composite deck and joint tends to keep the bridge girder ends from rotating, providing a positive moment restraint at the bottom of the continuity joint. Unfortunately, time-dependent effects such as temperature, creep, and shrinkage may cause the girders to camber upward and the continuity joint to form cracks. Changes in the surrounding climate can cause expansion and contraction within the girders, specifically the sun beating down on the top deck of a bridge each day is going to cause the deck to expand. This expansion will inevitably cause the girders to camber back upward. These effects can cause a positive moment to develop at the interior supports of the continuous structure that exceeds the capacity of the connection.

Unfavorable results from this cracking include a loss of continuity and corrosion of the joint reinforcement, furthering degradation of in-service bridges. This is a unique condition that does not emerge from simply supported connections and must be addressed.

1.2 Objectives & Scope of Work

The main objective of this study was to provide an adequate continuity joint repair solution for in-service bridges showing deterioration from time dependent effects. Using half-scale AASHTO Type II girders and three specialized concretes as repair materials

(ultra-high-performance concrete, fiber-reinforced self-consolidating concrete, and magnesium-alumino-liquid phosphate concrete), results from negative and positive moment flexural failures will be analyzed and compared amongst themselves and a control group. Six repair specimens' moment capacities (two from each repair material) will be determined in negative moment bending and three moment capacities (one from each repair material) will be determined in positive moment bending. The anticipated outcome of this research was to evaluate which specialized concrete groups, if any, restored full moment capacity following repair procedures after an initial cracking within the continuity joint.

In an effort to achieve the main objective of this research, the following scope of work was implemented:

- Research and review applicable literature.
- Develop a research strategy.
- Design and build formwork for research specimens.
- Cast twelve research specimens.
- Test control group specimens to flexural failure and record data.
- Crack continuity joints of repair specimens in positive moment region.
- Design repair reinforcement and formwork for repair specimens.
- Cast each specialized repair concrete.
- Test each repair specimens to flexural failure and record data.
- Analyze results and develop a comparative analysis between the repair specimens and control group.
- Develop conclusions and recommendations.
- Document information obtained from this study into a thesis.

1.3 Outline

This thesis is comprised of seven chapters and appendices. Chapter 1 provides background information relating to continuity joints, the problem current in-service bridges are facing due to time dependent effects, and this study's main objective and scope of work. Chapter 2 is a review of literature describing previous studies performed

on the topic of continuity joints in addition to properties and benefits of three specialized concretes used within this study. Specimen fabrication and casting procedures are detailed in Chapter 3. Laboratory testing arrangement and procedure, control group testing and results, and the initial cracking of specimens make up Chapter 4. Chapter 5 describes the continuity joint repair design, construction, and placement. The repair specimens' testing and results are described in chapter 6. Findings, conclusions, and recommendations are presented in Chapter 7. Finally, the appendices include complete load-deflection and load-strain curves from specimen testing.

2.0 Literature Review

This chapter contains a review of literature describing previous studies performed on the topic of continuity joints in addition to properties and benefits of three specialized concretes used within this study.

2.1 Connection of Simple-Span Precast Concrete Girders for Continuity

To improve the structural efficiency in concrete bridges of multiple spans, precast prestressed bridge girders are made continuous through cast-in-place decks and joints. Construction of this type of bridge connection has been commonly used throughout the United States since the 1960's. Once the deck and joint have cured, they allow the girders and composite deck to act continuous for any additional dead and live loads (Miller, et al. 2004). Prior to the final cured structure, placed girders behave as simply supported members with self-weight and the uncured composite deck as dead loads (Saadeghvaziri, et al. 2004). After continuity is established, the precast prestressed bridge girders camber upward due to time-dependent deformations. These time-dependent effects are due to temperature, creep, and shrinkage. The effects cause a restraint moment to develop at the interior supports of the continuous structure. This is a condition that does not emerge from simply supported connections. Figure 2-1 gives a visual representation of this type of system.

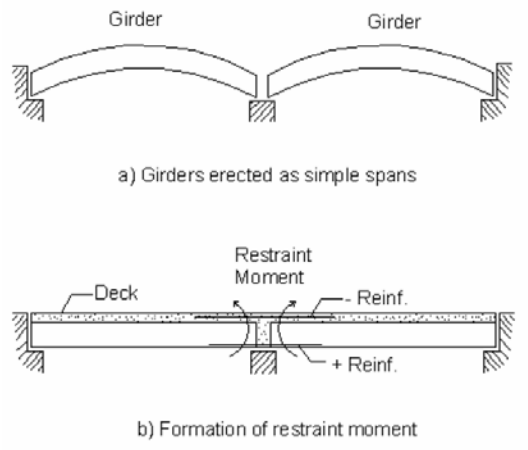

Figure 2-1:Formation of Positive Restraint Moment Under Time-Dependent Effects (Saadeghvaziri et al. 2004)

The continuity gained from the composite deck and joint tends to keep the bridge girder ends from rotating about the cross-sectional x-axis, providing a positive moment restraint at the bottom of the joint (Saadeghvaziri, et al. 2004). This restraint, with the addition of time-dependent effects, can cause cracking of the joint propagating upward from the positive moment region. These cracks can cause behavioral issues regarding continuity and create openings prone to joint reinforcement corrosion.

To prevent positive moment cracking in the joint, several studies by the Portland Cement Association in the 1960's recommended a moment connection be made between the girder ends and the joint. In these studies, various connection details were evaluated and reinforcing bars with hooked ends embedded in the ends of precast girders proved to be the most practical application for this type of moment restraint connection (Freyermuth, 1969).

A more recent study from 2004 by Miller et al. tested bent bars and bent strands with and without beam ends embedded into the continuity joint and additional stirrups or web bars within the joint. Figure 2-1 is an example of one configuration set-up for this research in elevation.

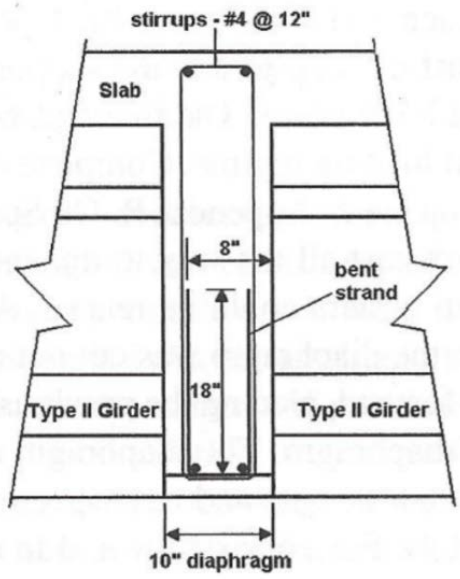

Figure 2-2:Bent Bar Specimen (Miller et al. 2004)

In this study, specimens' configurations were analytically determined through a model of a continuous two-span structure, using the deck and joint as the continuity element. The program developed by Miller et al. could compute internal moments within the continuity joint caused by creep from the girder and shrinkage from the girder and deck. To verify the program's accuracy, scaled I-girders from the Portland Cement Association's previous study were modeled and the program displayed an agreement to that experiment.

The test concluded that each positive moment restraint connection detail performed adequately, had separate advantages and disadvantages, and that selecting specific member details should be up to the engineer, the Department of Transportation, or both (Miller, et al. 2004).

2.2 Ultra-High-Performance Concrete for Repair of Damaged Continuity Joints

A recent new class of cementitious composites known as ultra-high-performance concrete (UHPC) has emerged from advancements in the material science of concrete. The fresh and hardened properties of this fiber-reinforced, portland cement-based product deliver performance that surpasses conventional concretes.

The Federal Highway Administration defines UHPC as a cementitious composite material composed of an optimized gradation of granular constituents, a water-to-cementitious materials ratio less than 0.25, and a high percentage of discontinuous internal fiber reinforcement (Graybeal, 2011). The mechanical properties of UHPC include compressive strength greater than 21.7 ksi (150 MPa) and sustained postcracking tensile strength greater than 0.72 ksi (5 MPa) (Graybeal, 2011). Durability and mechanical properties of UHPC create an advantageous use in highway infrastructure deterioration replacement and repair (Graybeal, 2014).

Unfortunately, using proprietary UHPC in applications to replace conventional concrete requires specially certified contractors and unique construction processes, causing it to be extremely expensive. Within the last decade, researchers across the United States have began developing non-proprietary UHPC using readily available materials to their regions. Pushing towards a more advantageous price point, research at the University of

Michigan (El-Tawil et al. 2016) and Montana State University – Bozeman (Berry et al. 2017) have achieved such non-proprietary UHPC mixes.

Researchers at the University of Oklahoma have recently optimized a non-proprietary UHPC mix design using readily available materials in the State of Oklahoma. The mix uses 10% silica fume, 30-40% GGBFS, Type I cement, a w/cm ratio of 0.2, an aggregate/cementitious material ratio of 1.0 when the aggregate is washed, fine sand, and sufficient HRWR reducer to produce a mortar flow of 7-8 in (McDaniel, 2017). This mix, named J3, will be one of the repair materials used in this study.

2.3 Fiber-Reinforced Self Consolidating Concrete for Repair of Damaged Continuity Joints

The recent increased use of self-consolidating concrete (SCC) in structural concrete repair applications may be based on its many advantages offered before and after hardening. One highly favorable advantage of SCC is its ability to flow under its own weight. This means that it is capable of forming in and around uneven surfaces without the use of mechanical vibration making it an ideal candidate for repair applications. Unfortunately, just like conventional concrete, self-consolidating concrete also shrinks which when restrained leads to development of stresses and eventually cracks throughout the process of curing. Applying self-consolidating concrete to an aged structural member may be subject to debonding itself across the concrete interfaces as it begins to shrink and crack. Within the last decade or so, researchers have investigated methods to control and combat this unfavorable property. Research done at the University of Sherbrooke found the best combination to reduce potential cracking of SCC was to add steel fibers and expansive agent to the mix (Kassimi, 2013). This type of mixture is commonly called fiber-reinforced self-consolidating concrete, or FR-SCC. The initial research by Kassimi was the starting point to move forward with evaluating and developing optimum fiber types and mixtures in the repair of full-scale reinforced concrete beams. The research showed that the fiber-reinforced self-consolidating mixtures were suitable for repair applications and can restore at least 95% of initial load-carrying capacity of structural elements made of conventional concrete. The beams repaired with steel and long multifilament polypropylene fiber-reinforced self-consolidating mixtures exhibited better

structural performance in terms of load carrying capacity and stiffness than those repaired with either monofilament polypropylene or hybrid fibers reinforced SCC (Kassimi, et al. 2014).

A recent study done at the University of Oklahoma (Choate, 2018) involved the repair of an AASHTO Type II girder using FR-SCC. This repair tested the girder in end region shear and proved to restore 83% of its original tested capacity. The FR-SCC mix used in this repair was developed in previous project at the University of Oklahoma (Wirkman, 2016) and incorporated macro polypropylene fibers and Komponent®, a shrinkage-compensating cement. This mix will be used as one of the repair materials in this study.

2.4 Magnesium-Alumino-Liquid Phosphate Concrete for Repair of Damaged Continuity Joints

Magnesium-Alumino-Liquid Phosphate (MALP) concrete incorporates a pre-packaged magnesium-alumino-aggregate dry powder with a mono-aluminum-liquid phosphate activator and is fast-setting with high-early strength. MALP was initially developed to patch concrete floors exposed to high-temperature spills and other punishing industrial activities (Fournier, 2014). This concrete has been recently introduced to state transportation agencies for repair of concrete bridge decks and expansion joint nosings. Because MALP does not need any water or specialized tools for mixing or placement the ingredients can be easily combined on-site for repair. Another advantage of MALP is that works really well in cold temperatures. One commercially available product, Phoscrete®, claims to be traffic-ready in thirty minutes. This allows for quick repairs and fast turnaround times for the structure to be back in working order. Phoscrete® can achieve 4,000 psi compressive strength after one hour and 7,000 psi seven days later. The rapid strength gain and fast-setting properties of Phoscrete® could make it a valuable asset in concrete repair. Unfortunately, limited information on performance of Phoscrete® as a repair material hinders its use. This specific magnesium-alumino-liquid phosphate concrete will be used as the third repair material in this study.

3.0 Methods & Approach

To aid in the construction of girders and their continuity joints in a laboratory-controlled environment, the specimens were scaled down to approximately half the size of an AASHTO Type II girder. In total, twelve girder-joint-girder specimens were constructed in two steps. The first step involved fabrication of steel reinforcement and concrete casting of half-length specimens. The second step involved joining two half-length specimens together via a cast-in-place deck and continuity joint.

3.1 Half-Scale AASHTO Type II Girders

3.1.1 Girder Design

The design of the girders for this research is the same design used in previous research at the University of Oklahoma (Mayhorn, 2016). This geometry replicates a girder taken out of service from a bridge spanning over the Arkansas River in Tulsa County, Oklahoma and is typical of many aging girders across Oklahoma.

The girder-joint-girder design consists of two half-length specimens each stretching 9’-0” in length with a 10” continuity joint and deck connecting them together. This fabrication process creates a final dimension of 18’-10” in length for each specimen. The height of the final specimen, including the deck, is 2’-3 1/8”. The geometry and dimensions are shown in Figure 3-1.

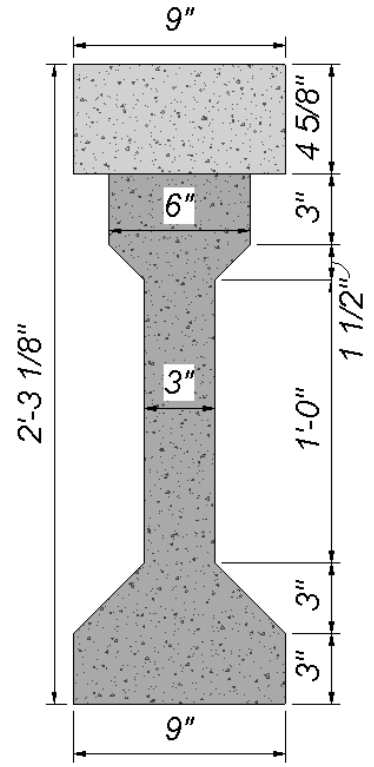

Figure 3-1:Girder Dimensions & Geometry

The continuity joint connecting each half-length specimen has an overall dimension of 10” (length) x 9” (width) x 2’-3 1/8” (height). This section is a rectangular prism outlining the width of the deck and bottom bell as well as the height of the overall specimen. Figure 3-2 shows the dimensions and geometry of the continuity joint section.

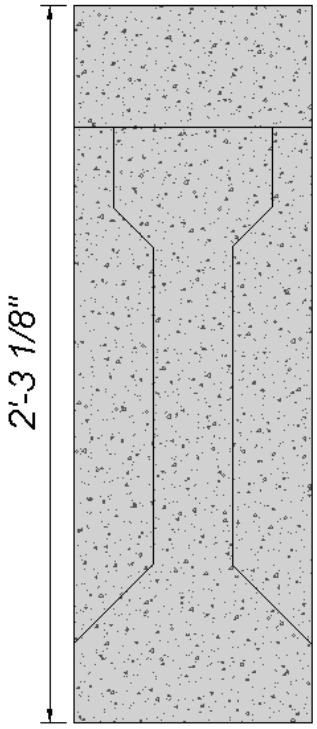

Figure 3-2:Continuity Joint Dimensions & Geometry

Joining the two half-length specimens via continuity joint and deck creates the final geometry of the girder-joint-girder specimen as shown in Figure 3-3.

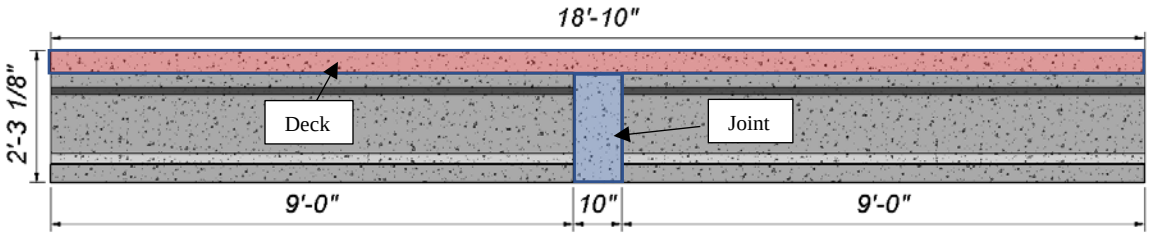

Figure 3-3:Girder-Joint-Girder Specimen

Steel reinforcement was designed and used for two separate load cases. The first load case was a static point-load at midspan, directly above the continuity joint, with the girder-joint-girder supported at each end. This load case simulates a flexural failure in the positive moment region of the joint based on a design moment capacity of 1.2 times the cracking moment in accordance with the AASHTO LRFD Code (2017). Longitudinal steel reinforcement with ninety-degree hooks placed at the bottom of the continuity joint was designed with the intention of yielding under the first load case. Unlike previous research, the reinforcement used in this study was mild steel. Each half-length specimen

received identical longitudinal reinforcement but offset from one another to allow for clearance within the joint while connecting together. Two No. 3 and No. 5 bars were placed within the girder sections and are shown in Figure 3-4 through Figure 3-5. Note that these bars extend beyond the face of the girder as they are reinforcement within the continuity joint.

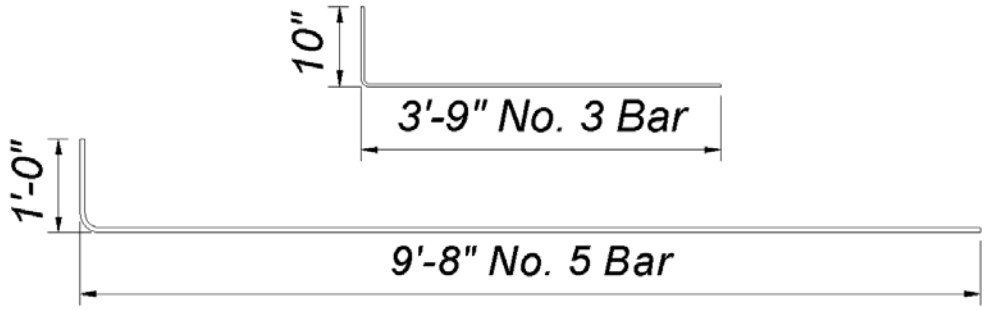

Figure 3-4:Hooked End Bar Dimensions

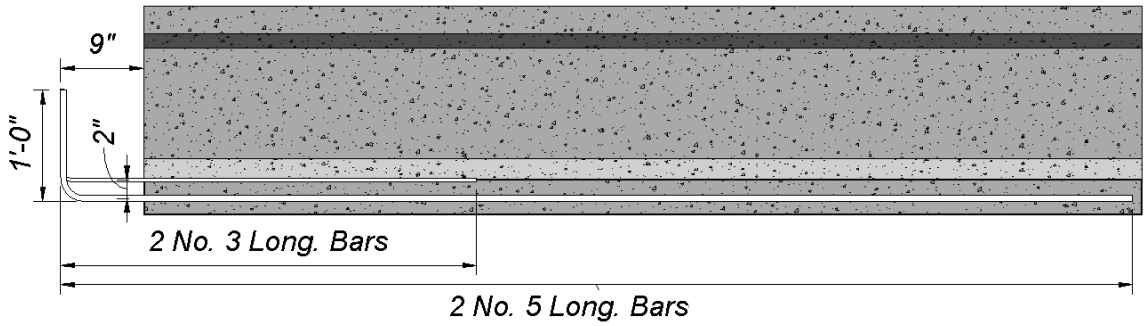

Figure 3-5:Hooked End Bar Placement

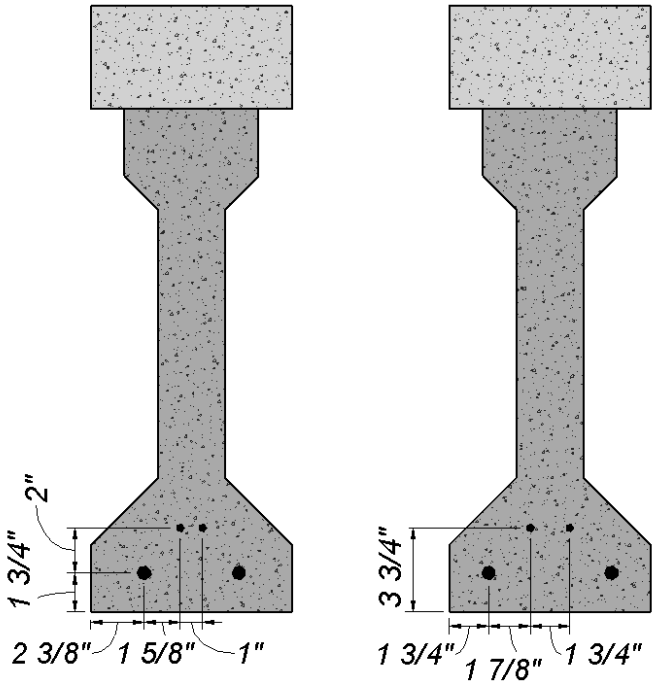

Figure 3-6:(Left) Inside Longitudinal Bars; (Right) Outside Longitudinal Bars

The second load case was two static point-loads, one at each end of the specimen, while being supported at midspan. This load case simulates live load on the deck, resulting in girder-joint-girder negative moment bending. Steel reinforcement placed within the deck should yield under the second load case. Four No. 5 bars were used in the design of the negative bending moment and were centered over the joint as designed for tests of UHPC continuity joints in previous research (Casey, 2019). Figure 3-7 and Figure 3-8 show the deck longitudinal reinforcement dimensions and placement.

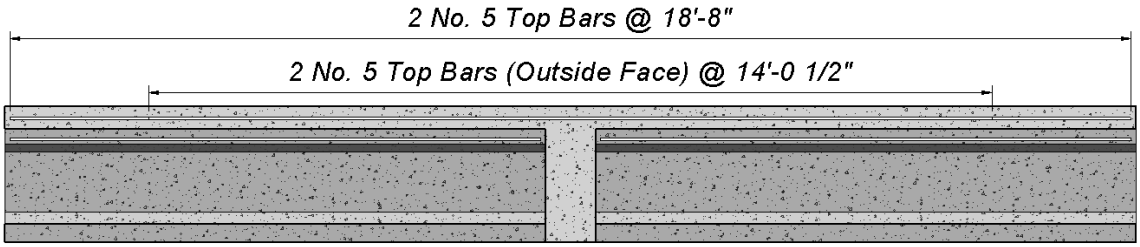

Figure 3-7:Deck Longitudinal Reinforcement

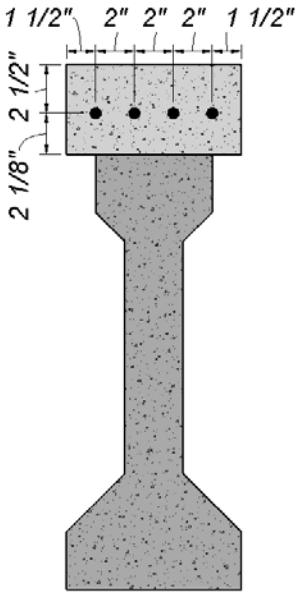

Figure 3-8:Deck Reinforcement Placement

Lastly, to ensure each load case fails as intended, shear reinforcement was accounted for during the design phase and adequate stirrups were placed within the specimens. Bent pairs of No. 3 stirrups were used in this design based on previous work (Mayhorn, 2016). The stirrups do not allow for any specimen to fail in shear during testing. The dimensions and spacing for each half-length specimen are shown in Figure 3-9 and Figure 3-10.

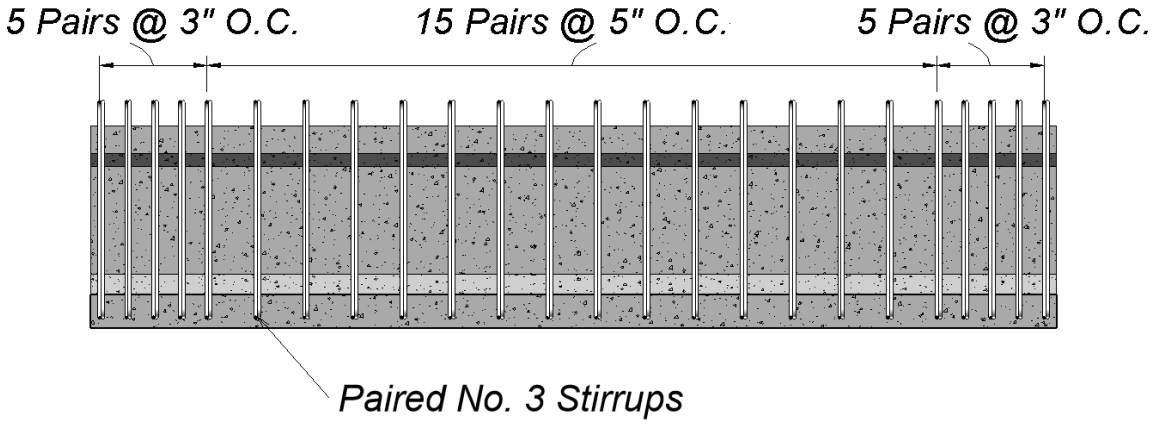

Figure 3-9:Half-Length Specimen Stirrup Spacing

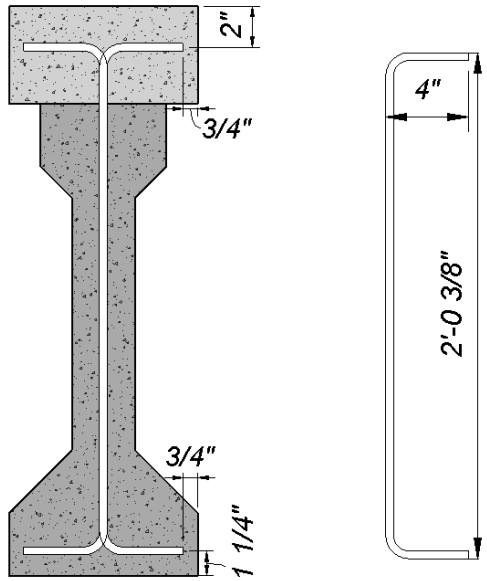

Figure 3-10:(Left) Stirrup Placement; (Right) Stirrup Dimensions

This concludes all the steel reinforcement for the specimens. Figure 3-11 through Figure 3-13 and Table 3-1 show the reinforcement types, spacing, and placement throughout the full-length specimens when joined together.

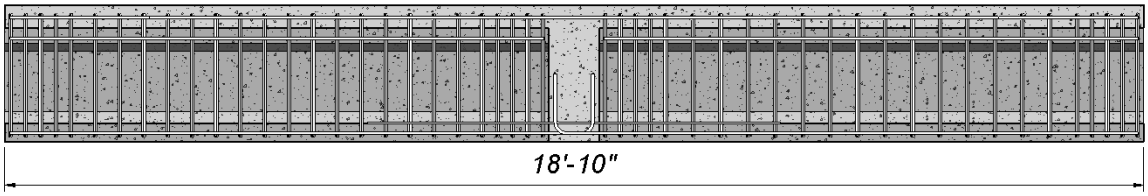

Figure 3-11:Full Specimen Steel Reinforcement

Figure 3-12:3-Dimensional Representation of Full-Length Specimen Steel Reinforcement

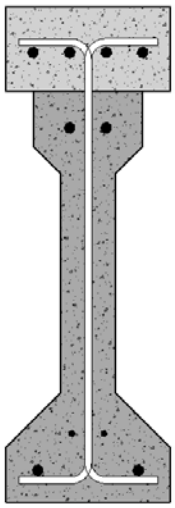

Figure 3-13:Cross Section of Steel Reinforcement

Table 3-1:Summary of Steel Reinforcement

Reinforcement Type	(QTY) Size @ Spacing	Length
Longitudinal Deck Reinforcement	(4) No. 5s @ 2” O.C.	(2): L = 18’ 8” (2): L = 14’ 1/2” (Centered over Joint)
Longitudinal Girder Compression Reinforcement	(2) No. 5s @ 2” O.C.	L = 8’ 9 3/4”
Longitudinal Girder Tension Steel Hooked into Continuity Joint	(2) Bent No. 5s @ 5 1/2” O.C. *OR* (2) Bent No. 5s @ 4 1/4” O.C.	Refer to Figure 3-4 and Figure 3-5 for accurate measurements
Mild Girder Tension Steel into Continuity Joint	(2) Bent No. 3s @ 1 1/4” O.C. *OR* (2) Bent No. 3s @ 3 1/4” O.C.	Refer to Figure 3-4 and Figure 3-5 for accurate measurements
Shear Reinforcement	(25) C-Shaped No. 3 Tied Pairs: (5) Pairs @ 3” O.C. (both ends) (15) Pairs @ 5” O.C. (middle)	Refer to Figure 3-9 Figure 3-10 for accurate measurements

All steel reinforcement used in this design is Grade 60, which has a minimum yield strength of 60 ksi. Prior to placement of reinforcement, tensile tests were performed on the steel batches as per ASTM A370 and the results are shown in Table 3-2.

Table 3-2:Steel Reinforcement Tensile Test Results

	MOE (ksi)	Yield (psi)	Ultimate (psi)
Test 1	26,618	62,546	102,668
Test 2	26,712	63,639	103,652
Test 3	30,105	63,368	103,698
Average	**27,812**	**63,184**	**103,339**

Based on the longitudinal reinforcement designs and tensile testing, nominal moment capacities were calculated for both positive and negative moment bending per ACI 318-14. The positive nominal moment capacity was calculated as 107.6 ft-k. The negative nominal moment capacity was calculated as 152.4 ft-k.

3.1.2 Girder Construction

To begin the process of constructing the girders steel reinforcement was cut, bent, and tied into cages. Each cage was built to be placed inside a half-length girder specimen. A total of 50 stirrups were used in this construction and tied in pairs. For ease of fabrication, the cages were constructed upside down using the bottom longitudinal reinforcement to act as supports to hang stirrups. Once the alignment and placement of the stirrups were achieved, they were then tied into place. Figure 3-14 shows one cage ready to be installed within the formwork before casting concrete.

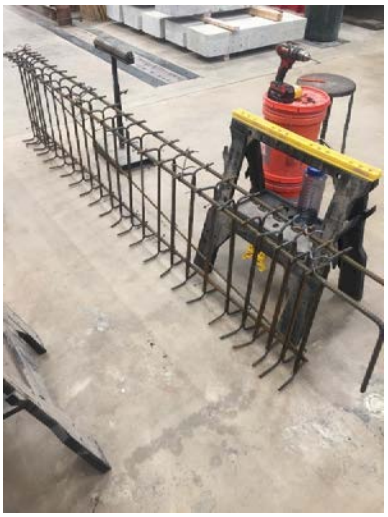

Figure 3-14:Half-Length Specimen Rebar Cage

Metal formwork for the casting was used to house the cages for the specimens. Used in previous research and built by an undergraduate student at the University of Oklahoma, these forms are 18’ in length with the AASHTO Type II profile. This allows for two half-length specimens to be cast at the same time. A total of four forms were used, yielding four half-length specimens per concrete pour. Figure 3-15 shows the arrangement of cages placed within the form.

Figure 3-15:Rebar Cages Within Formwork

Notice how two specimens are built using this formwork. A plywood divider between the two specimens, seen in the center of the metal form, separates the two specimens throughout the casting and curing processes. A No. 3 bar extends diagonally across each cage to alleviate any racking that may occur during the handling and placement of the cages. This reinforcement is not intended to be of any structural benefit after placement of cages within the formwork.

The plywood shown at the end of the forms not only keeps concrete from escaping during the casting process but also aligns the bottom longitudinal reinforcement. This alignment of the hooked ends of the reinforcement was crucial in that it allowed two half-length specimens to mate well prior to casting the deck and continuity joint. Baling wire was also wrapped around the hooked ends in order to keep them from shifting and rotating. A closer look at the formwork and hooked is shown in Figure 3-16.

Figure 3-16:Hooked Ends Formwork

As stated previously, each casting yielded four half-length specimens. To ensure the hooked ends would mate correctly, two different end forms were constructed like that of

Figure 3-16 – one for the inner reinforcement and one for the outer reinforcement. Each casting consisted of two of each type of formwork, yielding two final full-length specimens upon joining. The difference of each end form and the alignment dimensions is shown from the cross section of the final specimen in Figure 3-17.

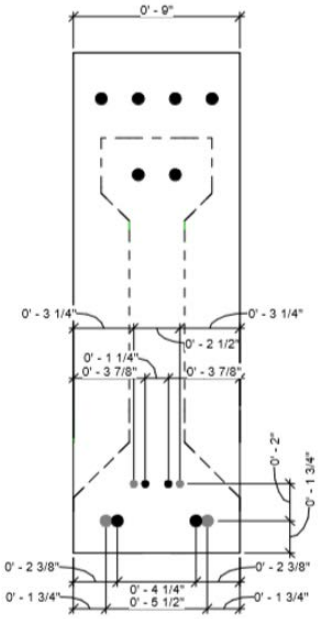

Figure 3-17:Hooked End Bar Mating Alignment

Plywood and construction grade lumber platforms were built for the casting process. These platforms allowed the specimens to sit level by way of shims beneath. Additionally, the platform let the metal forms to be clamped down ensure dimensional accuracy and stability throughout the casting process. To restrain the formwork from bulging away from the girder's centerline due to head pressure during the pouring process, square steel tube stock was fabricated to clamp across the tops of the formwork. Figure 3-18 below shows these clamps and the final stage of the formwork prior to casting.

Figure 3-18:Specimens Ready for Casting

3.1.3 Girder Casting

As per Oklahoma Department of Transportation 2019 Standard Specifications for Highway Construction, Section 701.01: Mix Design and Proportioning, Class AA concrete was used in this design for the girders, including the deck and continuity joint. Table 3-3 shows the specifications for this class of concrete.

Table 3-3:Concrete Class AA Specifications

Class of Concrete	Minimum Cement Content, lb/yd^3	Air Content, %	Water/Cement Ratio, lb/lb	Slump, in.	Minimum 28-day Compressive Strength, psi
AA	564	6.5 ± 1.5	0.25-0.44	2 ± 1	4,000

The ODOT mix design of Class AA concrete is shown in Table 3-4.

Table 3-4:ODOT Class AA Mix Design

Material:	**Weight/yd^3**	
Cement	588	lbs.
#57 Crushed Stone	1841	lbs.
Fine Aggregate	1281	lbs.
Water	232	lbs.
Glenium 7920	3	fl oz./cwt
MB AE-90	0.7	fl oz./cwt

The concrete was ordered and brought to the laboratory by truck from Dolese Bros. Company. The fresh concrete properties me the ODOT slump requirement and water-reducing admixture was added to the batch plant. The slump on site for each pour was 4-6". The actual mix design from Dolese Bros. Company used in this research is shown in Table 3-5.

Table 3-5:Dolese Bros. Mix Design

Material:	**Amount/yd^3**
Type 1 Portland Cement	588 lb
Coarse Aggregate (#67)	1841 lb
Fine Aggregate (Natural Sand)	1290 lb
Water	224 lb
HRWR	3.5 fl oz./cwt
AEA	0.70 fl oz./cwt

Each half-length specimen needed 6.61 ft^3 of concrete. An additional 0.88 ft^3 was used to fill three cylinders for compression testing for each pour. To expedite the casting process, the concrete was transported across the lab using a large, round-gate bucket attached to a top running single girder overhead crane. Figure 3-19 shows the concrete flowing from the truck's discharge chute to the round-gate bucket.

Figure 3-19:Filling Round-Gate Bucket with Concrete

Using the overhead crane to transport the concrete to the girder forms, the concrete was then discharged. This process was a four-person operation. One person manned the crane and moved the bucket down the girder while another released the concrete into the formwork. Once a sufficient amount of concrete was placed, the bucket was moved down the girder to begin adding more concrete into the formwork. Following behind this process was a two-person crew using a concrete vibrator. While one operated the vibrating end of the machine, another held the motor and supplied electrical power when needed. This process reduces the internal friction of the mix and removes any air pockets formed within the fresh concrete.

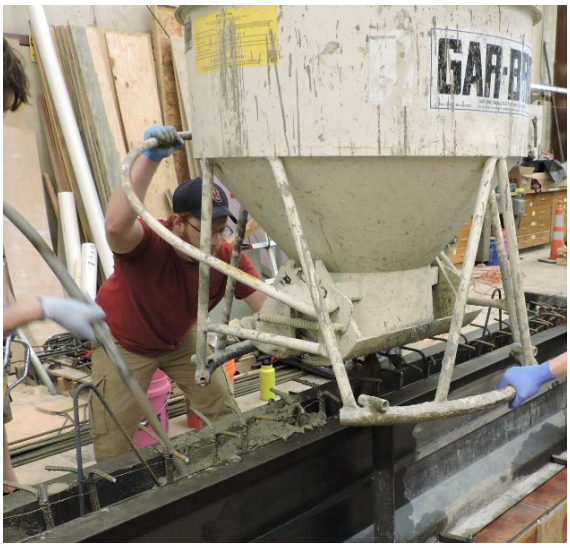

Figure 3-20:Pouring & Vibrating Concrete into Girder Formwork

Figure 3-20 shows the previously mention process in motion. There was one thing worth noting while pouring the concrete into the formwork. In order to allow the fresh concrete to flow unobstructed down through the girder's web and to the bottom bell, one of the top longitudinal No. 5 bars was removed. This increased the clearance of which the concrete could flow. Once the formwork was just about full of concrete, these bars were then re-tied to their original location. This was a relatively simple task, as the concrete was only filled up to the top of the formwork seen in the figure.

Also shown in Figure 3-20 are hooks to aid in transporting the specimens using the overhead crane. These hooks were made from No. 3 bars and extend 9" down into the girder and 3" above the eventual deck. Finally, the top surface of the girder was roughened which is the interface where the deck meets the girder. Transport hooks and two sets of poured girders are shown in Figure 3-21.

Figure 3-21:Completed Girder Casting

The half-length girder specimens were moist cured for seven days. Wet burlap was placed over all exposed concrete and was monitored throughout the seven days. In addition to the wet burlap, plastic sheeting covered the specimens to mitigate the evaporation of water. After the seven-day moist cure the half-length girders were stripped of all formwork and were ready to be joined together, as shown in Figure 3-22.

Figure 3-22:Half-Length Girder Specimens After Moist Cure

3.2 Continuity Joints

3.2.1 Continuity Joint Construction

Immediately following the seven-day moist cure the half-length girder specimens were then arranged to prepare for the casting of the deck and continuity joint. Figure 3-23 shows how the hooked ends of two specimens are able to mate together.

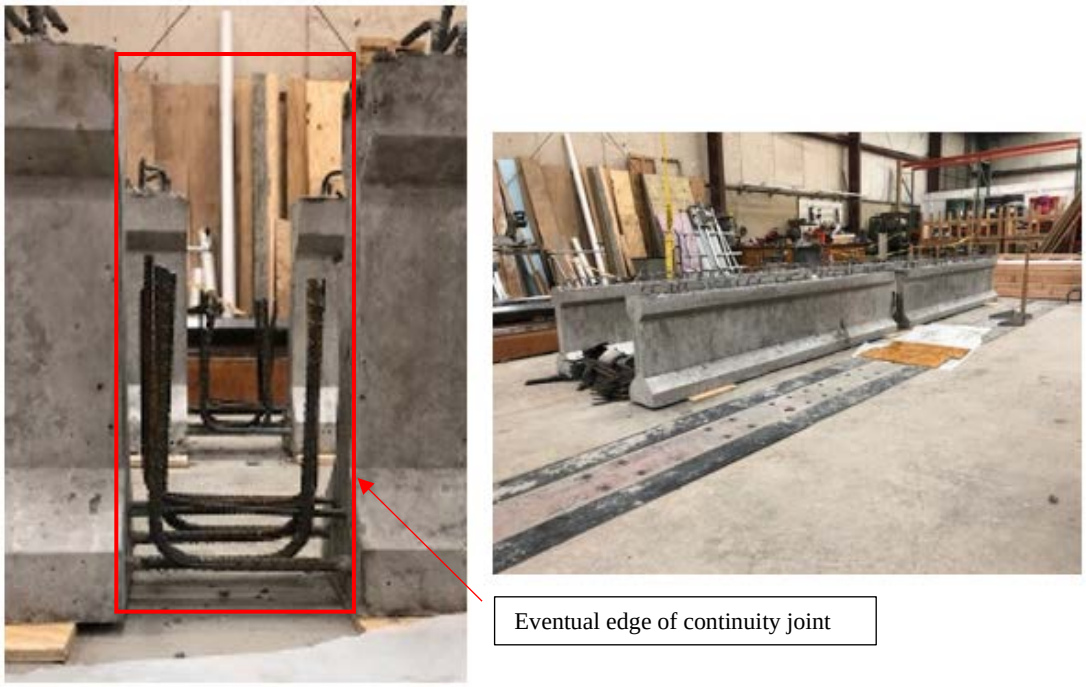

Figure 3-23:Orientation of Half-Length Girders Prior to Deck/Joint Casting

Plywood and construction grade lumber was again used to create the formwork for the continuity joint. Because the joint is a rectangular prism that extends out from either side of the bells and webs of the two half-length specimens, sheets of plywood were cut in the shape of the outer girder profile, including the deck. This allowed containment of the pour on the faces perpendicular to the length of the specimen. Plywood and lumber were used to house the two faces running parallel to the length of the specimens. Figure 3-24 shows how the continuity joint formwork comes together. The sheet of plywood on the floor was used for two reasons. The plywood maintained that the joint stay level with the two half-length girder specimens and allowed a stop block of wood at the base of the larger face of the joint. Much like the C-shaped clamps built for the top of the half-length

girder specimens, this stop-block would not allow movement of the formwork due to head pressure during the pour.

Figure 3-24: Continuity Joint Formwork

Figure 3-24 shows a piece of lumber stretched across the top of the joint. This lumber was set in place to keep the forms from bowing out during the pour. One problem with this method was that during the pour the round-gate bucket would drop concrete onto the wood and not into the joint. An easy remedy to this problem used in the pours to follow was to use a two F-style clamps across the joint, which worked very well.

3.3 Composite Deck Slab

3.3.1 Deck Slab Construction

After the half-length girder specimens were set in place with the mating hooked ends, the formwork for the deck was built. The formwork design was simple and built from plywood and construction lumber. Spanning the length of the half-length girders, 2x4s were used as the formwork of the underside lip of the deck. The deck is 9” wide, which protrudes 1.5” away from the top bell of the girder. Plywood cut to length was attached to these 2x4’s which encapsulated the side faces of the deck. These plywood pieces were 4.625” tall, the same height as the finished deck, and gave a perfect reference to trowel

the fresh concrete across. The deck design was also based on previous research (Casey, 2019). This system of formwork was set in place by way of supports acting as stilts. These stilts not only held the formwork in place but allowed the formwork to be installed without directly anchoring into the specimen. This aided in the process of demolding the specimens and the reuse of the formwork. Figure 3-25 shows the specimens ready for concrete placement.

Figure 3-25:Deck Formwork

Two strain gages, Figure 3-26, were applied to two of the deck reinforcement bars over the joint. One strain gauge was installed on one of the outer bars, and another on one of the inner bars. The gages were placed at the midpoint of each bar after the appropriate amount of grinding, sanding, and cleaning (lacquer thinner, acid, base) was applied to the area of interest. The midpoint of each bar corresponded to the center of the joint; the data that would come from this location is desired specifically for the second load case where the deck bars are supposed to fail after the joint has been repaired.

First, the longitudinal bars were ground down to the bare metal where the stain gauges would be installed. This process rids the bars of the mill scale and produces the shiny steel beneath. After grinding was complete, sandpaper was used to further prepare the metal surface. The sandpaper grits used, in order, were 80, 120, 180, 220, and 320. After this step, the surface was cleaned using an acid and base treatment.

Cyanoacrylate (CA) glue was used to adhere the strain gauge to the bar surface, Figure 3-26. Once the adhesive had time to dry completely, the strain gauge was covered in room-temperature-vulcanizing silicone (RTV). This provided the strain gauges a seal to mitigate water intrusion and also a bit of protection from falling concrete during pouring, Figure 3-27. The silicone was left to cure overnight and was then wrapped with aluminum tape. Zip ties were used to connect the strain gauge wires to the rebar and

provide strain relief if the wires are pulled during the placement of the concrete (Figure 3-28).

Figure 3-26:Strain Gauge Glued to Longitudinal Reinforcement

Figure 3-27:Room-Temperature-Vulcanizing Silicone (RTV) Covering Strain Gauge

Figure 3-28:Strain Gauges Attached to Longitudinal Reinforcement Ready for Install

The longitudinal reinforcement was installed, as shown in Figure 3-30, and tied to the stirrups. The strain gauge wires were incrementally zip tied down the longitudinal reinforcement to the first transport hook. Tape was used to cover the exposed strain gauge wires, labeling either inner or outer bar, and additional zip ties were used to attach the wires to the top of the transport hooks. This process kept the strain gauge wires protected throughout the pour and would allow access to the wires after the concrete cures. Figure 3-29 shows a strain gauge emerging from the top of the deck and tied to a transport hook.

Figure 3-29:Strain Gauge Wires Before Casting

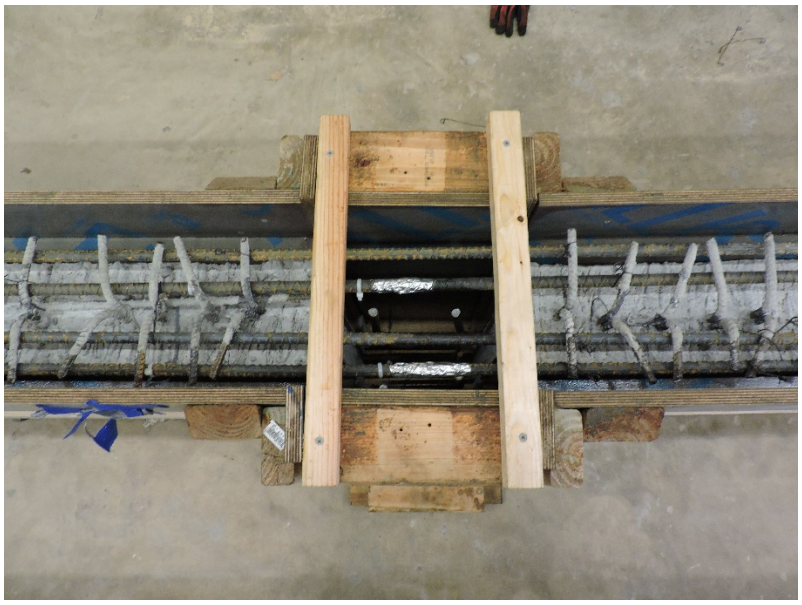

Figure 3-30:Top View of Continuity Joint Prior to Casting

Additional C-shaped clamps were built from 2x4's and 2x6's. These were used to keep the sides of the formwork from bulging throughout the casting process. One clamp per half-length specimen proved to be sufficient and was placed at each of their midspans. The clamps and the final formwork setup, ready for casting, are shown in Figure 3-31.

Figure 3-31:Two Girder-Joint-Girder Specimens Prior to Casting

3.3.2 Deck and Continuity Joint Casting

An amount of 5.5 ft^3 of concrete was needed for casting each deck and an amount of 1.17 ft^3 of concrete was needed for casting each joint, totaling 6.6 ft^3 for each full specimen. The process for casting the deck and joint was very much like casting the half-length girder specimens. The four-person crew had the same tasks as they did for the girder pour. One thing noted while casting the first deck and joint was that the clearance needed for vibrating the joint was hindered by concrete poured along the deck above the girder beforehand. This is shown in Figure 3-32.

Figure 3-32:Vibrating the Joint During Casting

The team decided that pouring the continuity joint prior to the deck along the girders allowed for better clearance for vibrating. This proved to be successful, and the method was used for the rest of the full-specimen castings. Figure 3-33 shows the complete girder-joint-girder specimen after final casting.

Figure 3-33:Girder-Joint-Girder Specimen After Final Casting

The full-length girder specimens were moist cured for seven days. Wet burlap was placed over all exposed concrete and was monitored throughout the seven days. In addition to the wet burlap, plastic sheeting covered the specimens to mitigate the evaporation of water. After the seven-day moist cure the full-length girders were stripped of all formwork to await testing.

3.4 Class AA Concrete Cylinder Compressive Strengths

Concrete cylinder compression testing was performed in accordance with ASTM C39. Table 3-6 shows the 28-day compressive strengths for the Class AA concrete used for the girder-joint-girder specimens. Unfortunately, data for only two cylinders on 7/19/2019 was obtained.

Table 3-6:Class AA Concrete Cylinder Compression Testing Results

Date Poured	**Compressive Strengths [psi]**			**Average [psi]**
3/1/2019	5848	5392	5760	**5670**
3/18/2019	5466	5410	5437	**5440**
4/3/2019	4285	4814	5087	**4730**
4/10/2019	5840	6028	6042	**5970**
6/20/2020	5004	4894	4545	**4810**
7/19/2020	4067	3924	N/A	**4000**
7/25/2020	3456	3667	3858	**3660**
8/22/2020	5486	5408	5248	**5380**
9/16/2020	5685	6276	5642	**5870**

4.0 Initial Girder Testing & Procedure

Three control specimens and nine repair specimens were tested at Donald G. Fears Structural Engineering Lab at the University of Oklahoma. This chapter will address the testing arrangement and procedure. Furthermore, results from the control specimens and initial cracking of the specimens to be repaired are provided within this chapter.

4.1 Specimen Testing Arrangement & Procedure

4.1.1 Specimen Testing Arrangement

The tests were arranged as a simply supported beam with a concentrated load at midspan at the location of the continuity joint. The concentrated load was applied by a hydraulic ram attached to a loading frame anchored to the strong floor. The clear span length of the specimens was 18’ 2”, bearing 4” on each end. This loading was only intended to produce positive moment in the joint and was not representative of how the girder-joint-girders would be supported in the field.

A 50-kip capacity calibrated load cell was placed directly below the hydraulic ram to monitor and record the applied load. A ½” layer of sand was placed between a 1” thick metal plate and the specimen’s deck. This layer of sand allowed the plate to be leveled by hand prior to placement of a cylindrical swivel spacer and load cell allowing the load to be normal to the surface of the deck of uniform area. The swivel spacer also allowed the load applied to make minor rotational adjustments for stability through the load path to the girder specimen. This setup is shown in Figure 4-1

Figure 4-1:Hydraulic Ram, Load Cell, Spacer, and Metal Plate Setup

Each end support consisted of a large concrete ecology block with an ODOT approved bridge bearing pad encased in neoprene resting on top. Figure 4-2 shows this setup with a girder-joint-girder specimen installed beneath the load frame.

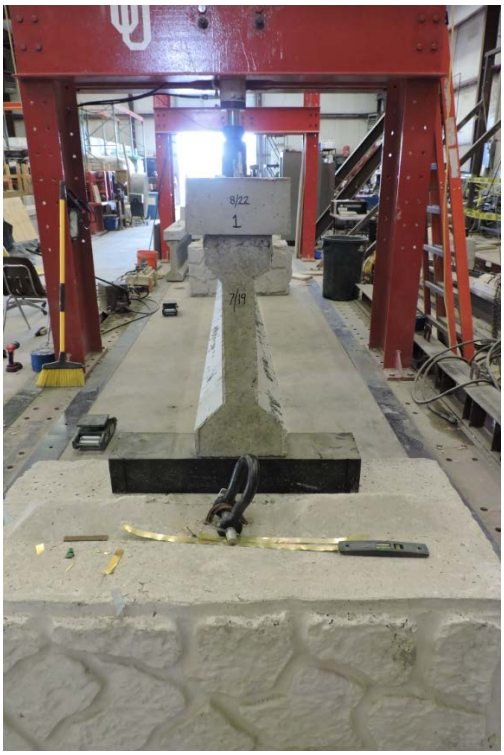

Figure 4-2:End Support Setup

Two wire potentiometers were placed on each side of the girder-joint-girder specimen at midspan to measure deflection while testing. Steel angles were epoxied to the face of the continuity joint to allow the wire potentiometers to connect to the specimen. This setup is shown in Figure 4-3.

Figure 4-3:Wire Potentiometer Setup

4.1.2 Specimen Testing Procedure

Each test specimen was installed beneath the load frame using the overhead crane. A plumb bob suspended from a string attached to the center of the hydraulic ram allowed the team of researchers to place the test specimens centered both laterally and longitudinally. After the test specimen was aligned with the hydraulic ram, the wire potentiometers, load cell, and strain gauges were attached to the data acquisition system. To ensure the data acquisition was working properly each sensor was tested for a signal change. After this check, each signal was tared to zero within the data acquisition system in preparation for testing.

Load was applied to each specimen by two 5-kip intervals until 10-kips were applied. Loading increments were then adjusted to 2-kip intervals for the remainder of testing. This allowed for better precision when locating cracks. Shear and flexural cracks were assessed between each interval. Cracks were traced with black permanent marker with the corresponding load written at the end of the crack.

Two separate scenarios would govern when each specimen had completed its testing. The first scenario was when the specimen would not take any more load, yielding the longitudinal reinforcement. This was a flexural failure. The second scenario was the initial cracking of the specimens to be repaired. Testing for this scenario was completed when the continuity joint had sufficient cracking that would simulate that of a damaged girder in the field.

Each specimen was unloaded when finished with testing.

4.2 Control Girder Testing and Results

Three girder-joint-girder specimens were tested to failure in negative moment bending. These specimens acted as the control group and are denoted as C1, C2, and C3 throughout this research. To simulate negative moment bending the team of researchers decided to flip the specimens upside down before installing them beneath the load frame. Loading the control group upside down resulted in a flexural failure in negative moment bending at the continuity joint. Figure 4-4 shows how this test setup looks prior to loading.

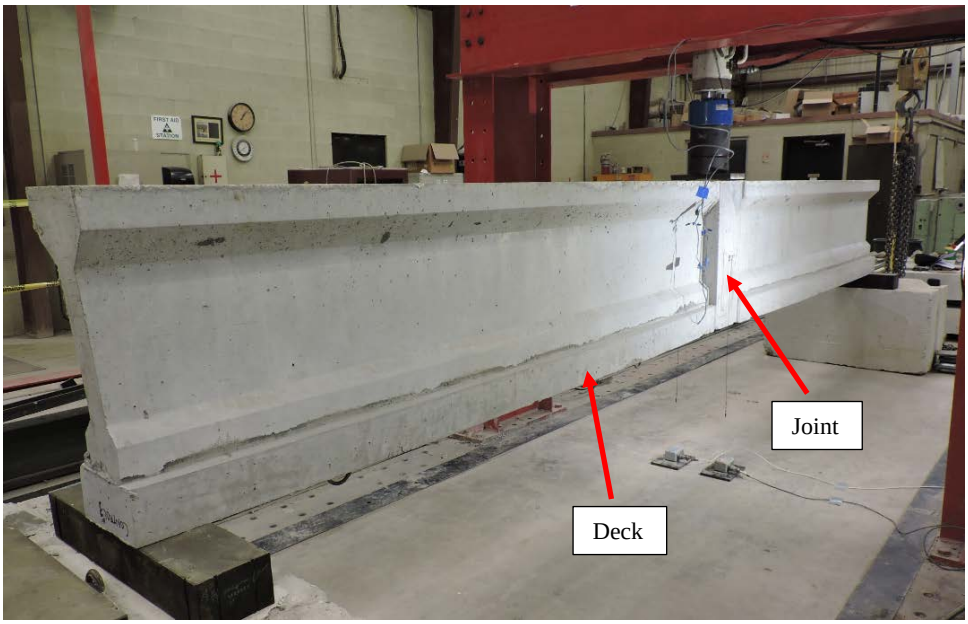

Figure 4-4:Control Beam Test Setup for Negative Moment Bending

4.2.1 Control Specimen (C1) Results

Initial shear cracking was observed within the web of the specimen at 10-kip loading and continued to propagate diagonally upward as the loading progressed. The vast majority of the shear cracking developed within the web occurred between 14-kip and 36-kip of loading. Traced and marked with the corresponding loading increment, the shear cracking is shown in Figure 4-5.

Figure 4-5:C1 Shear Cracking

At the same 10-kip loading interval, initial flexural cracking began to form in the continuity joint (Figure 4-6).

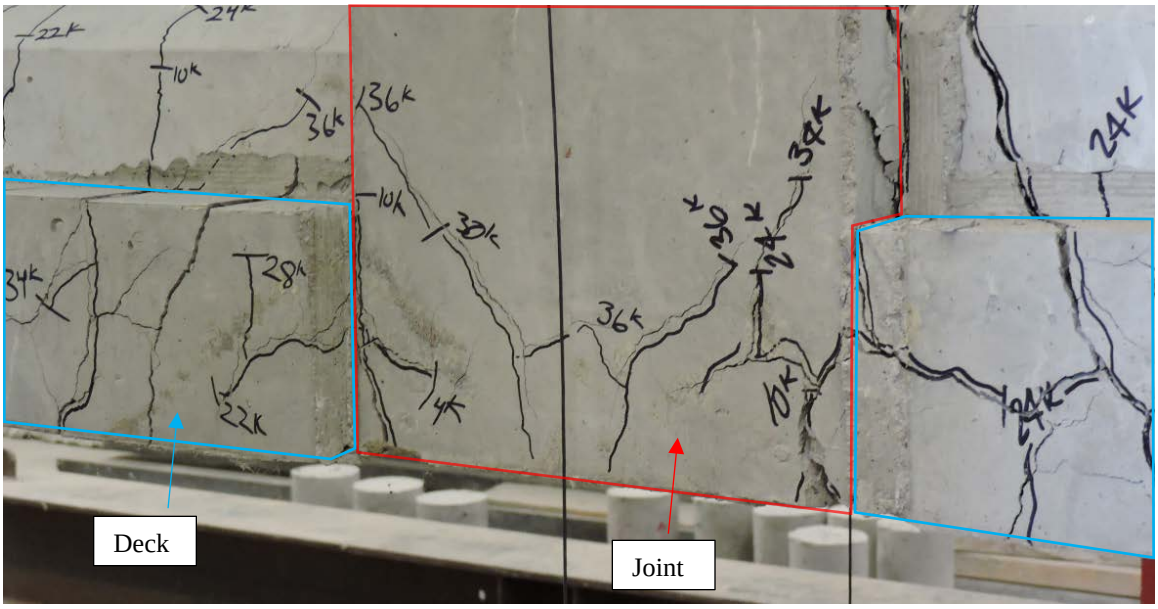

Figure 4-6:C1 Initial Cracking in Continuity Joint

These cracks continued to grow with increased loading. Flexural cracks at the girder-joint interface were observed on both sides of the specimen. As loading increased, these cracks not only continued propagating upward on the interface but also increased in width, showing visible joint separation (Figure 4-7 and Figure 4-8).

Figure 4-7:C1 Cracking at Girder-Joint Interface (Left Side)

Figure 4-8:C1 Cracking at Girder-Joint Interface (Right Side)

Figure 4-9 shows the girder-joint interface flexural cracking across the deck. This photo was taken after the specimen had been unloaded, removed from beneath the loading frame, and flipped right side up. The large cracks across the top of the deck indicate that the continuity joint had begun to detach from the two half-length girders. Figure 4-10 shows the overall girder-joint-girder specimen after testing.

Figure 4-9:C1 Girder-Joint Interface Cracking across the Deck

Figure 4-10:Deflected Shape of Unloaded C1 Specimen

Control specimen C1 showed a ductile behavior after 33,086 lb were applied, and had an ultimate load capacity of 44,601 lb. At the ultimate load, C1 had deflected an average of 2.28". Figure 4-11 shows the load-deflection curve of C1, which is typical of a beam flexural failure.

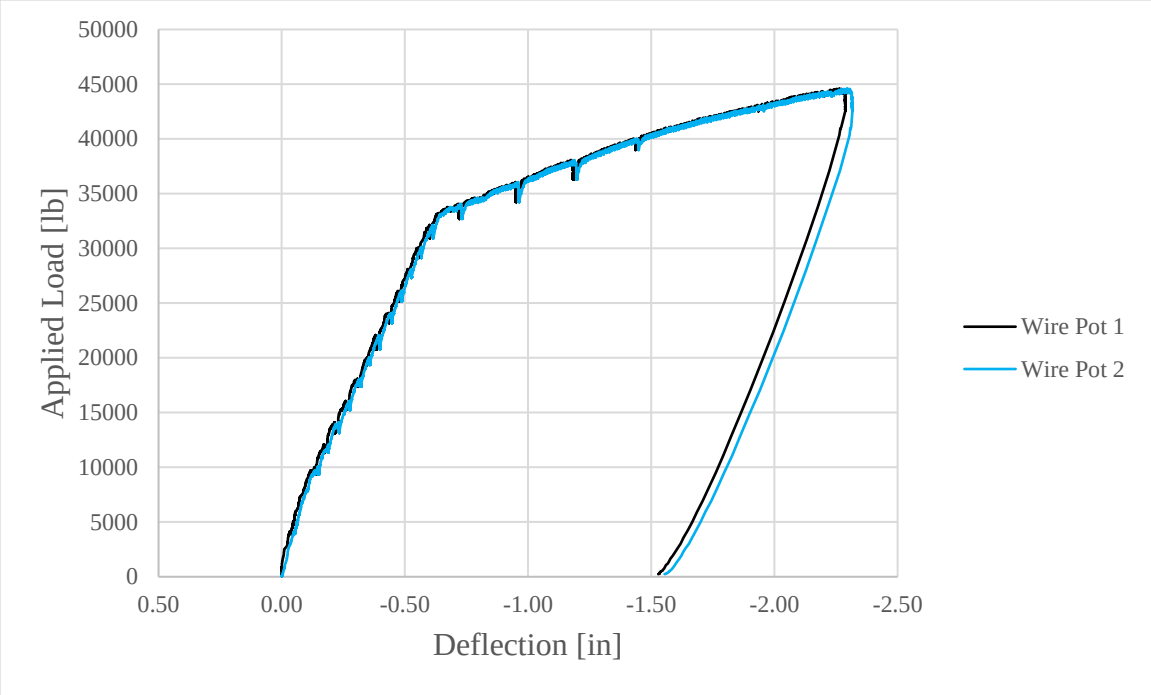

Figure 4-11:C1 Load-Deflection Curve

The outer longitudinal reinforcement for negative moment bending began to yield at a loading of 27,716 lb. This was the point at which the strain in the steel reached 0.00218 in/in. Figure 4-12 shows a plot of the load-strain curve of control specimen C1. The inner reinforcement's strain gauge appears to have lost signal during the loading process. There are a number of reasons this may have happened, which include detaching from the rebar, or an open circuit caused by a shifting of the strain gauge wires within the specimen. The complete set of load-strain curves can be found in the Appendix.

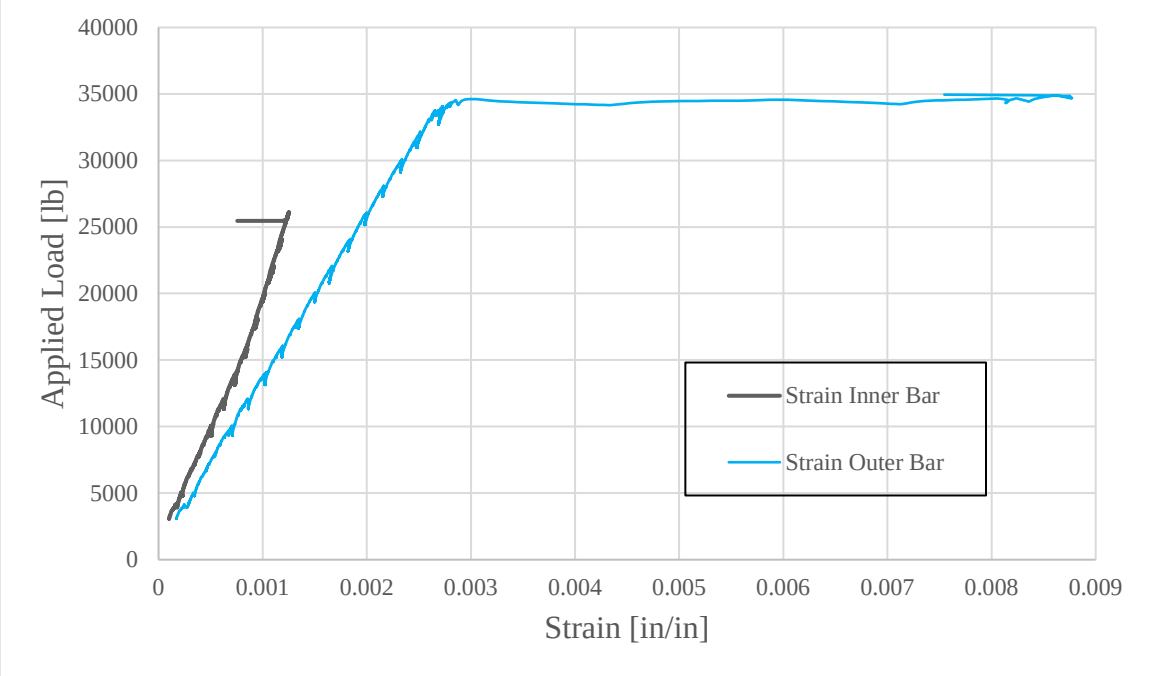

Figure 4-12:C1 Load-Strain Curve

4.2.2 Control Specimen (C2) Results

Initial shear cracking was observed within the web of the specimen at 10-kip loading and continued to propagate diagonally upward as the loading progressed. The vast majority of the shear cracking developed within the web occurred between 12-kip and 36-kip loading. Traced and marked with the corresponding loading increment, the shear cracking is shown in Figure 4-13.

Figure 4-13:C2 Shear Cracking

At the same 10-kip loading interval, initial flexural cracking began to form in the continuity joint (Figure 4-14).

Figure 4-14:C2 Initial Cracking in Continuity Joint

These cracks continued to grow with increased loading. Flexural cracks at the girder-joint interfaced were observed on both sides of the specimen. As loading increased, these

cracks not only continued propagating upward on the interface but also increased in width (Figure 4-15 and Figure 4-16).

Figure 4-15:C2 Cracking at Girder-Joint Interface (Left Side)

Figure 4-16:C2 Cracking at Girder-Joint Interface (Right Side)

Figure 4-17 shows the girder-joint interface flexural cracking across the deck. This photo was taken after the specimen had been unloaded, removed from beneath the loading frame, and flipped right side up. The large cracks across the top of the deck indicate that the continuity joint had begun to detach from the two half-length girders. Figure 4-18 shows the overall girder-joint-girder specimen after testing.

Figure 4-17:C2 Girder-Joint Interface Cracking Across the Deck

Figure 4-18:Deflected Shape of Unloaded C2 Specimen

Control specimen C2 showed a ductile behavior after 33,171 lb were applied, and had an ultimate load capacity of 44,620 lb. At the ultimate load, C2 had deflected 2.40”. Figure 4-19 shows the load-deflection curve of C2, which is typical for a beam flexural failure.

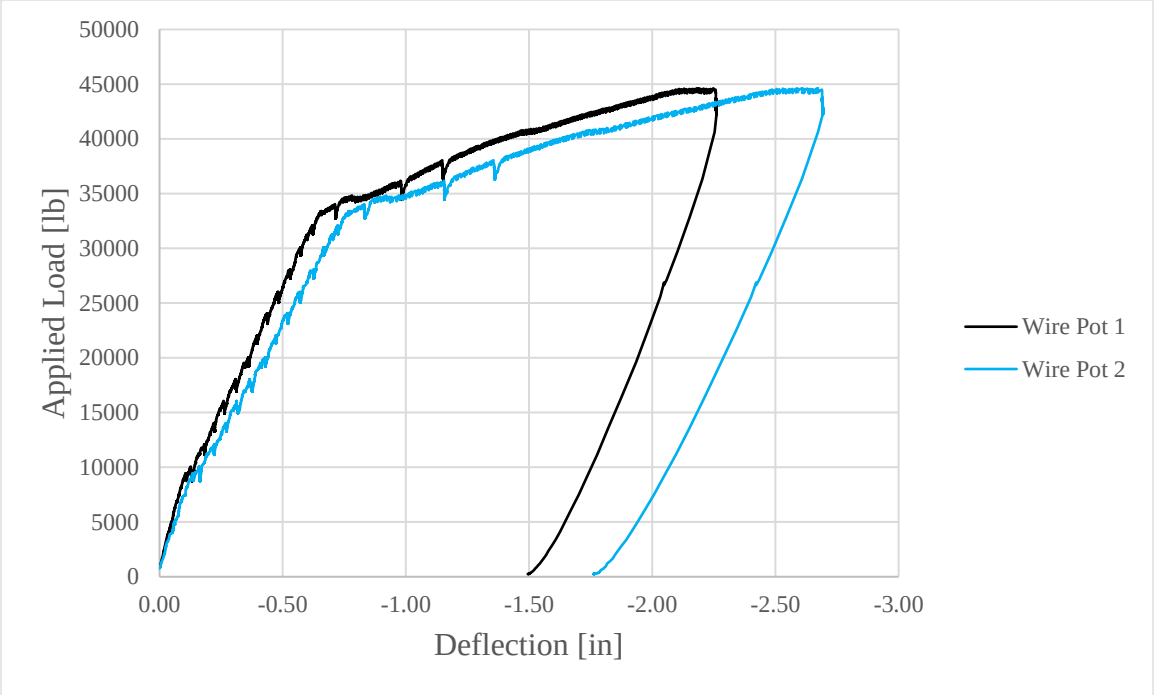

Figure 4-19:C2 Load-Deflection Curve

The inner longitudinal reinforcement for negative moment bending began to yield at a loading of 29,232 lb. The outer longitudinal reinforcement began to yield at a loading of 28,042 lb. These were the points at which the strain in the steel reached 0.00218 in/in. Figure 4-20 shows a plot of the load-strain curve of control specimen C1.

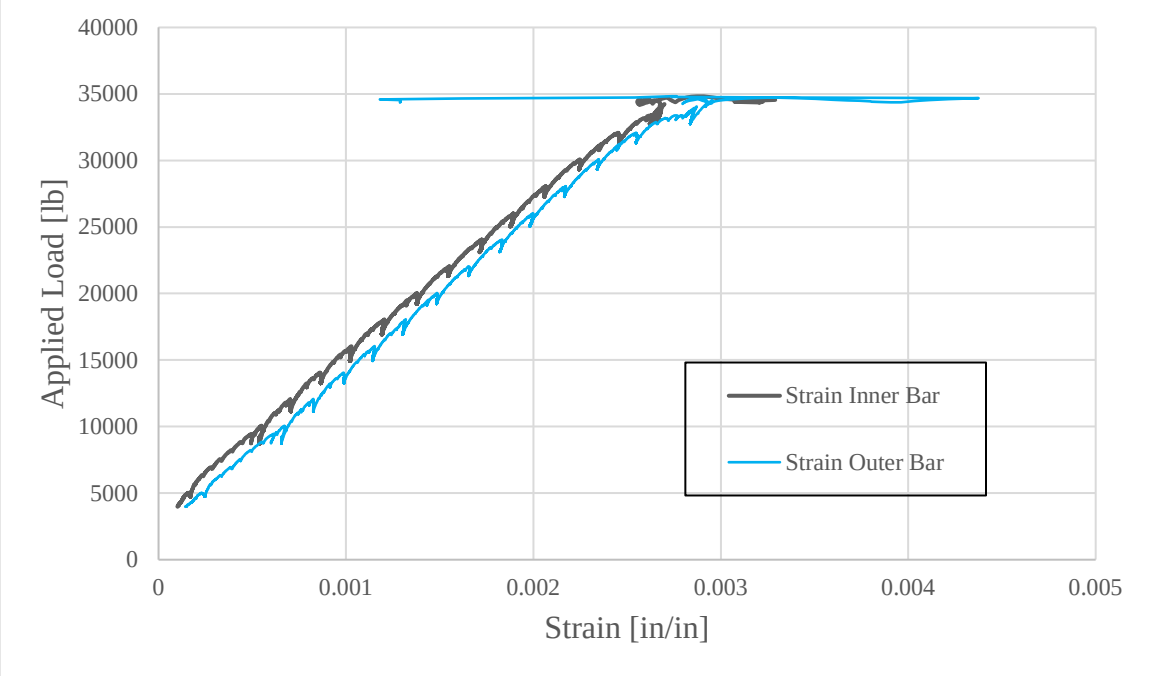

Figure 4-20:C2 Load-Strain Curve

4.2.3 Control Specimen (C3) Results

Initial shear cracking was observed within the web of the specimen at 10-kip loading and continued to propagate diagonally upward as the loading progressed. The vast majority of the shear cracking developed within the web occurred between 12-kip and 36-kip loading. Traced and marked with the corresponding loading increment, the shear cracking is shown in Figure 4-21.

Figure 4-21:C3 Shear Cracking

At the same 10-kip loading interval, initial flexural cracking began to form in the continuity joint. At the 16-kip loading increment a flexural crack propagated straight upward from the center of the continuity joint. This significant crack continued until 30-kips of load was applied before branching off into two flexure-shear cracks. These cracks terminated at 38-kip and 34-kip loading (Figure 4-22).

Figure 4-22:C3 Cracking in Continuity Joint

Flexural cracks at the girder-joint interface were observed on both sides of the specimen. As loading increased, these cracks not only continued propagating upward on the interface but also increased in width, showing visible joint separation. Figure 4-23 shows the girder-joint interface flexural cracking across the deck. The centerline flexural crack can also be seen. This photo was taken after the specimen had been unloaded, removed from beneath the loading frame, and flipped right side up. The large cracks across the top of the deck indicate that the continuity joint had begun to detach from the two half-length girders. Figure 4-24 shows the overall girder-joint-girder specimen after testing.

Figure 4-23:C3 Girder-Joint Interface and Centerline Cracking Across the Deck

Figure 4-24:Deflected Shape of Unloaded C3 Specimen

Control specimen C3 showed a ductile behavior after 32,223 lb were applied, and had an ultimate load capacity of 41,525 lb. At the ultimate load, C3 had deflected 2.16”. Figure 4-25 shows the load-deflection curve of C3, which is typical for a beam flexural failure.

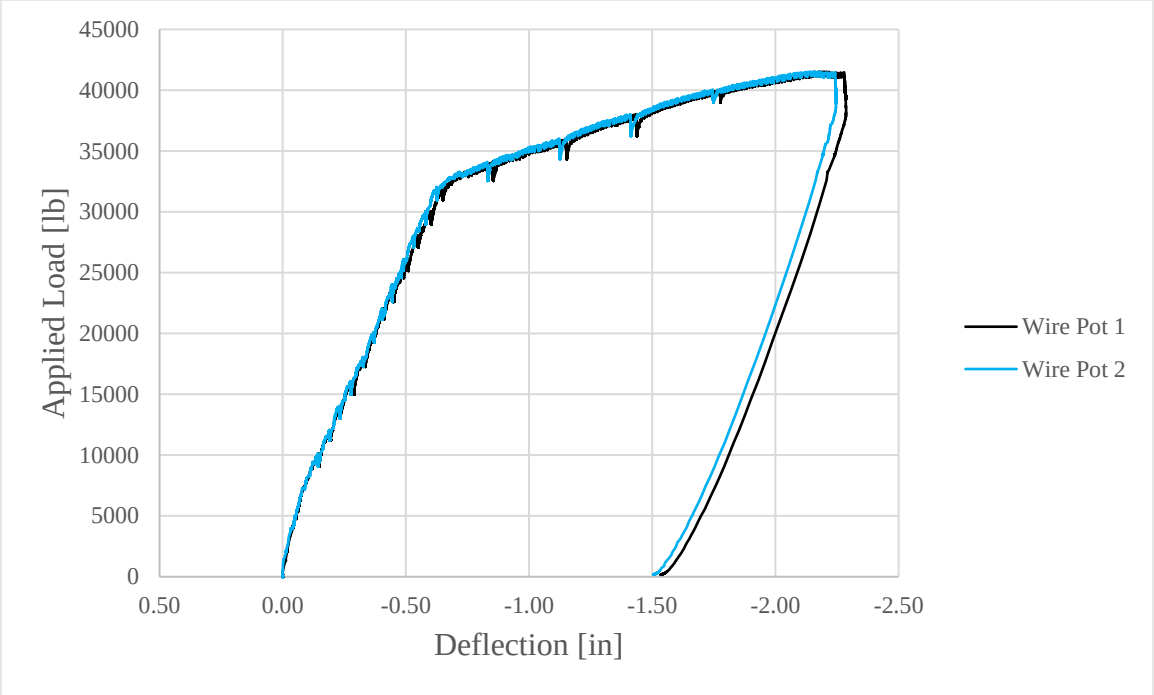

Figure 4-25:C3 Load-Deflection Curve

The inner longitudinal reinforcement for negative moment bending began to yield at a loading of 29,418 lb, which is inconsistent with the other strain gauge and all strain gauges from the other two control specimens. This may indicate a faulty reading. The outer longitudinal reinforcement began to yield at a loading of 31,322 lb. These were the points of which the strain in the steel reached 0.00218 in/in. Figure 4-26 shows a plot of the load-strain curve of control specimen C1.

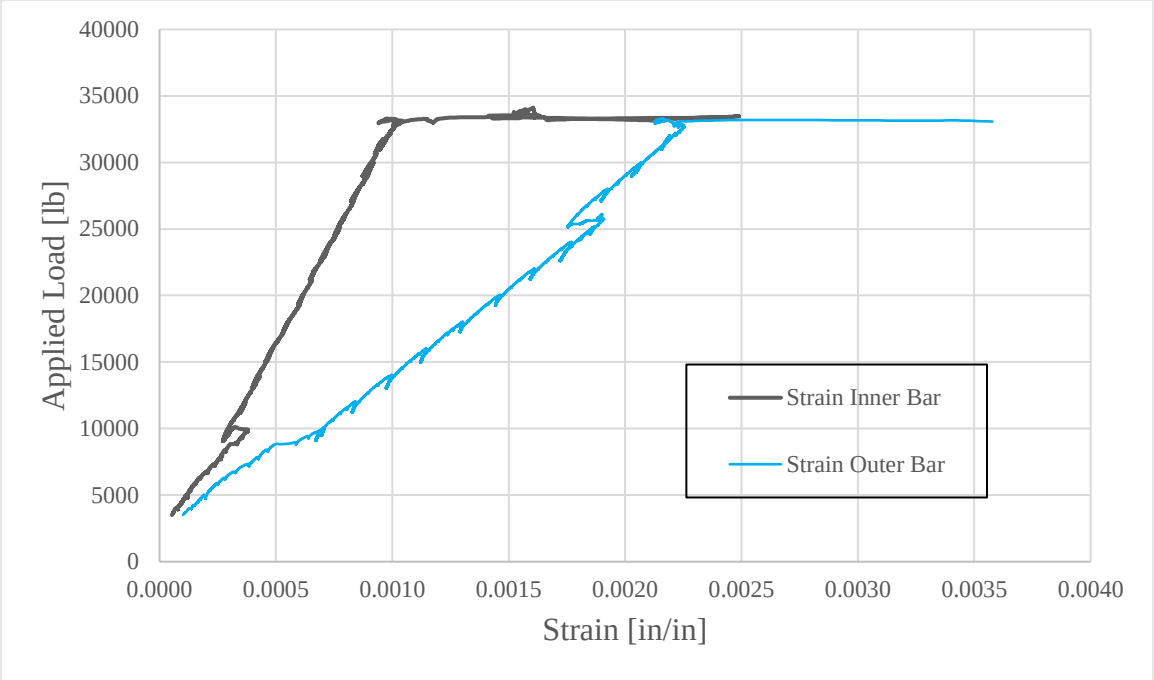

Figure 4-26:C3 Load-Strain Curve

4.2.4 Control Girder Testing Summary

Figure 4-27 shows a plot of all load-deflection curves of the control girder specimens. The results of these curves are very similar and show typical beam flexural failures.

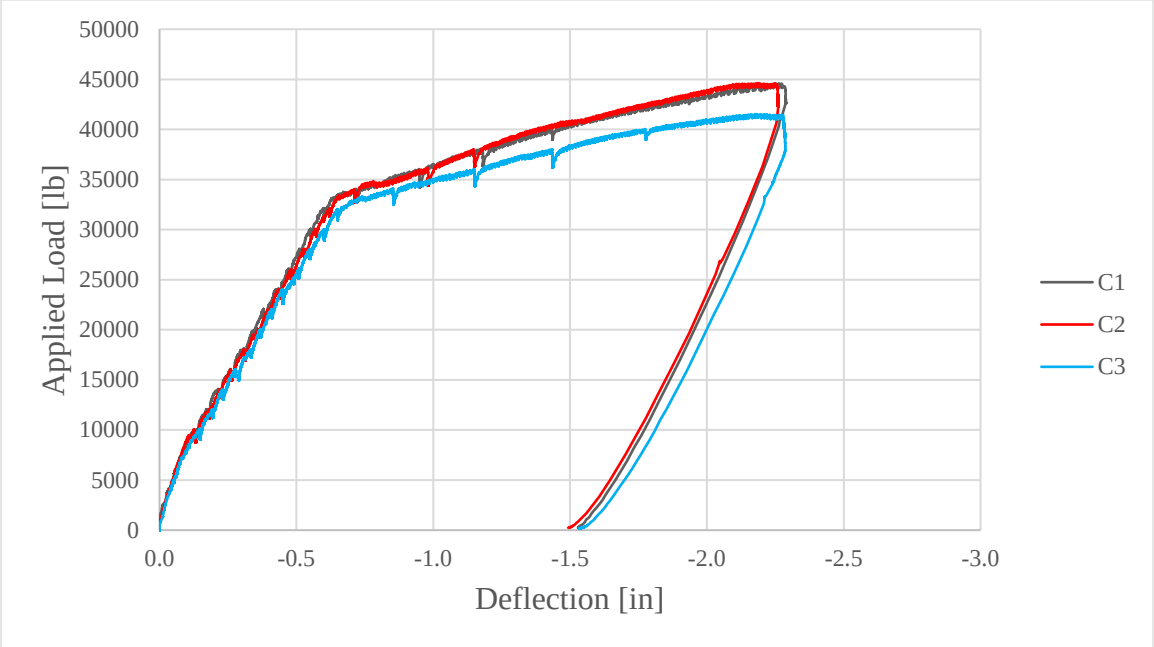

Figure 4-27:Load-Deflection Curves of Control Girder Specimens

4.3 Initial Cracking of Girders to be Repaired

The remaining nine girder-joint-girder specimens were loaded to induce cracking within their continuity joints. This process simulated the time-dependent effects out in the field which cause the bottom of the continuity joint to crack due to induced positive moment. Unlike the control group, the remaining nine specimens were loaded in positive moment bending. The data acquisition system was used in conjunction with the load cell only for these tests, outputting the load at which a sufficient amount cracking within the continuity joint replicated in-situ damage.

Besides loading in positive moment bending, the testing arrangement and procedure for the initial cracking of the repair girders was identical to that of the control specimens. Figure 4-28 shows this setup, which was used for all nine girder-joint-girder specimens.

Figure 4-28:Initial Setup Before Testing for Girders to Be Repaired

Specimens were divided into three groups. These groups corresponded to the material they were subsequently be repaired with. The nomenclature for each group within this research will be used as follows: R1-J3, R2-J3, and R3-J3 will be used for the group of specimens to be repaired with ultra-high-performance concrete; R1-FRSCC, R2-FRSCC, and R3-FRSCC will be used for the group of specimens to be repaired with fiber-reinforced self-consolidating concrete; R1-PHOS, R2-PHOS, and R3-PHOS will be used

for the group of specimens to be repaired with magnesium-alumino-liquid phosphate concrete (Phoscrete).

Specific to the J3 group only, a ½" notch was cut transversely across midspan on the bottom of each specimen. This notch was to promote cracking in the center of the joint, but did not yield any significant results.

4.3.1 First Set of Cracking (J3)

The first set of three specimens cracked were to be repaired with ultra-high-performance concrete (J3). At an applied load of 22,987 lb, sufficient cracking within the continuity joint of specimen R1-J3 had been achieved. Figure 4-29 through Figure 4-31 show joint cracking for R1-J3.

Figure 4-29:R1-J3 Rear Joint Face Initial Cracking

Figure 4-30:R1-J3 Bottom Joint Face Initial Cracking

Figure 4-31:R1-J3 Front Joint Face Initial Cracking

At an applied load of 23,020 lb, sufficient cracking within the continuity joint of specimen R2-J3 had been achieved. Figure 4-32 through Figure 4-34 show joint cracking for R2-J3.

Figure 4-32:R2-J3 Front Joint Face Initial Cracking

Figure 4-33:R2-J3 Bottom Joint Face Initial Cracking

Figure 4-34:R2-J3 Rear Joint Face Initial Cracking

At an applied load of 20,060 lb, sufficient cracking within the continuity joint of specimen R3-J3 had been achieved. Figure 4-35 through Figure 4-37 show joint cracking for R3-J3.

Figure 4-35:R3-J3 Front Joint Face Initial Cracking

Figure 4-36:R3-J3 Bottom Joint Face Initial Cracking

Figure 4-37:R3-J3 Rear Joint Face Initial Cracking

4.3.2 *Second Set of Cracking (FRSCC)*

The second set of three specimens cracked were to be repaired with fiber-reinforced self-consolidating concrete (FRSCC). At an applied load of 27,520 lb, sufficient cracking

within the continuity joint of specimen R1-FRSCC had been achieved. Figure 4-38 through Figure 4-40 show joint cracking for R1-FRSCC.

Figure 4-38:R1-FRSCC Front Joint Face Initial Cracking

Figure 4-39:R1-FRSCC Bottom Joint Face Initial Cracking

Figure 4-40:R1-FRSCC Rear Joint Face Initial Cracking

At an applied load of 21,430 lb, sufficient cracking within the continuity joint of specimen R2-FRSCC had been achieved. Figure 4-41 through Figure 4-43 show joint cracking for R2-FRSCC.

Figure 4-41:R2-FRSCC Front Joint Face Initial Cracking

Figure 4-42:R2-FRSCC Bottom Joint Face Initial Cracking

Figure 4-43:R2-FRSCC Rear Joint Face Initial Cracking

At an applied load of 21,415 lb, sufficient cracking within the continuity joint of specimen R3-FRSCC had been achieved. Figure 4-44 through Figure 4-46 show joint cracking for R3-FRSCC.

Figure 4-44:R3-FRSCC Front Joint Face Initial Cracking

Figure 4-45:R3-FRSCC Bottom Joint Face Initial Cracking

Figure 4-46:R3-FRSCC Rear Joint Face Initial Cracking

4.3.3 Third Set of Cracking (Phoscrete)

The third set of three specimens cracked were to be repaired with magnesium-alumino-liquid phosphate concrete (Phoscrete). At an applied load of 25,200 lb, sufficient amount of cracking within the continuity joint of specimen R1-PHOS had been achieved. Figure 4-47 through Figure 4-49 shows joint cracking for R1-PHOS.

Figure 4-47:R1-PHOS Front Joint Face Initial Cracking

Figure 4-48:R1-PHOS Bottom Joint Face Initial Cracking

Figure 4-49:R1-PHOS Rear Joint Face Initial Cracking

At an applied load of 24,720 lb, sufficient cracking within the continuity joint of specimen R2-PHOS had been achieved. Figure 4-50 through Figure 4-52 show joint cracking for R2-PHOS.

Figure 4-50:R2-PHOS Front Joint Face Initial Cracking

Figure 4-51:R2-PHOS Bottom Joint Face Initial Cracking

Figure 4-52:R2-PHOS Rear Joint Face Initial Cracking

At an applied load of 25,180 lb, sufficient cracking within the continuity joint of specimen R3-PHOS had been achieved. Figure 4-53 through Figure 4-55 show joint cracking for R3-PHOS.

Figure 4-53:R3-PHOS Front Joint Face Initial Cracking

Figure 4-54:R3-PHOS Bottom Joint Face Initial Cracking

Figure 4-55:R3-PHOS Rear Joint Face Initial Cracking

4.3.4 Initial Cracking Load Summary of Results

Table 4-1 shows a summary of the initial cracking loads for each specimen to be repaired. The loads represent the point at which the research team noticed enough cracking within each specimen to simulate in situ degradation.

Table 4-1:Initial Cracking Load Summary

Specimen Name	**Load at Sufficient Joint Cracking [lb]**
R1-J3	22,987
R2-J3	23,020
R3-J3	20,060
R1-FRSCC	27,520
R2-FRSCC	21,430
R3-FRSCC	21,415
R1-PHOS	25,200
R2-PHOS	24,720
R3-PHOS	25,180
Average:	**23,504**

5.0 Continuity Joint Repair

The continuity joint repairs for the nine specimens consisted of three different specialized concretes. The first set of specimens were repaired with an ultra-high-performance concrete mix (J3). The second set of specimens were repaired with a fiber-reinforced self-consolidating concrete mix (FR-SCC). The final set of specimens were repaired with a magnesium-alumino-liquid concrete mix (Phoscrete). This chapter will describe the joint repair design, construction, and casting procedures.

5.1 Joint Repair Design

The continuity joint repair design was based on the time-dependent effects of temperature loading on reinforced concrete continuous girder bridges. Changes in the surrounding weather can cause expansion and contraction within the girders which may result in unfavorable internal stresses. Sections 3 and 4 of AASHTO LRFD (2017) were used to establish a steel reinforcement design that would counteract these time-dependent effects.

5.1.1 Steel Reinforcement Repair Design

By considering a temperature gradient within a concrete girder bridge using AASHTO LRFD 3.12.3, internal stresses and structural deformations were determined in accordance with the provisions of AASHTO LRFD Article 4.6.6. Because plane sections remain plane, a curvature is imposed on the superstructure to accommodate the linearly variable component of the temperature gradient (AASHTO LRFD, 2017). Section C4.6.6 gives the equation for this rotation due to a vertical temperature gradient, shown in Equation 1.

Equation 1:AASHTO C4.6.6-3

$$\phi = \frac{\alpha}{I_c}\iint T_G z dw dz = \frac{1}{R}$$

Where:

$\alpha = coefficient\ of\ thermal\ expansion;\ 6 * 10^{-6}/_{\circ\mathrm{F}}$

$I_c = inertia\ of\ cross-section;\ 15{,}507\ in^4$

$T_G = temperature\ gradient;\ 46°\text{F}$

$z = vertical\ distance\ from\ center\ of\ gravity\ of\ cross-section;\ 13.56"$

$w = width\ of\ element\ in\ cross-section;\ 9"$

Setting the State of Oklahoma as the location, the temperature gradient of 46°F was found from AASHTO LRFD Table 3.12.3-1, using Solar Radiation Zone 2 from AASHTO LRFD Figure 3.12.3-1. Evaluating Equation 1 gives a rotation per unit length corresponding to the girder-joint-girder specimens used in this research of $\phi = 0.00001459$.

The moment developed at the pier for a two-span structure needed to eliminate deflection where the temperature gradient flexes the structure into a segment of a circle in the vertical plane is given by Equation 2:

Equation 2:AASHTO C4.6.6-7

$$M_c = \frac{3}{2} E I_c \phi$$

Evaluating Equation 2 gave a moment value of 102 k-ft. Therefore, the amount of positive reinforcement needed was calculated as 0.752 in^2 of 60 ksi mild steel, or four No. 4 bars.

In this design, reinforcement was placed in two locations at the bottom of the continuity joint. The lower reinforcement was designed to be placed within the bottom bell, 2.75" on center from the bottom of the specimen. The upper reinforcement was designed to be placed in the bottom of the web, 6.25" on center above the bottom of the specimen.

The web repair reinforcement was designed to be two U-shaped No. 4 bars which legs extended horizontally across the face of the continuity joint. Each leg of each U-shaped bar was designed to lap with one another, consisting of a minimum development length of 9.49" and standard hook geometry as per ACI 25.4.3.1 (2014) and ACI 25.3.1 (2014), respectively. Figure 5-1 shows the top repair reinforcement.

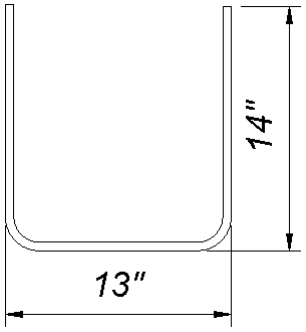

Figure 5-1:Top Repair Reinforcement Shape & Dimensions

The bottom repair reinforcement was designed to be two U-shaped No. 4 bars which legs extended halfway into the bottom bell. The reason for this was for ease of the installment of the rebar. Each leg was anchored into the bottom bell 4.5” to provide the necessary bond strength using a Hilti HIT-HY 200-R epoxy. The bottom repair reinforcement was also designed with a standard hook geometry as per ACI 25.3.1 (2014). Figure 5-2 shows the bottom repair reinforcement shape and dimensions.

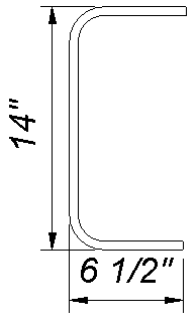

Figure 5-2:Bottom Repair Reinforcement Shape & Dimensions

5.1.2 Concrete Repair Design

The outer edge of all repair reinforcement was placed 1.5” from all faces of the original continuity joint, giving an edge to center distance of 1.75”. The design allowed the minimum inside bend diameter of the bars to be 3” in accordance with ACI Table 25.3.1. The placement of repair reinforcement is shown in Figure 5-3.

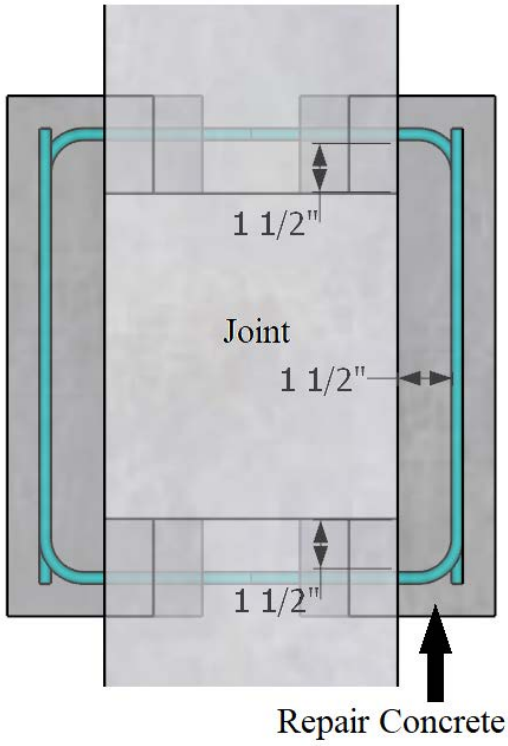

Figure 5-3:Top View of Repair Reinforcement Design

As per ACI 25.4.3.2 (2014), the repair reinforcement hooks were spaced to allow at least 2.5” of side cover (normal to the plane of hooks). The cover beyond the hooks (horizontal distance parallel to the bars) was designed to be 1”, giving the concrete overlay a thickness of 3”. This cover was not intended for kickout of the bars as they were epoxied into the specimen and were designed with durability in mind. The front and 3-dimensional views of the repair reinforcement design are shown in Figure 5-4 and Figure 5-5. Note that the upper repair reinforcing bars are vertically offset ¼” along their longitudinal length to allow for lapping and were installed through the web.

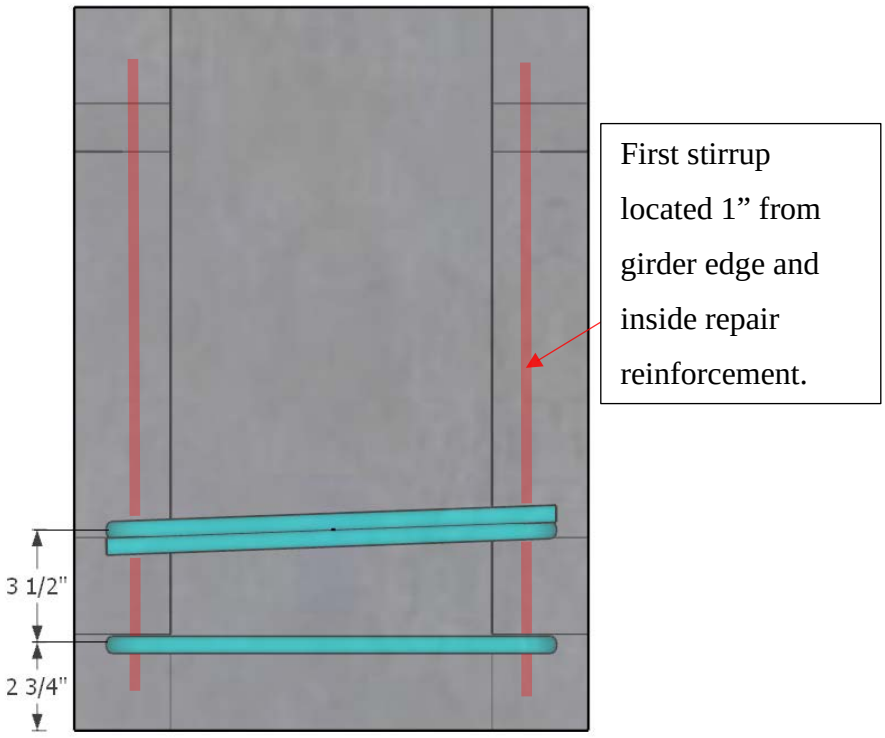

Figure 5-4:Front View of Repair Reinforcement Design

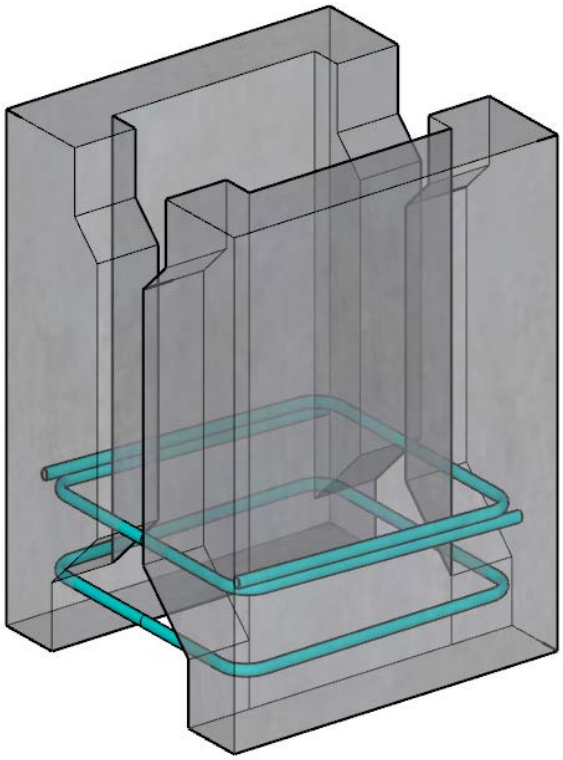

Figure 5-5:3-Dimensional View of Repair Reinforcement Design

5.1.3 Horizontal Shear Design

Horizontal shearing forces between the front face of the continuity joint and repair concrete's interface were considered during the design. A 34-kip design load, obtained from the control specimen data, was used for these calculations. Negative moment bending causes a stress block within the bottom bell of the girder-joint-girder specimen with an area of 21.9 in^2. This stress block was transformed to the cross-sectional area of the repair concrete, requiring a horizontal shearing force of 14.9 kips to maintain equilibrium.

A total of twelve, ¼" x 2 ¾" Tapcon screw anchors were used to transfer this shearing force across the interface between the original girder concrete and the repair concrete. With an embedment length of 1 ½" and concrete compressive strength of 4,000 psi, the total design capacity of the Tapcon screws was rated at 16.6 kips as per the manufacturer's performance tables. Six screw anchors were designed to be installed on each front face of the continuity joint.

5.2 Joint Repair Construction

Repair reinforcement was cut, bent, and placed within the repair specimens in accordance with the design. One strain gauge was placed on one bottom reinforcing bar for each specimen to obtain data during testing. Formwork was fabricated to house the repair joint for casting each of the repair concretes.

5.2.1 Joint Repair Reinforcement

An injectable adhesive anchor, Hilti HIT-HY 200-R, was used to install the repair reinforcement. As per the Hilti Product Technical Guide, 5/8" holes were drilled through the vertical face of the bottom bell and the web of each specimen. To aid in the process of drilling out the 9" long hole in the bottom bell, a 5" long bit was used to bore from both sides. The allowed for better alignment of the overall void and quicker turnaround. The 5/8" hole in the web was drilled with ease using the same bit. The centerline of each hole was drilled 1.75" longitudinally from the side faces of the joint. This dimension allowed clearance from any vertical stirrup placed within the original specimen. A visual representation of the location of these holes is shown in Figure 5-6 and Figure 5-7.

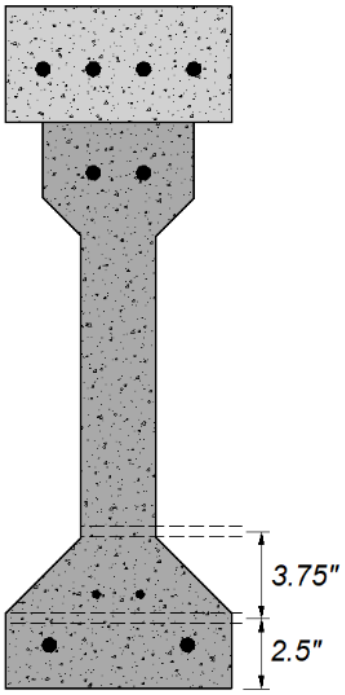

Figure 5-6:Vertical Location of Drilled Holes for Repair Reinforcement

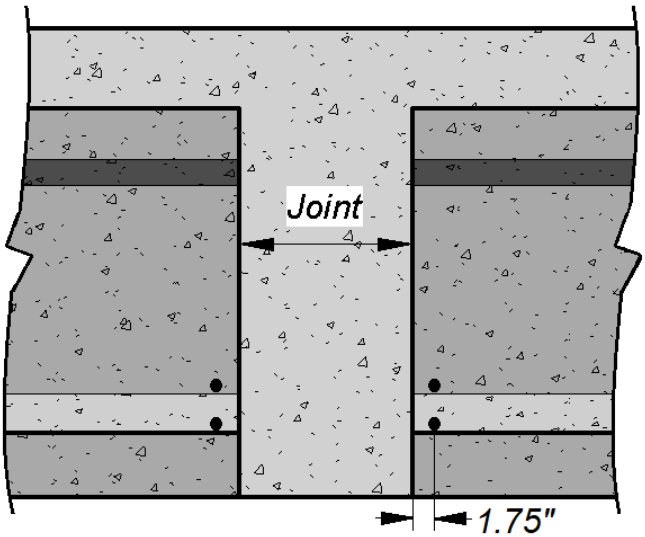

Figure 5-7:Horizontal Location of Drilled Holes for Repair Reinforcement

After coring out each hole of the specimens, an air compressor with a blow gun attachment was used to clear out any remaining dust particles left behind. This process helped the injectable adhesive adhere to the inside surfaces of the concrete holes.

No. 4 bars were installed as designed. Approximately 1 oz. of adhesive was used in each hole to anchor the reinforcement. The top reinforcing bars were tied together and

orientated as horizontally as possible. Each reinforcing bar was left overnight to cure before any additional work on the specimens continued. Figure 5-8 shows the installation of the repair reinforcement.

Figure 5-8:Installation of Repair Reinforcement

A diamond grinding wheel was used with an angle grinder to roughen the repair surface. This process was done to increase the interface bond between the repair concretes and the cracked specimens, allowing for shorter lap length the design calculation. After roughening each surface, a water only pressure washer was used to eliminate concrete dust trapped within the concrete pores left by the grinding wheel. Figure 5-9 shows the roughened surface of a girder-joint-girder specimen.

Figure 5-9:Roughened Surface of Areas to Be Repaired

One strain gauge was installed on one bottom repair bar of each specimen using the same procedure as previously stated. To ensure a smooth surface to adhere to, sanding the location of the strain gauge was done after installation. This order of operations allowed any scratches or markings created while installing, tying, grinding, or pressure washing to be removed prior to placing the strain gauges. Figure 5-10 shows the final set up of the repair reinforcement strain gauges.

Figure 5-10:Strain Gauge Installed on Repair Reinforcement

5.2.2 Joint Repair Formwork

Plywood and construction grade lumber was again used to create the formwork for the continuity joint repair. Much like the formwork to create the initial continuity joint, sheets of plywood were cut in the shape of the outer girder profile. The only difference in these shapes were that they extended farther away from the girder and did not include the profile of the deck above. Because these pieces were for reuse and that each girder profile was not exactly the same, silicone was used to fill any gaps between the side formwork and the girder specimens. In addition to the silicone, high-strength adhesive tape was used to hold the side formwork to the web of the specimens. Figure 5-11 shows how the repair formwork mates with the girder profile.

Figure 5-11:Repair Formwork for Side Face

The front face formwork of the repair was built much like the initial continuity joint's formwork. The outer dimensions of this formwork were 18" wide by 22.5" tall. A small cut was made 3" above the bottom of the 2x4 formwork to allow the strain gauge wires to pass through. This passage was also filled with silicone to mitigate any leak of repair concrete.

A sheet of plywood on the floor was once again used for the repair pours. The stop block would not allow movement of the formwork due to head pressure during the pour, and silicone was used between the base and the side pieces. Small wooden wedges were used between the top of the formwork and the bottom of the deck. These helped keep pressure between the formwork and the floor plywood. Figure 5-12 shows the final setup of the joint repair formwork.

Figure 5-12:Repair Joint Formwork Final Setup

5.3 Mixing & Placing Repair Concretes

Each repair concrete was mixed and placed at Fears Lab. Each side of the girder-joint-girder repairs needed 0.77 ft^3 of repair concrete. The repair specimens were poured in groups of three corresponding to the type of concrete used. Five-gallon buckets were used to pour each material into the top of the formwork. Pouring continued until the joint repair concrete had filled to the bottom of the deck. Each concrete flowed very well around the sides of the repair with no vibration needed.

5.3.1 UHPC (J3) Repair Mixing & Placement

The J3 mixture, Table 5-1, was mixed using a spiral blade mixer with the capacity of 21 ft^3. One batch of 5 ft^3 of the J3 mix was enough to fill the repair forms and cylinders for compression testing. The mix began with combining all the dry materials into the mixer. The dry materials were mixed for ten minutes. After the dry mixing, half of the Glenium

7920 was added to the water which was then added to the dry mix slowly over the course of two minutes. The rest of the Glenium 7920 was added directly to the mixer after a period of one minute. As soon as this mixture began to flow, Dramix OL 13/0.2 steel fibers were added and given three minutes to distribute throughout the mixture.

The J3 was transported from the mixer to the three repair specimens using 5-gallon buckets. The team worked quickly to pour the repair concrete into the forms and cylinders for testing. The J3 repair was cured for 7 days before removing the formwork around the continuity joint.

Table 5-1:UHPC (J3) Mixture Proportions

J3:	**Weight/yd^3**	
Type I Cement	1179.6	lb.
GGBFS	589.8	lb.
Silica Fume	196.6	lb.
Steel Fibers	264.5	lb.
Fine Masonry Sand	1966	lb.
Water	393.2	lb.
Glenium 7920	19.5	oz.

5.3.2 FR-SCC Repair Mixing & Placement

The FR-SCC mixture, Table 5-2, was mixed using the same spiral blade mixer as the UHPC. One batch of 5 ft^3 of the FR-SCC mix was enough to fill the repair forms and cylinders for compression testing.

The mix began with combining all the aggregates and half the amount of water and mixing for one minute. The water to cement ratio was 0.562. The air entrainer was poured into the sand prior to combining the aggregates and water. Fly ash, cement, and Komponent were then added immediately following in that order. The Glenium 7920 and the rest of the water were added slowly until desired flow had been met. Once the

mixture was flowable, MasterFiber MAC Matrix macrosynthetic fibers and one dose of citric acid was added to the mix. Additional doses of citric acid were added to the mixer every 15 minutes until casting of the repairs had been completed. These doses were reduced proportionally to the amount of concrete still left in the mixer.

The FR-SCC was transported from the mixer to the three repair specimens using 5-gallon buckets. The team worked quickly to pour the repair concrete into the forms and cylinders for testing. The FR-SCC repair was moist cured with wet burlap for 7 days before removing the formwork around the continuity joint.

Table 5-2:FR-SCC Mixture Proportions

FR-SCC	**Weight/yd^3**	
Type I Cement	412.5	lb.
Fly Ash	225.0	lb.
Komponent	112.5	lb.
Water	249.8	lb.
Coarse Aggregate	1267.6	lb.
Fine Aggregate	1429.0	lb.
Air Entrainer	8.2	oz
Glenium 7920	61.9	oz.
Citric Acid	6.3	oz.
Macrosynthetic Fibers	7.7	lb.

5.3.3 Phoscrete Repair Mixing and Placement

The mixing procedure provided for the proprietary mixture, Phoscrete, was used to prepare the material. The mix ratio, 18.75% wet to dry, had already been established from the manufacturer's kit. The large mixer at Fears Lab was not used for this set of repairs. Because of the fast-setting properties of Phoscrete, roughly 8-minute set time, the

research team decided to mix one 55 lb bag of dry mix and one 10 lb jug of liquid activator individually in 5-gallon buckets. A urethane auger, supplied from the manufacturer, attached to a 10-amp variable speed drill was used during the mixing process.

To begin, the Phoscrete liquid activator was poured into a clean bucket. While mixing with the drill and auger, the dry mix was quickly added to the bucket and was mixed for one minute. Immediately following mixing, the crew lifted the bucket to pour the Phoscrete into the repair specimens' formwork. While some of the research team focused on pouring the already mixed concrete into the repairs, the rest of the team began a new batch in a new bucket immediately. This process continued to repeat itself until all repairs and compression cylinders had been cast.

The Phoscrete expanded slightly while setting up. This was of no concern as the technical data provided by the manufacturer addresses this and it did not affect the outcome of the repairs.

5.3.4 28-Day Repair Concrete Compressive Strengths

Concrete cylinder compression testing was performed in accordance with ASTM C39. Table 5-3 shows the 28-day compressive strengths for each of the repair concretes. Unfortunately, data for only two cylinders of FR-SCC was obtained.

Table 5-3:28-Day Repair Concrete Compressive Strengths

Repair Material	**Compressive Strength (psi)**
UHPC (J3)	19,318
	20,491
	20,907
Average	**20,239**
FR-SCC	6,010
	8,126
Average	**7,068**
Phoscrete	4,483
	4,510
	4,337
Average	**4,443**

6.0 Repaired Girder Testing & Results

Nine repair specimens were tested at Donald G. Fears Structural Engineering Lab at the University of Oklahoma. The first specimen from each repair group, denoted as R1-J3, R1-FRSCC, and R1-PHOS were tested to failure in positive moment bending. The remaining two specimens from each group were tested to failure in negative moment bending. This chapter will address the testing arrangement, testing procedure, and results.

6.1 Negative Moment Testing Arrangement

The arrangement for testing the repair specimens in negative moment bending was identical to the setup and procedure specified in Section 4.1, Specimen Testing Arrangement & Procedure. As with the control group, each repair specimen tested in negative moment bending was flipped upside down using the overhead crane prior to placement beneath the loading frame. Two wire pots were used for all repair specimen testing. Inputs to the data acquisition system included two strain gauges from the deck reinforcement, one strain gauge from the repair reinforcement, two wire pots used for deflection, and the load cell.

6.2 Ultra-High-Performance Concrete Repair Testing & Results

6.2.1 R1-J3 Repair Results

R1-J3 was tested to failure in positive moment bending. Shear cracking and flexural cracking were observed during testing on the girder webs and either sides of the of the repaired continuity joint, respectively, and are shown in Figure 6-1.

Figure 6-1:R1-J3 Shear & Flexural Cracking

There were no noticeable cracks on the longitudinal face of either side of the repair joint. Small surface cracks were observed on the transverse faces of the joint. Large cracks at the girder-joint interfaces continued to widen for the duration of the testing process. These cracks are shown in Figure 6-2 and Figure 6-3.

Figure 6-2:R1-J3 Girder-Joint Interface Crack (Right)

Figure 6-3:R1-J3 Girder-Joint Interface Crack (Left)

Crushing of the deck was observed in the compression zone on either side of the steel loading plate and is shown in Figure 6-4. This is common for a flexural failure after significant yielding of the flexural reinforcement and resulting strains. Figure 6-5 shows the overall girder-joint-girder repair specimen after testing. Note the failed specimen appears to consist of three separate members – each half girder and the continuity joint.

Figure 6-4:R1-J3 Deck Crushing

Figure 6-5:Deflected Shape of R1-J3

Specimen R1-J3 showed a ductile behavior after 23,466 lb were applied, and had an ultimate load capacity of 34,785 lb. At the ultimate load, R1-J3 deflected an average of 3.73”. Figure 6-6 shows the load-deflection curve of R1-J3, which is very typical for a beam flexural failure.

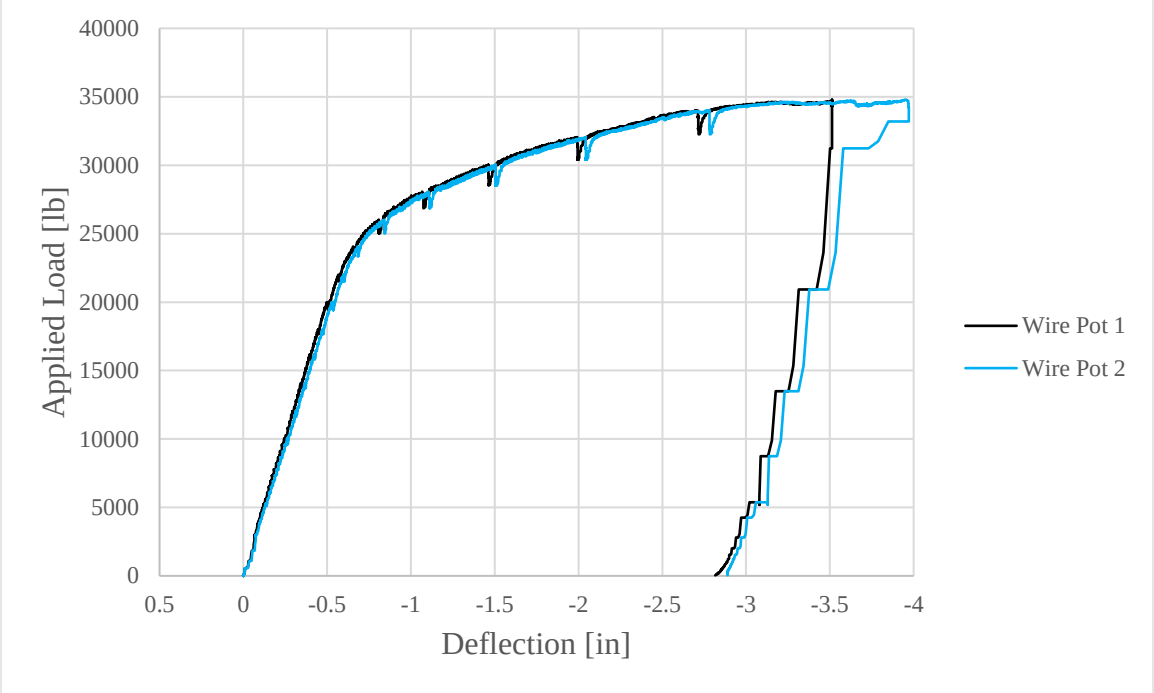

Figure 6-6:R1-J3 Load-Deflection Curve

The repair reinforcement bars had negligible strain under loading with a maximum value of 2.2E-05 in/in. This may be due to the original hooked longitudinal reinforcement still taking significant load. The inner and outer deck reinforcement had maximum compression strains of -0.00032 in/in and -0.00025 in/in, respectively. After this point, both bars began to decompress and eventually go into tension as the load increased. A possible reason for this may be due to the compression zone of the girder-joint-girder specimen rising above the deck reinforcement as loading increased beyond the linear-elastic range. Load-strain curve for R1-J3’s steel reinforcement is shown in Figure 6-7.

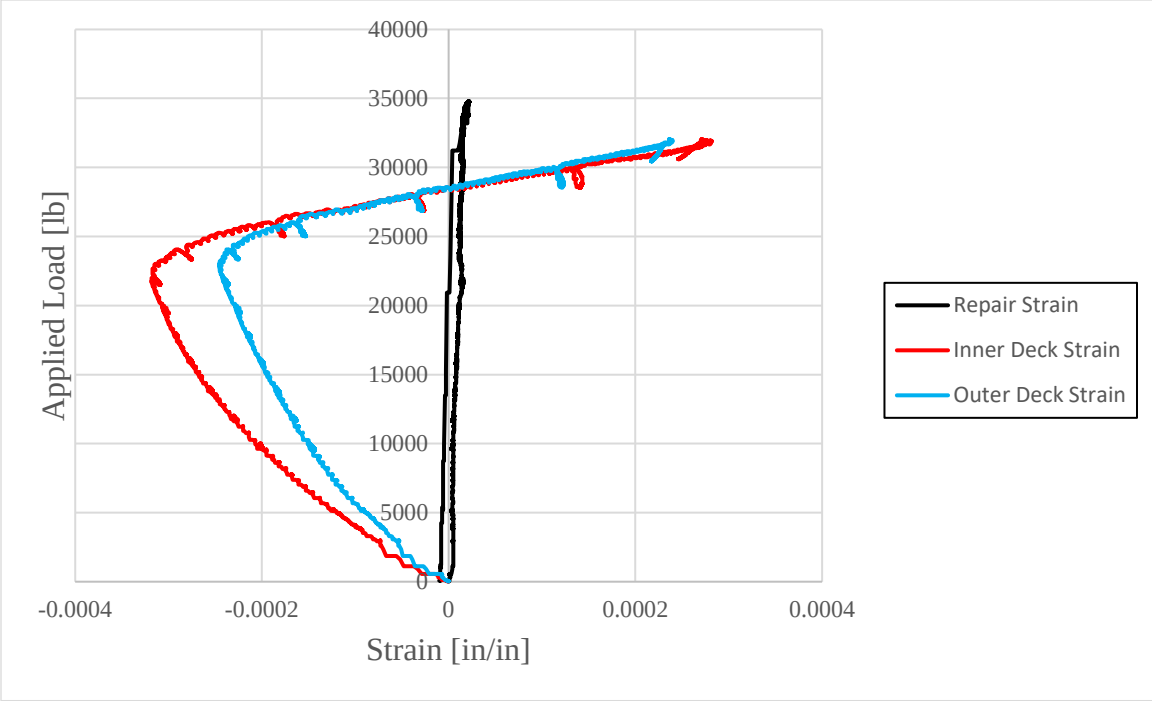

Figure 6-7:R1-J3 Load-Strain Curves

The load-strain curves have been truncated for ease of the reader's interpretation. The complete set of load-strain curves can be found in the Appendix.

6.2.2 R2-J3 Repair Results

R2-J3 was tested to failure in negative moment bending. Shear cracking and flexural cracking were observed during testing on the girder webs and either sides of the of the repaired continuity joint, respectively, and are shown in Figure 6-8.

Figure 6-8:R2-J3 Shear & Flexural Cracking

Small surface cracks were observed on the transverse faces of the joint. Large cracks at the girder-joint interfaces continued to widen for the duration of the testing process. These cracks are shown in Figure 6-9, Figure 6-10, and Figure 6-11. Significant flexural cracks within the deck are shown in Figure 6-9 and Figure 6-11.

Figure 6-9:R2-J3 Girder-Joint Interface Cracking (Front Left)

Figure 6-10:R2-J3 Girder-Joint Interface Cracking (Front Right)

Figure 6-11:R2-J3 Girder-Joint Interface Cracking (Back Right)

Shown in Figure 6-12, no noticeable cracks on the longitudinal face of either side of the repair joint were found.

Figure 6-12:R2-J3 Continuity Joint Repair After Testing

Figure 6-13 shows the overall girder-joint-girder repair specimen after testing.

Figure 6-13:Deflected Shape of R2-J3

Specimen R2-J3 showed a ductile behavior after 33,426 lb were applied, and had an ultimate load capacity of 46,024 lb. At the ultimate load, R2-J3 deflected an average of 3.65”. Figure 6-14 shows the load-deflection curve of R2-J3, which is very typical of a beam flexural failure.

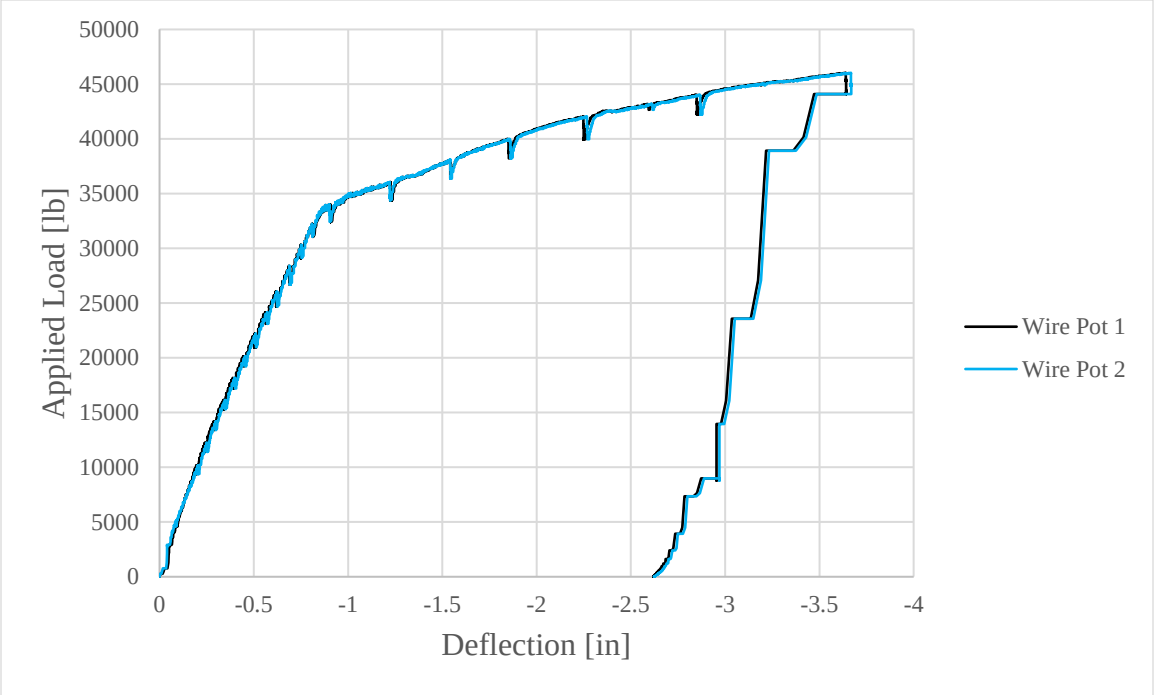

Figure 6-14:R2-J3 Load-Deflection Curve

The outer longitudinal reinforcement in the deck began to yield at a loading of 29,469 lb. Figure 6-15 shows a plot of the load-strain curves of repair specimen R2-J3. The inner reinforcement's strain gauge appears to have lost signal during the loading process. The complete set of load-strain curves can be found in the Appendix.

The repair reinforcement strained in compression until a loading of 36,705 lb, then appears to have gone into tension until ultimate loading.

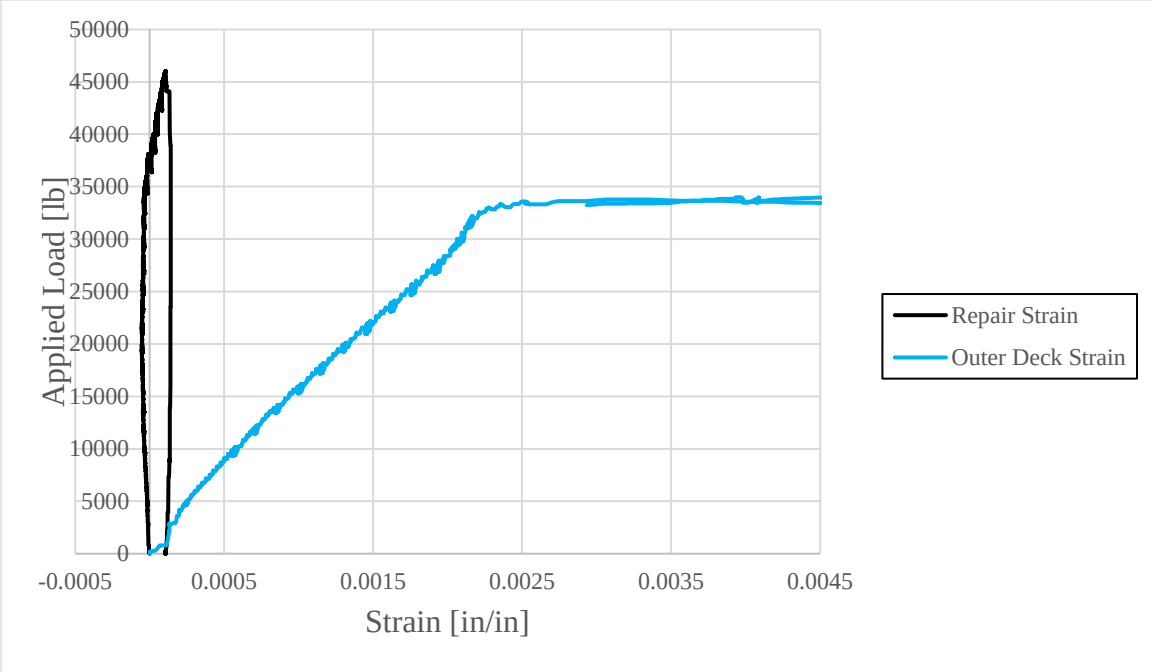

Figure 6-15:R2-J3 Load-Strain Curve

6.2.3 R3-J3 Repair Results

R3-J3 was tested to failure in negative moment bending. Shear cracking and flexural cracking were observed during testing on the girder webs and either sides of the of the repaired continuity joint, respectively, and are shown in Figure 6-16

Figure 6-16:R3-J3 Shear & Flexural Cracking

Small surface cracks were observed on the transverse faces of the joint. Large cracks at the girder-joint interfaces continued to widen for the duration of the testing process.

These cracks are shown in Figure 6-17 and Figure 6-18. Additionally, significant flexural cracks within the deck are shown in Figure 6-19

Figure 6-17:R3-J3 Girder-Joint Interface Cracking (Right)

Figure 6-18:R3-J3 Girder-Joint Interface Cracking

Figure 6-19:R3-J3 Continuity Joint Repair After Testing

No noticeable cracks on the longitudinal face of either side of the repair joint were found. Figure 6-20 shows the overall girder-joint-girder repair specimen after testing.

Figure 6-20:Deflected Shape of R3-J3

Specimen R3-J3 showed a ductile behavior after 33,446 lb were applied, and had an ultimate load capacity of 46,001 lb. At the ultimate load, R3-J3 deflected an average of 3.48". Figure 6-21 shows the load-deflection curve of R3-J3, which is very typical of a beam flexural failure.

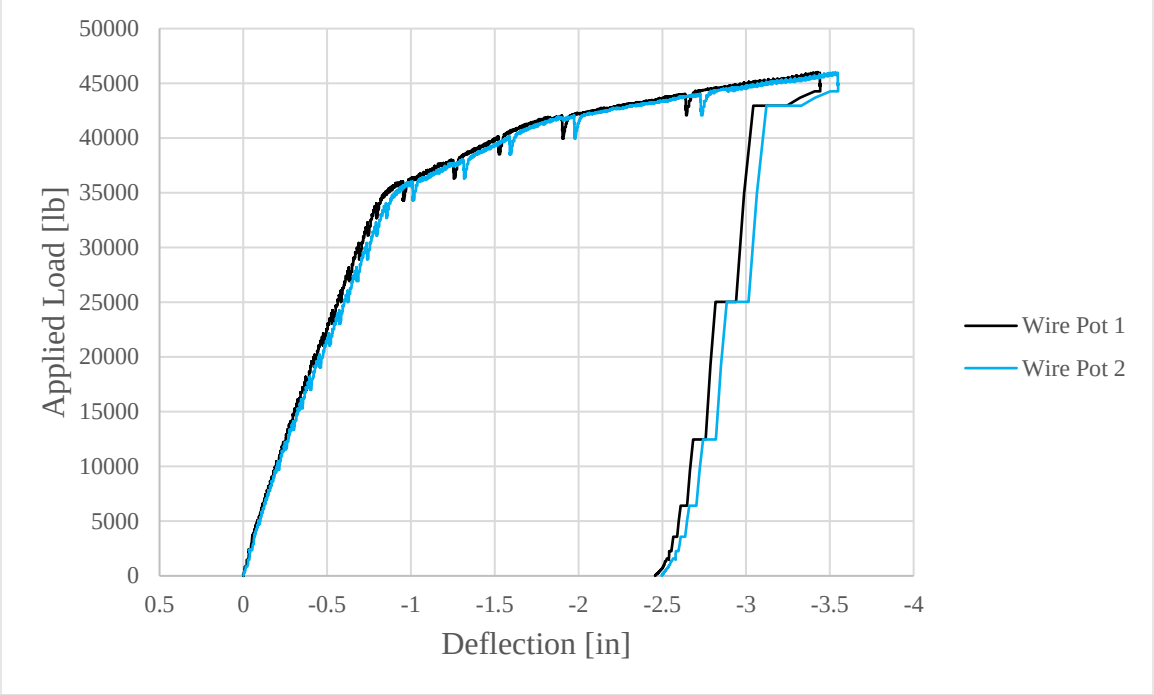

Figure 6-21:R3-J3 Load-Deflection Curve

The outer longitudinal reinforcement in the deck began to yield at a loading of 31,104 lb. Figure 6-22 shows a plot of the load-strain curves of repair specimen R3-J3. The inner reinforcement's strain gauge appears to have lost signal during the loading process. The complete set of load-strain curves can be found in the Appendix.

The repair reinforcement strained in compression until a loading of 43,935 lb, then appears to have gone into tension until ultimate loading.

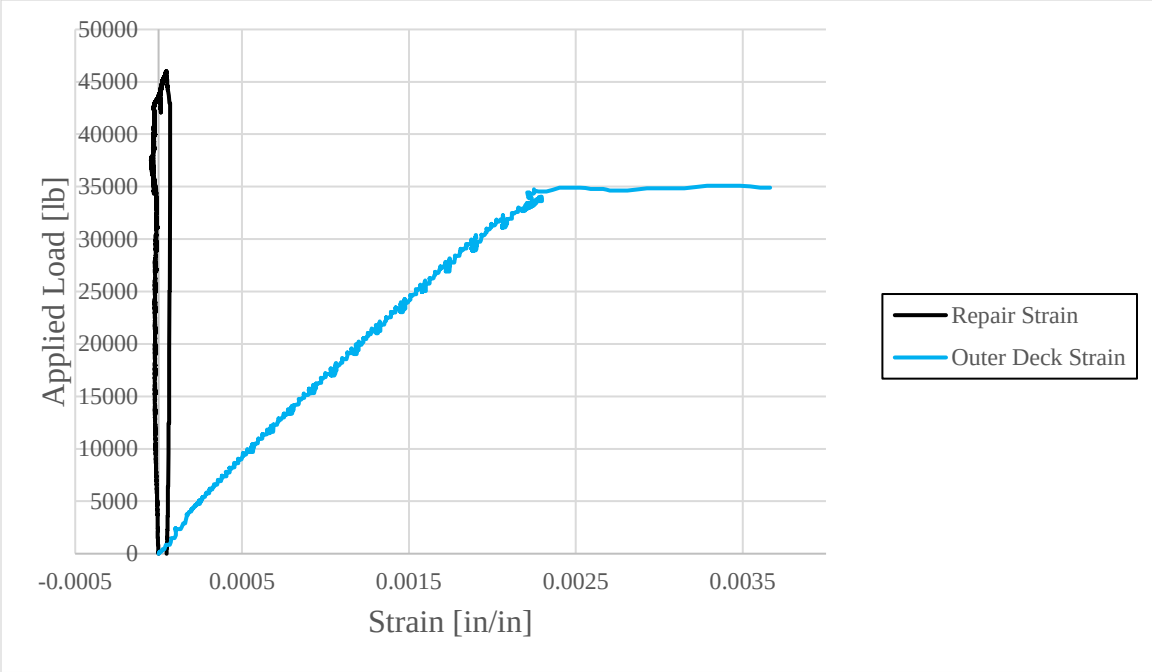

Figure 6-22:R3-J3 Load-Strain Curve

6.3 Fiber Reinforced Self Consolidating Concrete Repair Testing & Results

6.3.1 R1-FRSCC Repair Results

R1-FRSCC was tested to failure in positive moment bending. Shear cracking and flexural cracking were observed during testing on the girder webs and either sides of the of the repaired continuity joint, respectively, and are shown in Figure 6-23.

Figure 6-23:R1-FRSCC Shear & Flexural Cracking

There were no noticeable cracks on the longitudinal face of either side of the repair joint. Flexural cracks were observed on the transverse faces of the joint and at the girder-joint interface. These cracks are shown in Figure 6-24, Figure 6-25, and Figure 6-26

Figure 6-24:R1-FRSCC Joint Transverse Face Cracking (Back Right)

Figure 6-25:R1-FRSCC Girder-Joint Interface Cracking (Front Right)

Figure 6-26:R1-FRSCC Girder-Joint Interface Cracking (Front Left)

Flexural cracks from Figure 6-24 extended through the entire girder-joint-girder specimen and is explicitly shown in Figure 6-27.

Figure 6-27:R1-FRSCC Flexural Cracking Through Entire Specimen

Figure 6-28 shows the overall girder-joint-girder repair specimen after testing. Note the failed specimen appears to consist of three separate members – each half girder and the continuity joint.

Figure 6-28:Deflected Shape of R1-FRSCC

Specimen R1-FRSCC showed a ductile behavior after 25,606 lb were applied, and had an ultimate load capacity of 32,889 lb. At the ultimate load, R1-FRSCC deflected an average of 2.48”. Figure 6-29 shows the load-deflection curve of R1-FRSCC, which is very typical of a beam flexural failure.

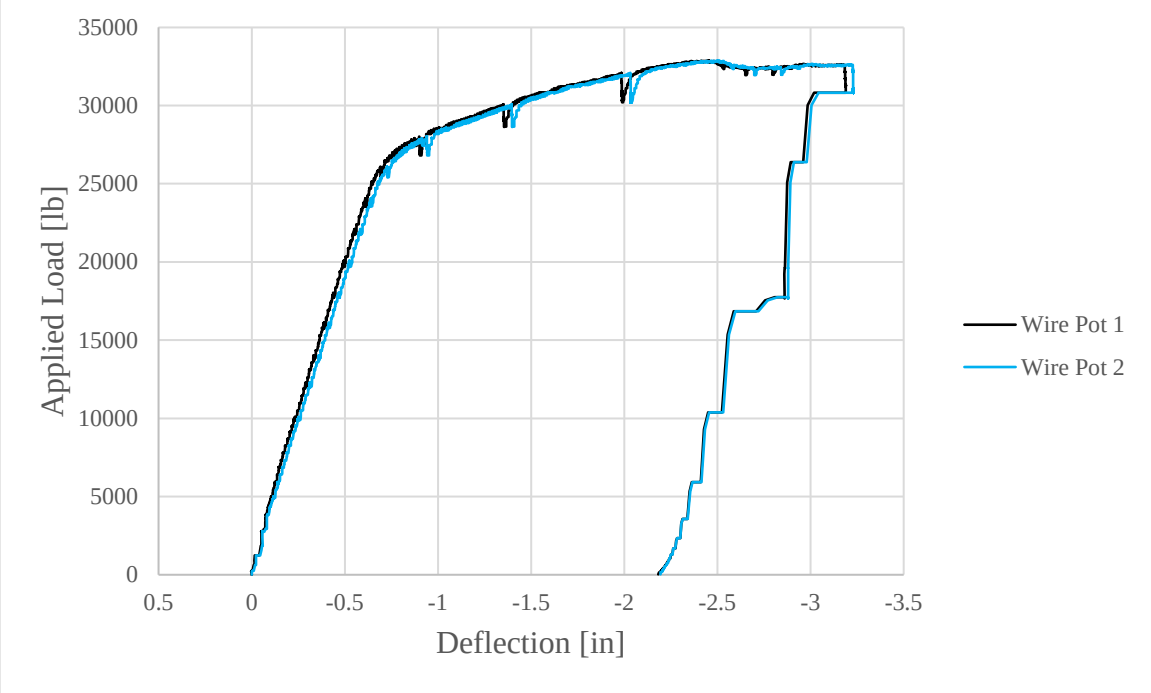

Figure 6-29:R1-FRSCC Load-Deflection Curve

The repair reinforcement bars did not yield but did undergo tension strain with a maximum value of 0.00041 in/in. This may be due to the original hooked longitudinal reinforcement still taking significant load. The inner and outer deck reinforcement had maximum compression strains of -0.00021 in/in and -0.00131 in/in, respectively. After this point, both bars began to decompress and eventually go into tension as the load increased. A possible reason for this may be due to the compression zone of the girder-joint-girder specimen rising above the deck reinforcement as loading increased beyond the linear-elastic range. Load-strain curves for R1-FRSCC's steel reinforcement are shown in Figure 6-30.

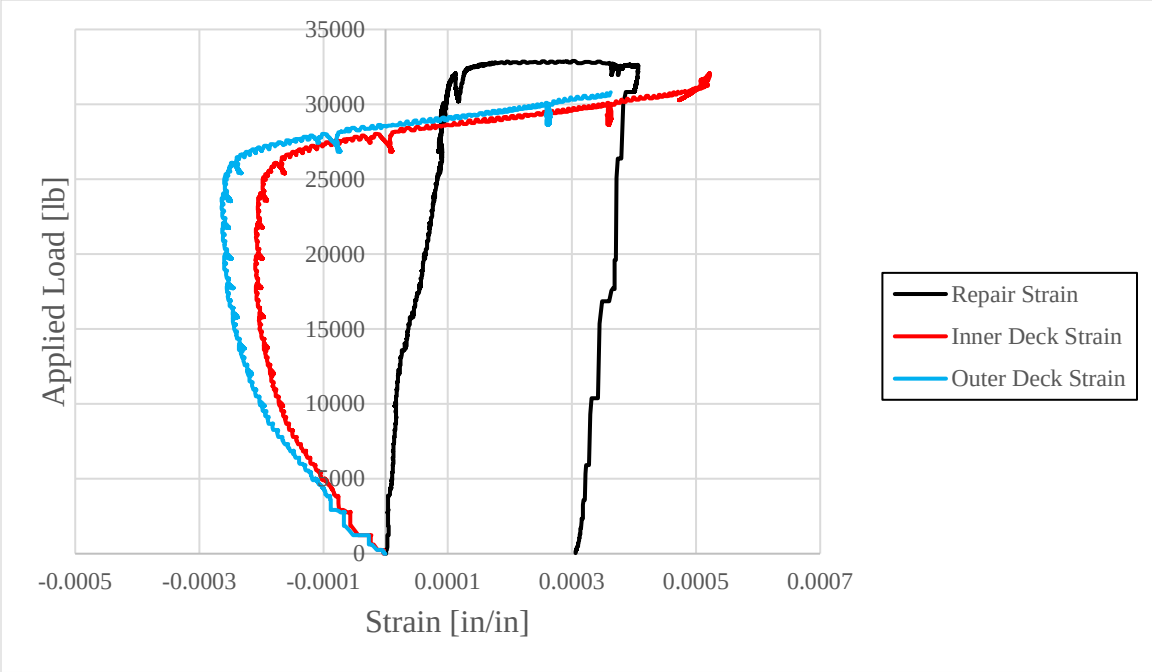

Figure 6-30:R1-FRSCC Load-Strain Curve

The load-strain curves have been truncated for ease of the reader's interpretation. The complete set of load-strain curves can be found in the Appendix.

6.3.2 R2-FRSCC Repair Results

R2-FRSCC was tested to failure in negative moment bending. Shear cracking and flexural cracking were observed during testing on the girder webs and either sides of the of the repaired continuity joint, respectively, and are shown in Figure 6-31.

Figure 6-31:R2-FRSCC Shear & Flexural Cracking

Significant flexural cracking was observed on all four transverse faces of the continuity joint. These cracks also extended onto the longitudinal faces of the continuity joint and can be seen in Figure 6-32, Figure 6-33, Figure 6-34, and Figure 6-35. Note that additional longitudinal face cracks and a substantial amount of flexural cracking within the deck can also be seen.

Figure 6-32:R2-FRSCC Joint Cracking, Longitudinal & Transverse Faces (Front Left)

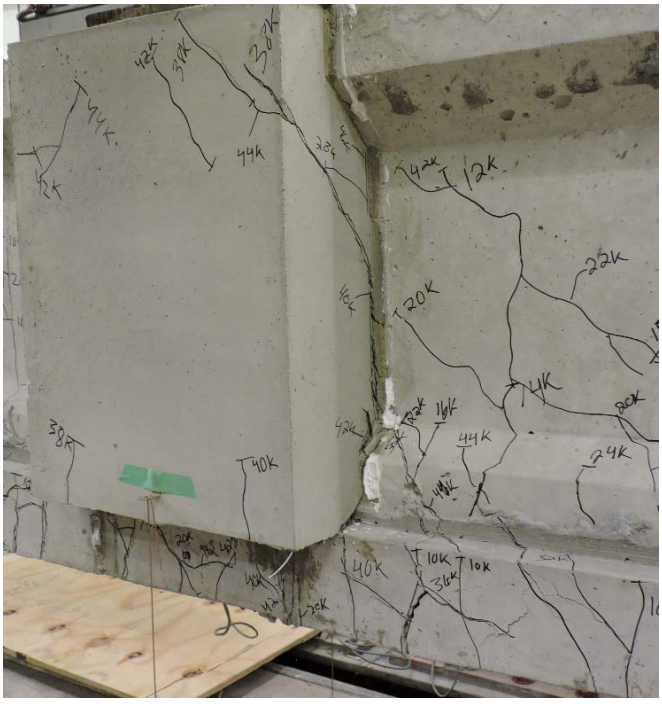

Figure 6-33:R2-FRSCC Joint Cracking, Longitudinal & Transverse Faces (Front Left)

Figure 6-34:R2-FRSCC Joint Cracking, Longitudinal & Transverse Faces (Back Left)

Figure 6-35:R2-FRSCC Joint Cracking, Longitudinal & Transverse Faces (Back Right)

Figure 6-36 shows the overall girder-joint-girder repair specimen after testing.

Figure 6-36:Deflected Shape of R2-FRSCC

Specimen R2-FRSCC showed a ductile behavior after 33,393 lb were applied, and had an ultimate load capacity of 46,006 lb. At the ultimate load, R2-FRSCC deflected an average of 2.75". Figure 6-37 shows the load-deflection curve of R2-FRSCC, which is very typical of a beam flexural failure.

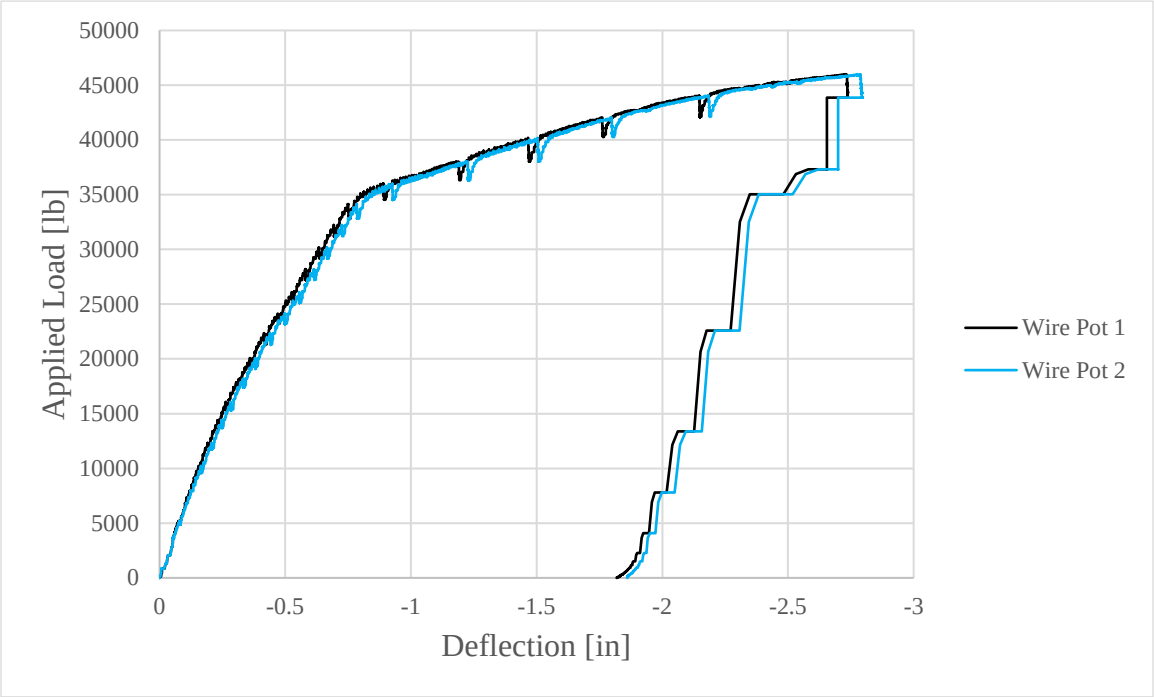

Figure 6-37:R2-FRSCC Load-Deflection Curve

The repair reinforcement underwent compression strain and had a maximum strain of -0.000107 in/in. The outer longitudinal reinforcement in the deck began to yield at a loading of 29,340 lb. The inner longitudinal reinforcement in the deck began to yield at a loading of 29,552 lb. Figure 6-38 shows a plot of the load-strain curves of repair specimen R2-FRSCC. The load-strain curves have been truncated for ease of the reader's interpretation. The complete set of load-deflection curves can be found in the Appendix.

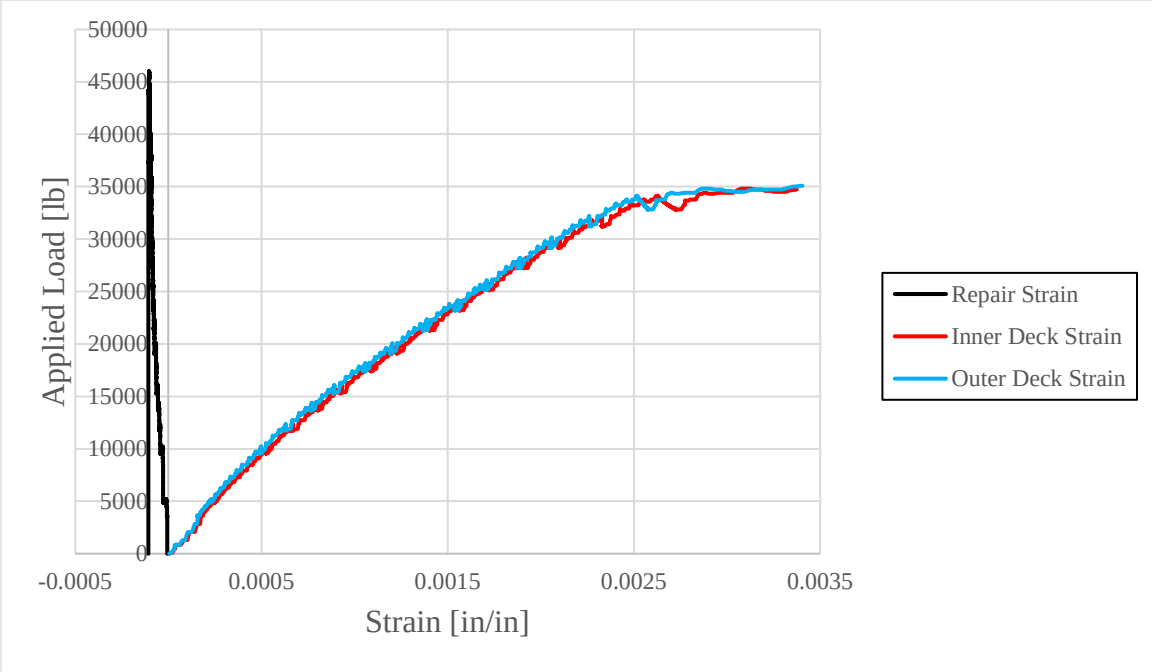

Figure 6-38:R2-FRSCC Load-Strain Curve

6.3.3 R3-FRSCC Repair Results

R3-FRSCC was tested to failure in negative moment bending. Shear cracking and flexural cracking were observed during testing on the girder webs and either sides of the of the repaired continuity joint, respectively, and are shown in Figure 6-39.

Figure 6-39:R3-FRSCC Shear & Flexural Cracking

Significant flexural cracking was observed on all four transverse faces of the continuity joint. These cracks also extended onto the longitudinal faces of the continuity joint and can be seen in Figure 6-40, Figure 6-41, and Figure 6-42. Note that additional

longitudinal face cracks and a substantial amount of flexural cracking within the deck can also be seen.

Figure 6-40:R3-FRSCC Joint Cracking, Longitudinal & Transverse Faces (Front Left)

Figure 6-41:R3-FRSCC Joint Cracking, Longitudinal & Transverse Faces (Front Right)

Figure 6-42:R3-FRSCC Joint Cracking, Longitudinal & Transverse Faces (Back Left)

A considerable crack formed within the deck, just outside of the continuity joint, and continuously widened throughout the loading process. This crack propagated upward and into the joint which can be seen in Figure 6-43.

Figure 6-43:R3-FRSCC Deck Cracking

Unfortunately, a photograph of the girder-joint-girder repair specimen's deflected shape after testing was not taken.

Specimen R3-FRSCC showed a ductile behavior after 34,698 lb were applied, and had an ultimate load capacity of 46,008 lb. At the ultimate load, R3-FRSCC deflected an average of 2.81". Figure 6-44 shows the load-deflection curve of R3-FRSCC, which is very typical of a beam flexural failure.

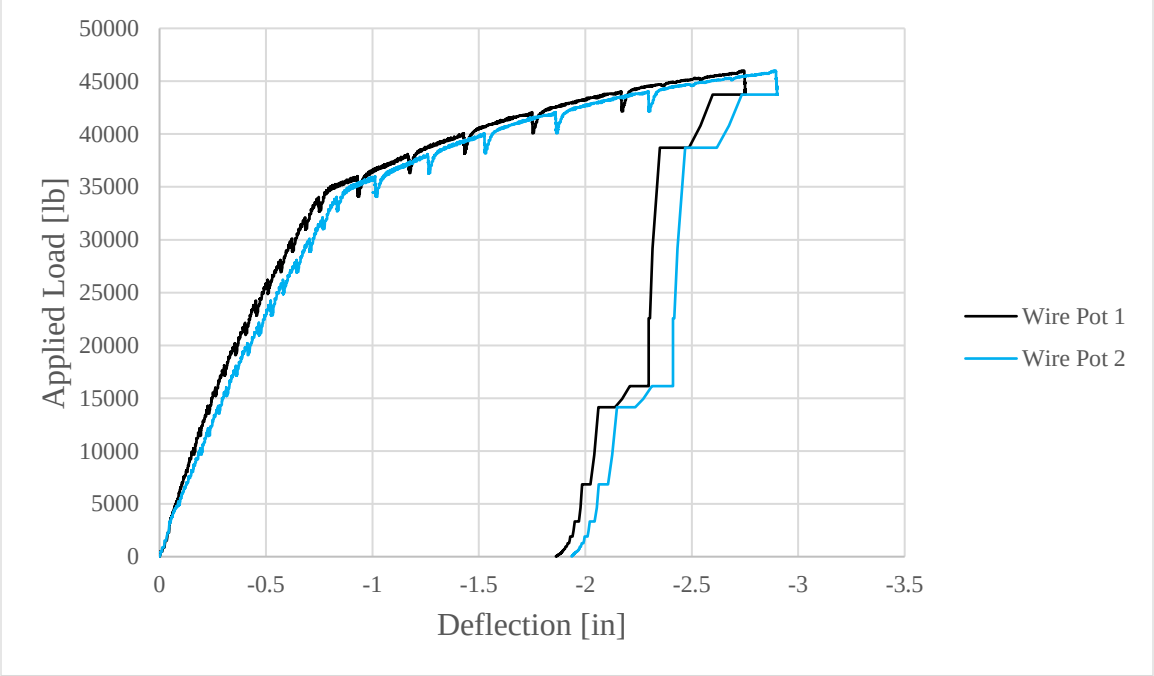

Figure 6-44:R3-FRSCC Load-Deflection Curve

The outer longitudinal reinforcement in the deck began to yield at a loading of 28,295 lb. The inner longitudinal reinforcement in the deck began to yield at a loading of 28,711 lb. The repair reinforcement did not yield and had a maximum compression strain of -0.000101 in/in. At 31,668 lb, the repair reinforcement went into tension. A possible reason for this may be due to the compression zone of the girder-joint-girder specimen rising above the repair reinforcement as loading increased beyond the linear-elastic range.

Figure 6-45 shows a plot of the load-strain curves of repair specimen R3-FRSCC. The load-strain curves have been truncated for ease of the reader's interpretation. The complete set of load-strain curves can be found in the Appendix.

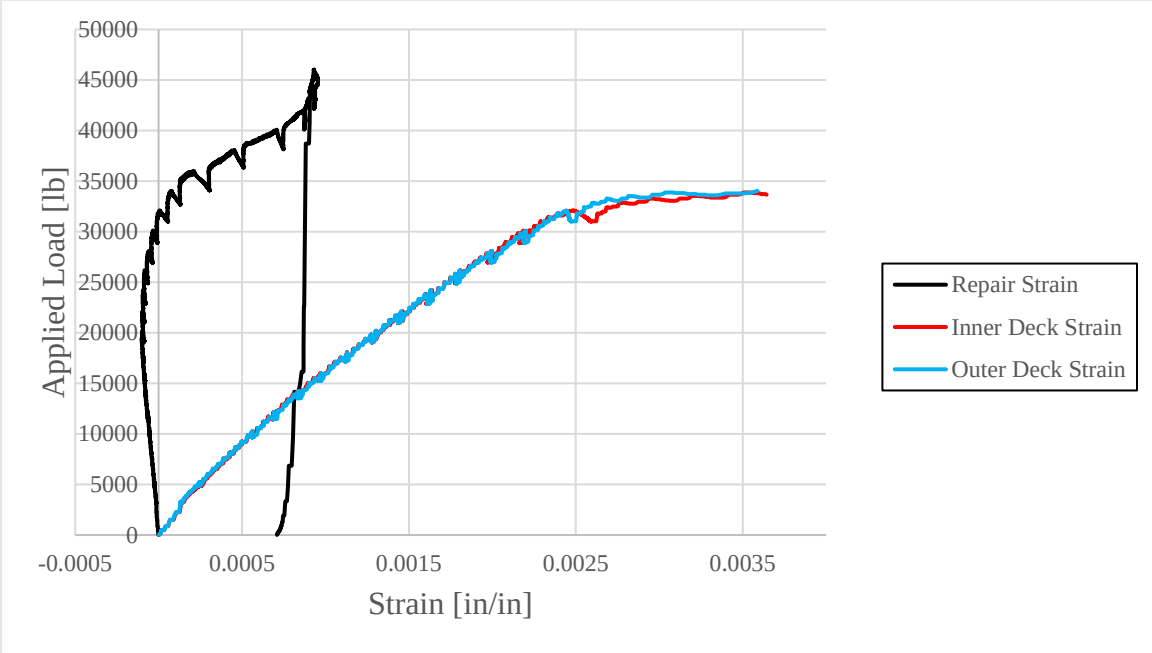

Figure 6-45:R3-FRSCC Load-Strain Curve

6.4 Phoscrete Repair Testing & Results

6.4.1 R1-PHOS Repair Results

R1-PHOS was tested to failure in positive moment bending. Shear cracking and flexural cracking were observed during testing on the girder webs and either sides of the of the repaired continuity joint, respectively, and are shown in Figure 6-46.

Figure 6-46:R1-PHOS Shear & Flexural Cracking

There were no noticeable cracks on the longitudinal face of either side of the repair joint. Flexural cracking was observed on all four transverse faces of the continuity joint. None of these cracks appeared to have extended onto the longitudinal faces of the continuity joint as shown in Figure 6-47, Figure 6-48, Figure 6-49, and Figure 6-50.

Figure 6-47:R1-PHOS Girder-Joint Interface & Joint Transverse Face Cracking (Front Left)

Figure 6-48:R1-PHOS Girder-Joint Interface & Joint Transverse Face Cracking (Front Right)

Figure 6-49:R1-PHOS Girder-Joint Interface & Joint Transverse Face Cracking (Back Left)

Figure 6-50:R1-PHOS Girder-Joint Interface & Joint Transverse Face Cracking (Back Right)

Significant cracking within the bottom bell of the girder-joint-girder specimen was observed at the location of the continuity joint. The two original half-girder specimens separated away from the joint under loading. The bottom of the original and repaired continuity joint is shown in Figure 6-51.

Figure 6-51:R1-PHOS Girder-Joint Separation

Figure 6-52 shows the overall girder-joint-girder repair specimen after testing. Note the failed specimen appears to consist of three separate members – each half girder and the continuity joint.

Figure 6-52:Deflected Shape of R1-PHOS

Specimen R1-PHOS showed a ductile behavior after 17,226 lb were applied, and had an ultimate load capacity of 23,421 lb. At the ultimate load, R1-PHOS deflected an average of 1.70”. Figure 6-53 shows the load-deflection curve of R1-PHOS, which is fairly typical of a beam flexural failure although the plateau is not as flat as normally observed. This may be due to bond or slip failure within the joint.

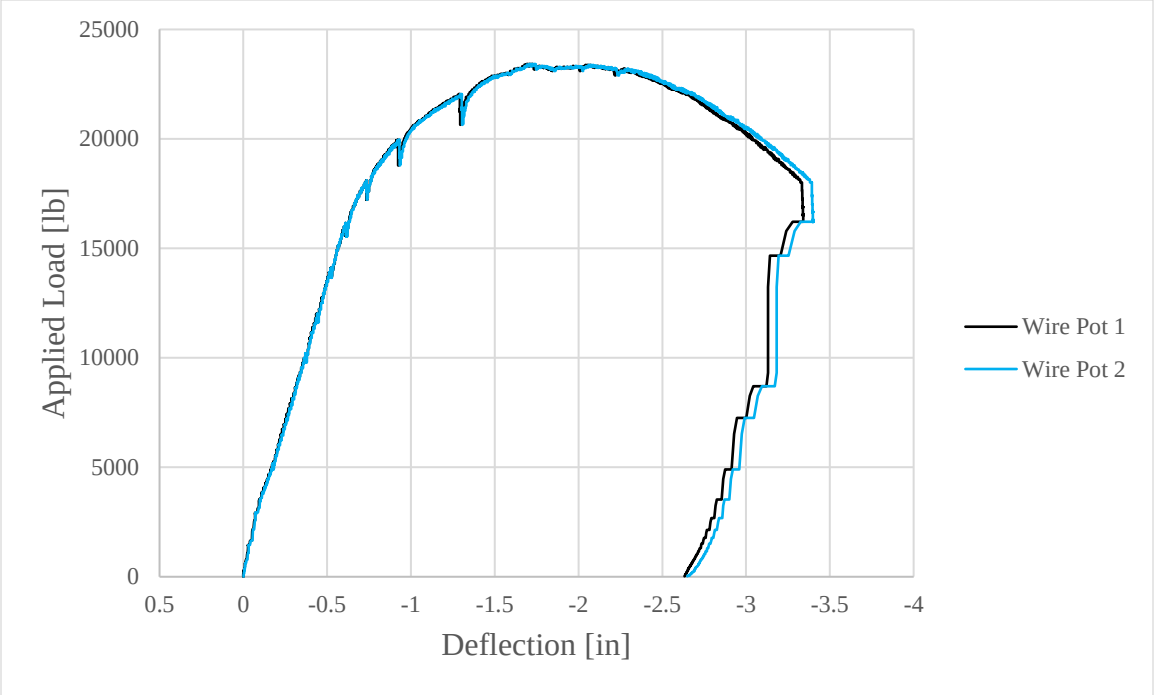

Figure 6-53:R1-PHOS Load-Deflection Curve

The repair reinforcement bars had minimal strain under loading with a maximum value of 0.000999 in/in. This may be due to the original hooked longitudinal reinforcement still taking significant load. The inner and outer deck reinforcement initially underwent compression strain. After roughly 13,915 lb were loaded, both bars went into tension and continued to strain as the load increased. The outer deck reinforcement yielded in tension at a loading of 19,982 lb. The inner deck reinforcement yielded in tension at a loading of 19,854 lb. Both the inner and outer deck reinforcement yielded after the ultimate load was achieved and while the girder-joint-girder was allowed to deflect with additional load applied. A possible reason for the bars yielding in tension may be due to the compression zone of the girder-joint-girder specimen rising above the deck reinforcement as loading increased beyond the linear-elastic range. Load-strain curves for R1-PHOS's steel reinforcement is shown in Figure 6-54.

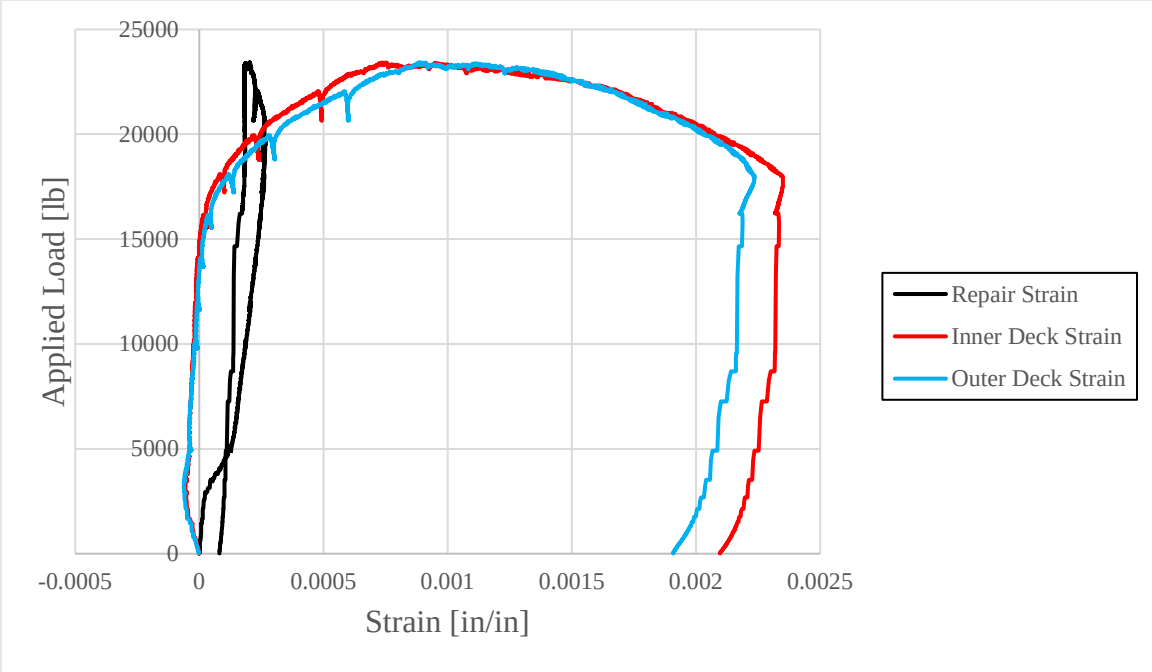

Figure 6-54:R1-PHOS Load-Strain Curve

6.4.2 R2-PHOS Repair Results

R2-PHOS was tested to failure in negative moment bending. Shear cracking and flexural cracking were observed during testing on the girder webs and either sides of the repaired continuity joint, respectively, and are shown in Figure 6-55.

Figure 6-55:R2-PHOS Shear & Flexural Cracking

Flexural cracking was observed on all four transverse faces of the continuity joint. Many of these cracks also extended onto the longitudinal faces of the continuity joint and can be seen in Figure 6-56, Figure 6-57, and Figure 6-58. Note that additional longitudinal face cracks can also be seen.

Figure 6-56:R2-PHOS Joint Cracking, Longitudinal and Transverse Faces (Front Left)

Figure 6-57:R2-PHOS Joint Cracking, Longitudinal and Transverse Faces (Front Right)

Figure 6-58:R2-PHOS Joint Cracking, Longitudinal and Transverse Faces (Back Right)

Flexural cracking extending across the deck is shown in Figure 6-59.

Figure 6-59:R2-PHOS Deck Cracking

Figure 6-60 shows the overall girder-joint-girder repair specimen after testing.

Figure 6-60:Deflected Shape of R2-PHOS

Specimen R2-PHOS showed a ductile behavior after 32,507 lb were applied, and had an ultimate load capacity of 46,037 lb. At the ultimate load, R2-PHOS deflected an average of 2.80". Figure 6-61 shows the load-deflection curve of R2-PHOS, which is very typical of a beam flexural failure.

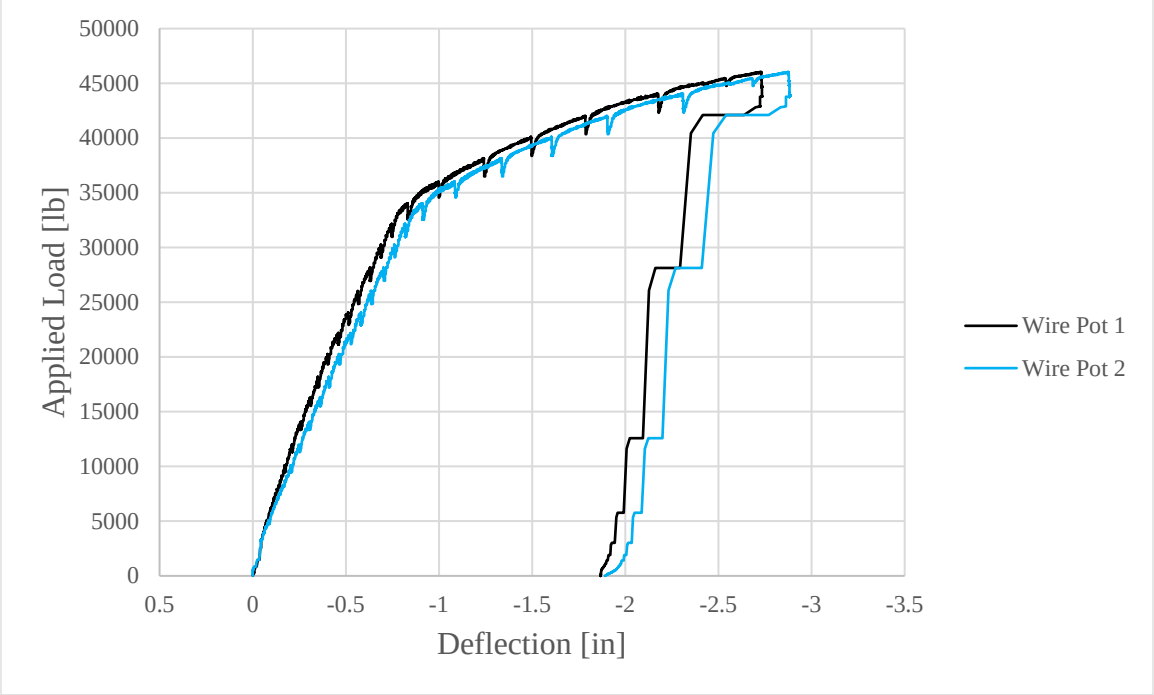

Figure 6-61:R2-PHOS Load-Deflection Curve

Specimen R2-PHOS's inner longitudinal reinforcement in the deck began to yield at a loading of 27,778 lb. The outer deck reinforcement lost signal during the loading process. The repair reinforcement strained in compression until a loading of 33,847 lb. At this loading, the repair bars began tension straining until the ultimate load was achieved. A possible reason for this may be due to the compression zone of the girder-joint-girder specimen rising above the repair reinforcement as loading increased beyond the linear-elastic range.

Figure 6-62 shows a plot of the load-strain curves of repair specimen R2-PHOS. The load-strain curves have been truncated for ease of the reader's interpretation. The complete set of load-strain curves can be found in the Appendix.

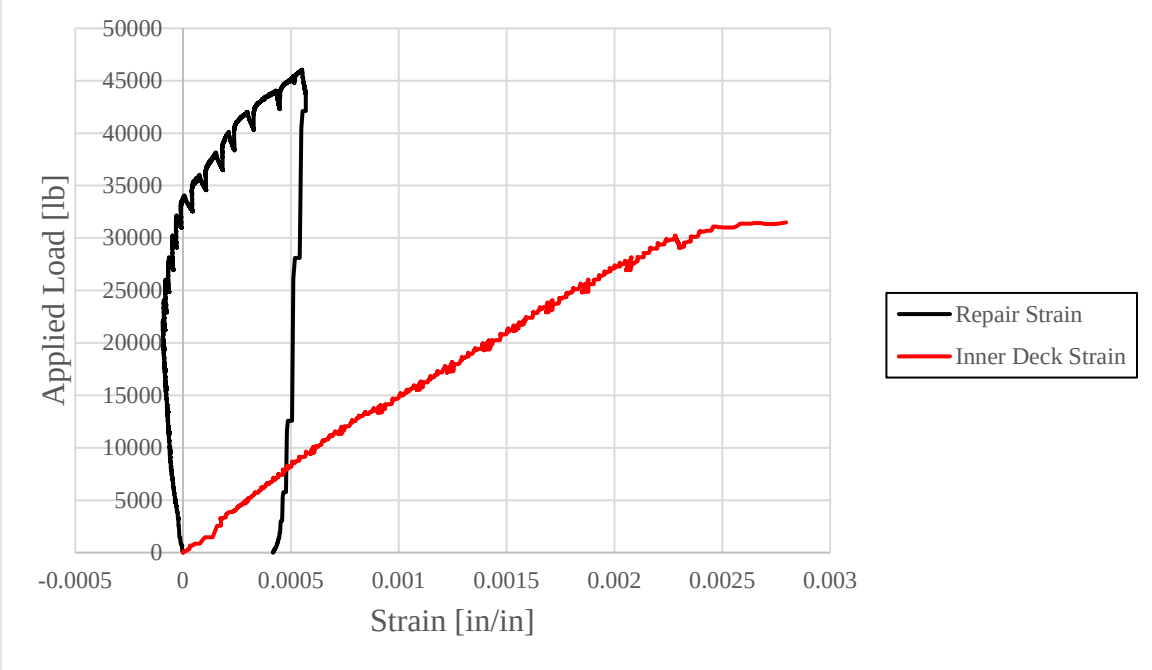

Figure 6-62:R2-PHOS Load-Strain Curve

6.4.3 R3-PHOS Repair Results

R3-PHOS was tested to failure in negative moment bending. Shear cracking and flexural cracking were observed during testing on the girder webs and either sides of the repaired continuity joint, respectively, and are shown in Figure 6-63 and Figure 6-64.

Figure 6-63:R3-PHOS Shear & Flexural Cracking (Front Left)

Figure 6-64:R3-PHOS Shear & Flexural Cracking (Front Right)

Limited flexural cracking was observed on the longitudinal and transverse faces of the repaired continuity joint. The only considerable crack at the girder-joint interface is shown in Figure 6-65. This crack initiated at the deck, propagated upward and across the joint's transverse face, and terminated on the longitudinal face of the joint around a loading of 46 kips.

Figure 6-65:R3-PHOS Girder-Joint Interface Cracking (Front Left)

Flexural cracking of the other transverse faces of the joint are shown in Figure 6-66, Figure 6-67, and Figure 6-68.

Figure 6-66:R3-PHOS Joint Transverse Face Cracking (Front Right)

Figure 6-67:R3-PHOS Joint Transverse Face Cracking (Back Left)

Figure 6-68:R3-PHOS Joint Transverse Face Cracking (Back Right)

Flexural cracking extending across the deck is shown in Figure 6-69

Figure 6-69:R3-PHOS Deck Cracking

Figure 6-70 shows the overall girder-joint-girder repair specimen after testing.

Figure 6-70:Deflected Shape of R3-PHOS

Specimen R3-PHOS showed a ductile behavior after 34,742 lb were applied, and had an ultimate load capacity of 46,130 lb. At the ultimate load, R3-PHOS deflected an average of 2.07". Figure 6-71 shows the load-deflection curve of R3-PHOS, which is very typical for a beam flexural failure.

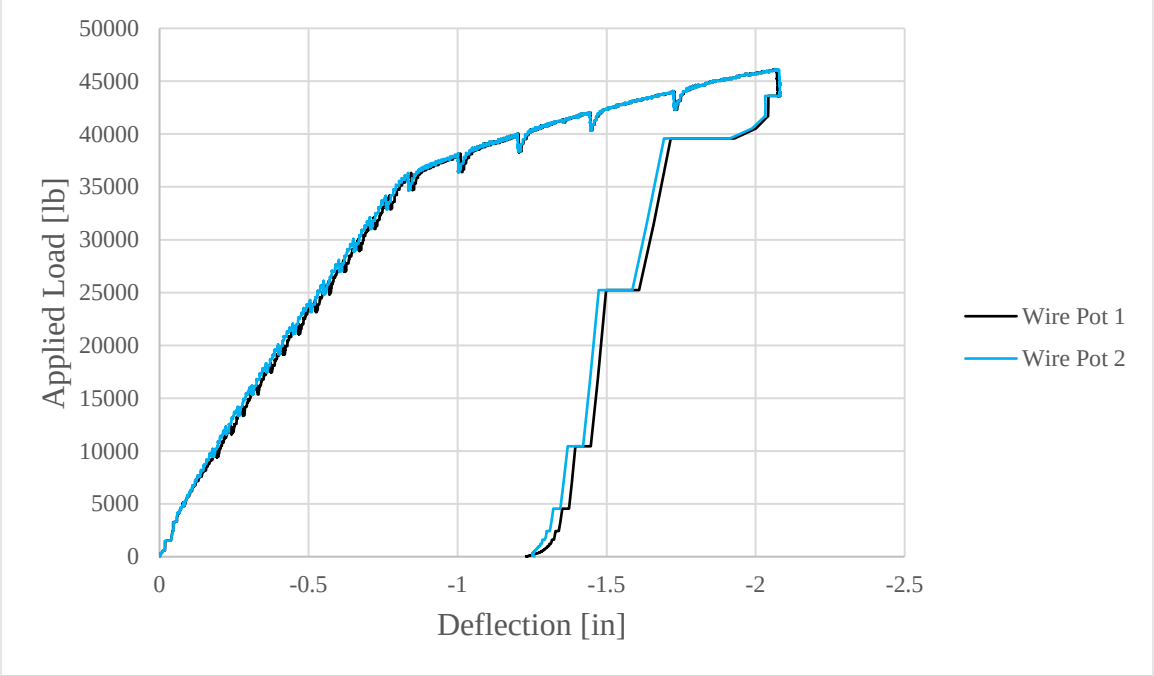

Figure 6-71:R3-PHOS Load-Deflection Curve

Specimen R3-PHOS's inner longitudinal reinforcement in the deck began to yield at a loading of 26,403 lb. The outer deck reinforcement began to yield at a loading of 27,448 lb. The repair reinforcement strained in compression until a loading of 43,178 lb. At this loading, the repair bars began tension straining until the ultimate load was achieved. A possible reason for this may be due to the compression zone of the girder-joint-girder specimen rising above the repair reinforcement as loading increased beyond the linear-elastic range.

Figure 6-72 shows a plot of the load-strain curves of repair specimen R3-PHOS. The load-strain curves have been truncated for ease of the reader's interpretation. The complete set of load-strain curves can be found in the Appendix.

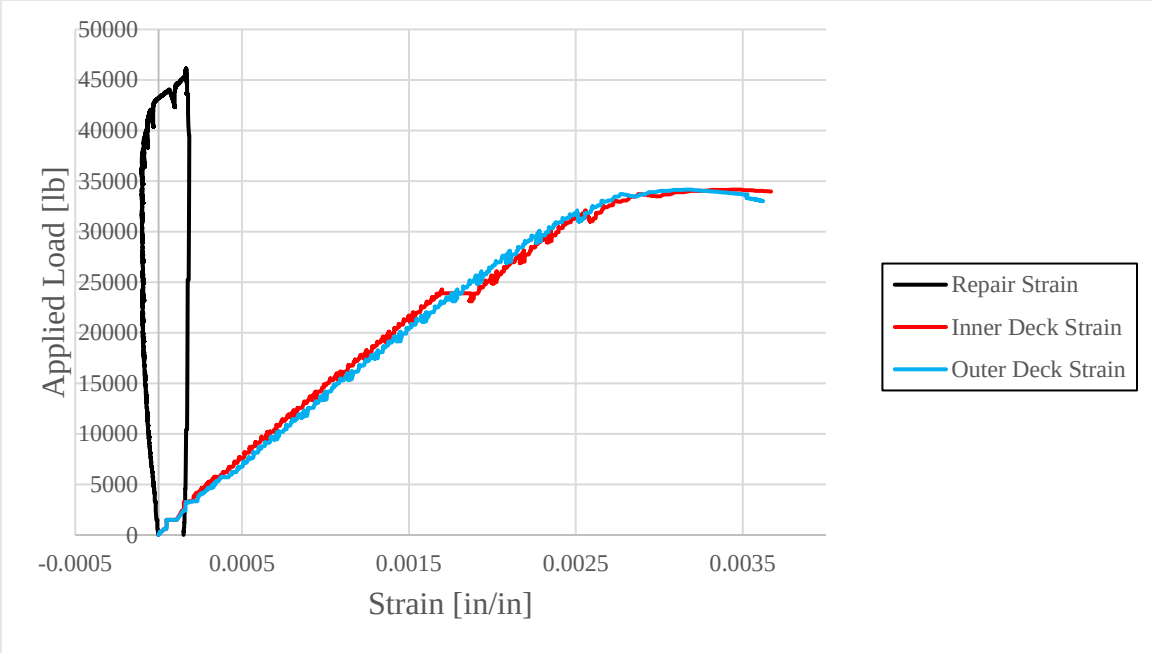

Figure 6-72:R3-PHOS Load-Strain Curve

6.5 Results Summary

Table 6-1 provides a summary of results for the positive moment bending tests.

Table 6-1:Positive Moment Bending Results

Positive Moment Bending Results			
Specimen	Ductile Behavior Load [lb]	Ultimate Load[lb]	Deflection [in]
R1-J3	23,466	34,785	3.73
R1-FRSCC	25,606	32,889	2.48
R1-PHOS	17,226	23,421	1.70

Table 6-2 provides a summary of results for the negative moment bending tests. Because the load cell's capacity was 50 kips, loading was partially stopped at roughly 46 kips.

Table 6-2:Negative Moment Bending Results

Negative Moment Bending Results			
Specimen	Ductile Behavior Load [lb]	Ultimate Load [lb]	Deflection [in]
R2-J3	33,426	46,024	3.65
R3-J3	33,446	46,001	3.48
R2-FRSCC	33,393	46,006	2.75
R3-FRSCC	34,698	46,008	2.81
R2-PHOS	32,507	46,037	2.80
R3-PHOS	34,742	46,130	2.07

7.0 Findings, Conclusions & Recommendations

The primary goal for this study was to establish adequate repair solutions for cracked continuity joints on existing precast, prestressed concrete girder-joint-girder bridges in the state of Oklahoma using three specialized concretes. The following chapter presents the findings, conclusions, and recommendations of this study for the repair of cracked girder-joint-girder bridge continuity joints based on the testing presented in Chapter 4 and Chapter 6.

Over the course of this research, twelve half-scale AASHTO Type II girder specimens were constructed and tested at the University of Oklahoma. Three specimens were tested to flexural failure in negative moment bending which served as the control group. The remaining nine specimens were cracked, repaired, and tested to flexural failure in either positive or negative moment bending. The initial cracking of the repair specimens simulated in situ damage to continuity joints caused by time-dependent effects.

7.1 Findings

7.1.1 Positive Moment Testing of R1-J3, R1-FRSCC, & R1-PHOS

- All positive moment repairs restored full flexural capacity when compared to the theoretical nominal moment strength, 107.6 ft-k.
- The repair reinforcement in specimens R1-J3, R1-FRSCC, and R1-PHOS did not yield under loading of a positive moment flexural failure.
- Deck reinforcement in all positive moment repair specimens initially strained in compression, followed by tension strain.
- Specimen R1-PHOS's deck reinforcement was the only reinforcement to yield, which was in tension.
- No signs of any cracking on the longitudinal faces of the positive moment repair specimens were observed.
- R1-J3 had the least amount of girder-joint interface cracking, while R1-PHOS had the most.
- R1-FRSCC and R1-PHOS both had significant transverse face joint cracking.

- All positive moment repair specimens' deflected shapes appear to consist of three separate segments – each half girder and the continuity joint.

The initial cracking loads and positive moment test results for the repair group are summarized in Table 7-1 and Table 7-2, respectively. All three specimens had an induced moment greater than the theoretical nominal moment capacity during the initial cracking phase. Ultimate flexural capacity for repaired specimens R1-J3 and R1-FRSCC far exceeded both the initial cracking moment and the theoretical moment capacity. Ultimate flexural capacity for repaired specimen R1-PHOS was 93% of its initial cracking moment but still exceeded the theoretical moment capacity. The ductile behavior load was the breaking point where an increase in deflection was observed with little increase in load.

Table 7-1:Initial Cracking Results of Positive Moment Repair Specimens

Initial Cracking Results of Positive Moment Repair Specimens		
Specimen	Load Applied [lb]	Moment [k-ft]
R1-J3	22,987	108.2
R1-FRSCC	27,520	129.6
R1-PHOS	25,200	118.6

Table 7-2:Repair Group Positive Moment Bending Results

Repair Group Positive Moment Bending Results					
Specimen	Ductile Behavior Load [lb]	Ultimate Load [lb]	Deflection [in]	Ductile Moment [k-ft]	Ultimate Moment [k-ft]
R1-J3	23,466	34,785	3.73	110.5	163.8
R1-FRSCC	25,606	32,889	2.48	120.6	154.9
R1-PHOS	17,226	23,421	1.70	81.1	110.3

A summary of load-deflection curves for each positive moment repair specimen is shown in Figure 7-1. It is very apparent that the ultimate load after repairing specimen R1-PHOS was significantly less, roughly 30%, than that of R1-J3 and R1-FRSCC. This is particularly interesting as the initial cracking load of R1-PHOS was near the average of the three specimens' initial cracking loads.

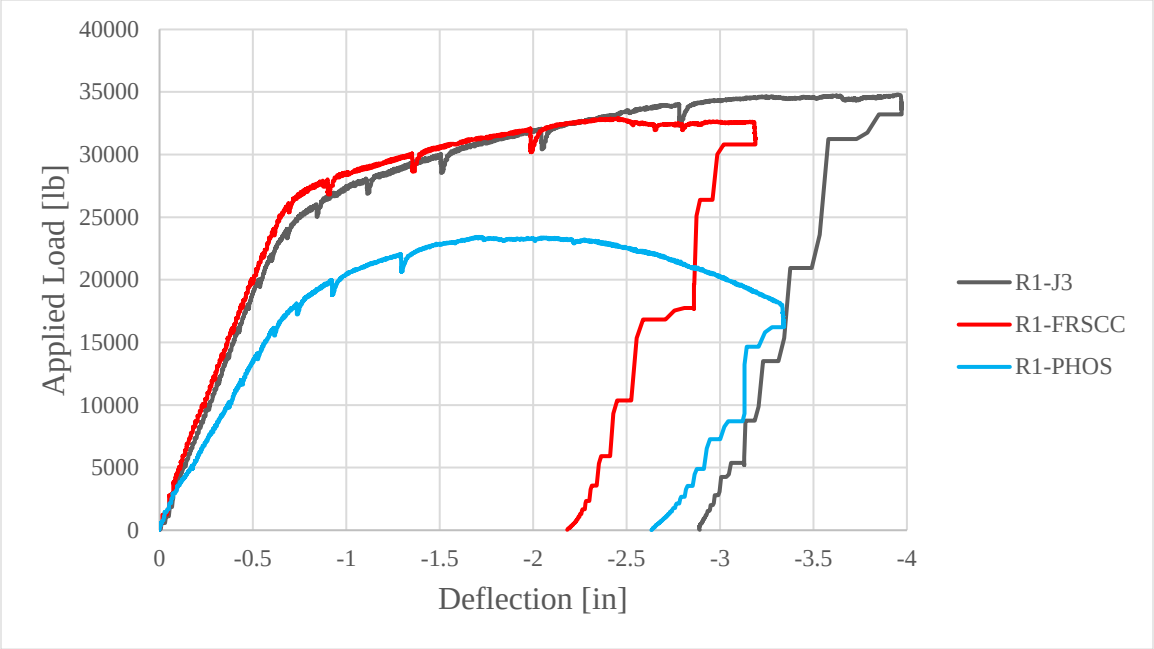

Figure 7-1:Summary of Positive Moment Repair Specimen Load-Deflection Curves

7.1.2 Negative Moment Testing of Repaired Specimens

- All negative moment repairs restored full moment capacity when compared to the theoretical calculated nominal moment, 152.4 ft-k.
- All repair reinforcement strain gauge data shows initial compression straining, followed by tension straining. No repair reinforcement yielded.
- Deck reinforcement in all negative moment repair specimens yielded.
- All specimens showed substantial flexural cracking spanning across the deck in the region of the continuity joint.
- The FRSCC specimens showed the greatest amount of flexural cracking on both the longitudinal and transverse faces of the joint of any group. The FRSCC specimens also showed significant girder-joint-girder interface separation.
- The J3 specimens showed no sign of flexural cracking on their longitudinal joint faces and a limited amount on the transverse faces. The J3 specimens also showed significant girder-joint-girder interface separation.
- The PHOS specimens showed limited cracking on the longitudinal and transverse joint faces and at the girder-joint-girder interface.

The negative moment test results for the repair group and the control group are summarized in Table 7-3 and Table 7-4, respectively. The ultimate moment for all repairs exceeded the ultimate moment of the control group, demonstrating that the flexural capacity had been fully restored following the repair procedures.

Table 7-3:Repair Group Negative Bending Results

Repair Group Negative Moment Bending Results					
Specimen	Ductile Behavior Load [lb]	Ultimate Load [lb]	Deflection [in]	Ductile Moment [k-ft]	Ultimate Moment [k-ft]
R2-J3	33,426	46,024	3.65	157.4	216.7
R3-J3	33,446	46,001	3.48	157.5	216.6
R2-FRSCC	33,393	46,006	2.75	157.2	216.6
R3-FRSCC	34,698	46,008	2.81	163.4	216.6
R2-PHOS	32,507	46,037	2.80	153.1	216.8
R3-PHOS	34,742	46,130	2.07	163.6	217.2

Table 7-4:Control Group Negative Moment Bending Results

Control Group Negative Moment Bending Results					
Specimen	Ductile Behavior Load [lb]	Ultimate Load[lb]	Deflection [in]	Ductile Moment [k-ft]	Ultimate Moment [k-ft]
C1	33,086	44,601	2.28	155.8	210.0
C2	33,171	44,620	2.40	156.2	210.1
C3	32,223	41,525	2.16	151.7	195.5

Summaries of load-deflection curves for each negative moment repair specimen and control specimens are shown in Figure 7-2 and Figure 7-3, respectively. The repair specimens showed almost identical behavior to the control specimens throughout the range of loading. All repair specimens exceeded the ultimate deflections of the control specimens, with the exception of specimen R3-PHOS, which had a deflection of 2.07”.

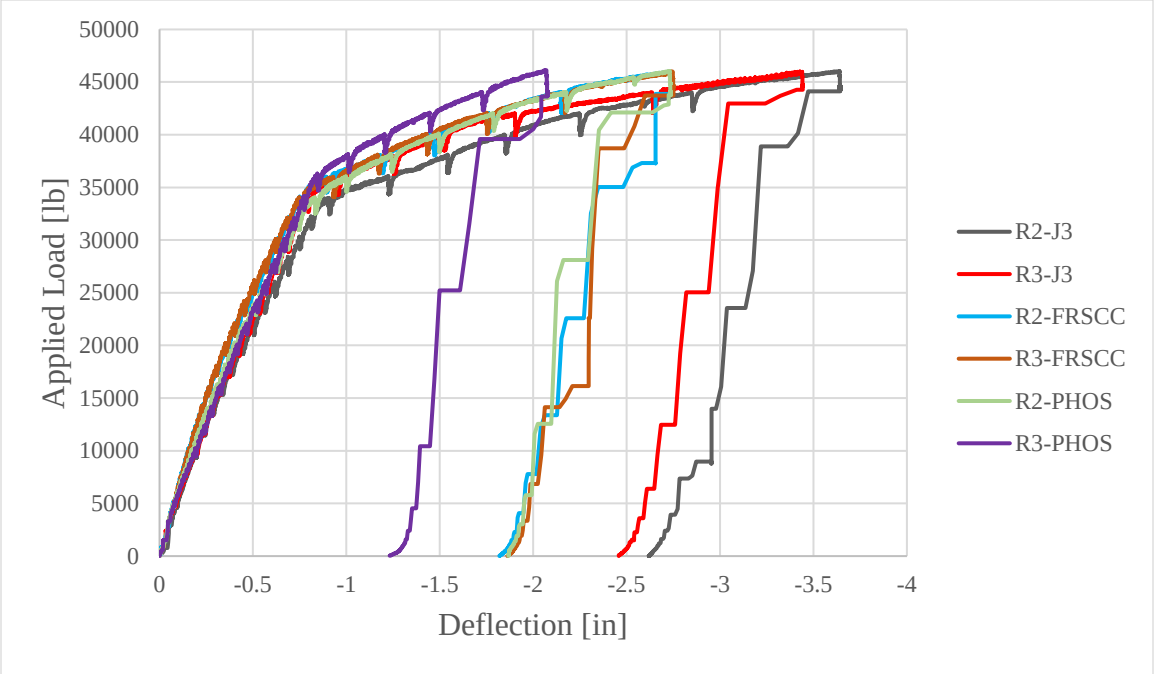

Figure 7-2:Summary of Negative Moment Repair Specimen Load-Deflection Curves

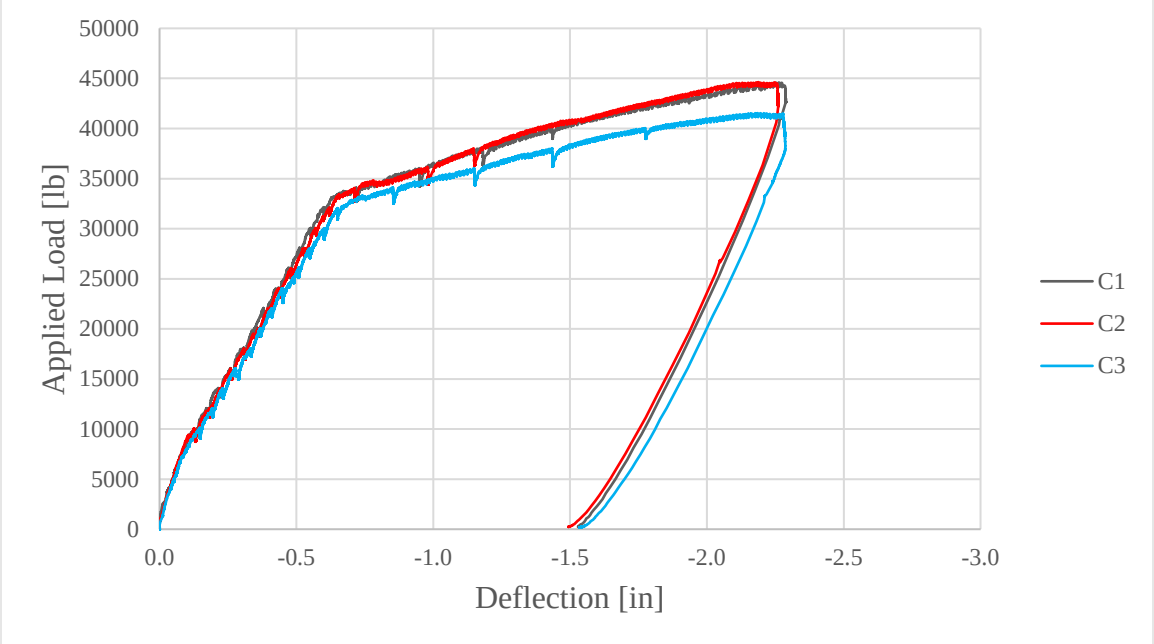

Figure 7-3:Summary of Negative Moment Control Group Load-Deflection Cures

All six repair specimens had a positive moment induced within 12.3% of the theoretical calculated nominal moment, 107.6 ft-k, during the initial cracking. Table 7-5 gives a summary of results of the initial cracking of the negative repair specimens.

Table 7-5:Initial Cracking Results of Negative Moment Repair Specimens

Initial Cracking Results of Negative Moment Repair Specimens		
Specimen	Load Applied [lb]	Moment [k-ft]
R2-J3	23,020	108.4
R3-J3	20,060	94.4
R2-FRSCC	21,430	100.9
R3-FRSCC	21,415	100.8
R2-PHOS	24,720	116.4
R3-PHOS	25,180	118.6

7.2 Conclusions

- All three repair materials restored the full positive and negative flexural capacities of the damaged continuity joints.
- All three repair materials restored the typical load-deflection response of a reinforced concrete flexural element over the full range of loading.
- The positive moment reinforcement in the continuity joints for all specimens reached yield during the pre-cracking phase, representing the most severe level of damage the joint could receive.
- The FR-SCC was the easiest of the three repair materials to place, followed by the J3 UHPC material, and finally the Phoscrete.

7.3 Recommendations

- The J3 UHPC offers the best balance between ease of placement and overall performance. With little to no cracking on the repaired faces, the J3 UHPC provides the best long-term resistance to weather exposure for the internal reinforcing bars.
- Perform the same study with a reduced cross-sectional area of repair reinforcement.
- Perform the same study with a reduced repair concrete overlay thickness of 2”.
- Perform the same study with one set of repair reinforcing bars installed in the bottom bell only by increasing their cross-sectional area. This would reduce labor time and eliminate the need for lapping U-shaped bars in the web.

- Data providing bottom longitudinal reinforcement behavior during positive moment bending testing may be provided in future research by additional strain gauges placed on these bars. The study herein suggests these bars continued to take load after the initial cracking and during the repair testing.

8.0 References

(AASHTO), American Association of State Highway and Transportation Officials. 2017. *AASHTO LRFD Bridge Design Specifications, Customary U.S. Units.* Vol. 8th Edition.

American Concrete Institute. 2014. *Building Code Requirements for Structural Concrete (ACI 318-14).* Vol. 7th. Farmington Hills, MI: American Concrete Institute.

ASTM A370. 2020. *Standard Test Methods and Definitions for Mechanical Testing of Steel Products.* West Conshohocken, PA: ASTM International.

ASTM C39. 2020. *Standard Test Method for Compressive Strength of Cylindrical Concrete Specimens.* West Conshohocken, PA.

Berry, Michael, Richard Snidarich, and Camylle Wood. 2017. *Development of Non-Proprietary Ultra-High-Performance Concrete.* FHWA/MT-17-010/8237-001, Civil Engineering, Montana State University - Bozeman, Helena: Montana Department of Transportation.

Casey, Conner. 2019. *Ultra-High Performance Concrete for Connections of Precast, Prestressed Girders Made Continuous for Live Load.* Master's Thesis, Civil Engineering and Environmental Science, University of Oklahoma, Norman, OK: University of Oklahoma .

Choate, Jacob. 2018. *Implementing FRSCC as a Repair Material for AASHTO Prestressed Concrete Girders.* Master's Thesis, Civil Engineering and Environmental Science, University of Oklahoma, Norman, OK: University of Oklahoma.

El Tawil, Sherif, Mouhamed Alkaysi, Antoine Naaman, Will Hansen, and Zhichao Liu. 2016. *Development, Characterization and Applications of a Non-Proprietary Ultra-High-Performance Concrete for Highway Bridges.* RC-1637, University of Michigan, Lansing: Michigan Department of Transportation.

Fournier, Paul. 2014. "Bridge Maintenance Experts Evaluate MALP Concrete Repair Technology." *Constructioneer* (Associated Construction Publications) 4-6.

Freyermuth, Clifford L. 1969. "Design of Continuous Highway Bridges with Precast, Prestressed Concrete Girders." *PCI Journal* 14-39.

Graybeal, Ben. 2014. *Design and Construction of Field-Cast UHPC Connections.* Research, Development, and Technology, Turner-Fairbank Highway Research Center, McLean, VA: U.S. Department of Transportation Federal Highway Administration.

Graybeal, Ben. 2011. *Ultra-High Performance Concrete.* Research, Development, and Technology, Turner-Fairbank Highway Research Center, McLean, VA: U.S. Department of Transportation Federal Highway Administration.

Kassimi, Fodhil. 2013. *Development and Performance of Fiber-Reinforced Self-Consolidating Concrete for Repair Applications.* Universite de Sherbrooke, Sherbrooke, Canada: ProQuest Dissertations Publishing. https://search.proquest.com/docview/1520158859?accountid=12964.

Kassimi, Fodhil, Kamal Khayat, and Ahmed K. El-Sayed. 2014. "Performance of Fiber-Reinforced Self-Consolidating Concrete for Repair of Reinforced Concrete Beams." *ACI Structural Journal* 1277-1286.

Mayhorn, Darion. 2016. *Investigation of the Effects of End Region Deterioration of Precast, Prestressed Concrete Bridges.* Master's Thesis, Civil Engineering and Environmental Science, University of Oklahoma, Norman, OK: University of Oklahoma.

McDaniel, Amy. 2017. *Development of Non-Proprietary Ultra-High-Performance Concrete Mix Designs.* Master's Thesis, Department of Civil Engineering and Environmental Science, University of Oklahoma, Norman, OK: University of Oklahoma, 1-100.

Miller, Richard A., Reid Castrodale, Amir Mirmiran, and Makarand Hastak. 2004. *Connection of Simple-Span Precast Concrete Girders for Continuity.* Federal Highway Administration & National Cooperative Research Program, Washington, D.C.: Transportation Research Board.

Saadeghvaziri, Mohamad Ala, William R. Spillers, and Libin Yin. 2004. *Improvement of Continuity Connection over Fixed Piers.* Department of Civil and Environmental Engineering, New Jersey Institute of Technology, Newark, NJ: U.S. Department of Transportation Federal Highway Administration.

Wirkman, Corey. 2016. *Performance of Fiber-Reinforced Self-Consolidating Concrete for Repair of Bridge Sub-Structures.* Master's Thesis, Civil Engineering and Environmental Science, University of Oklahoma, Norman, OK: University of Oklahoma.

9.0 Appendix

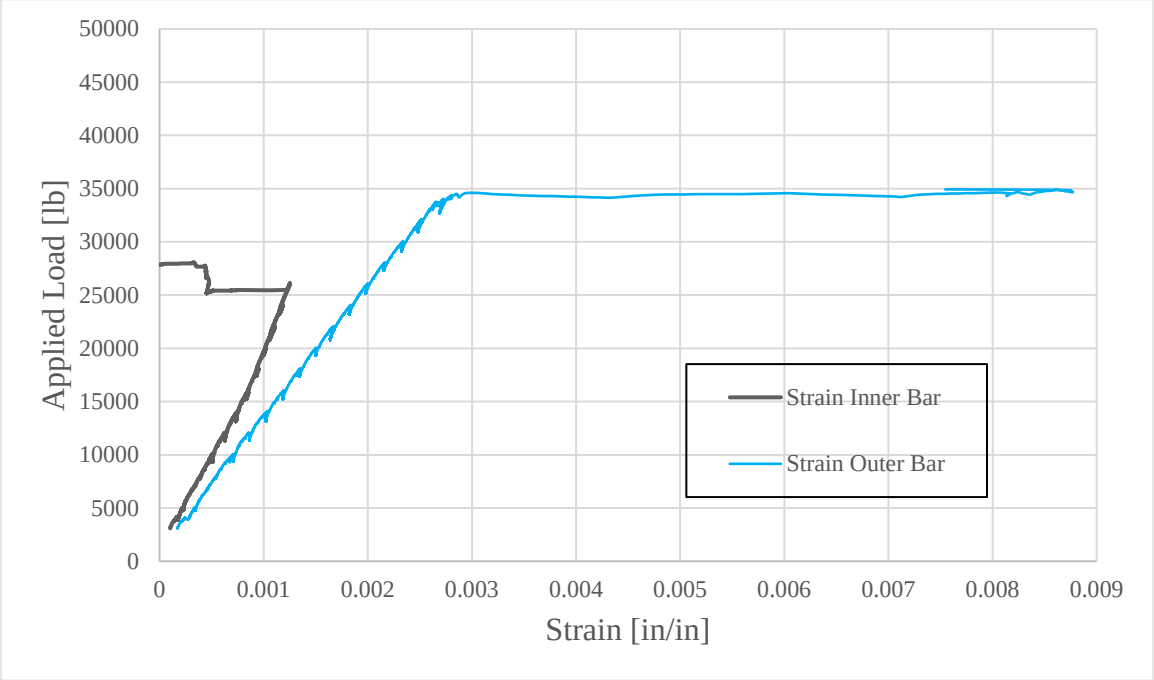

Figure 9-1:Specimen C1 Full Load-Strain Curve

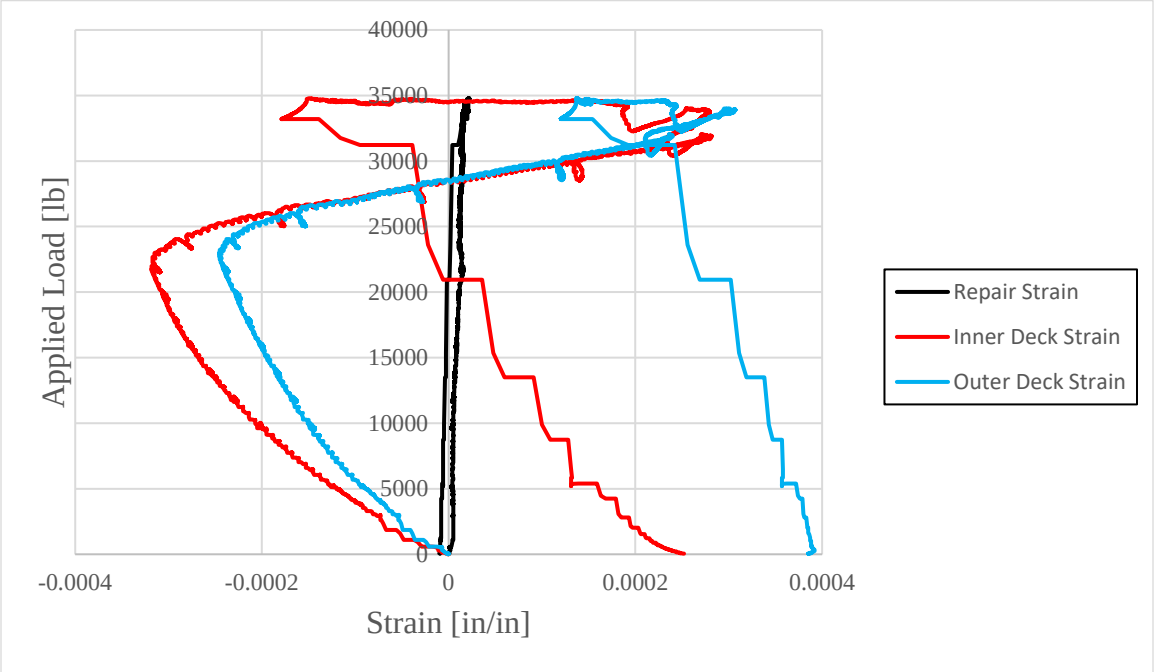

Figure 9-2:Specimen R1-J3 Full Load-Strain Curve

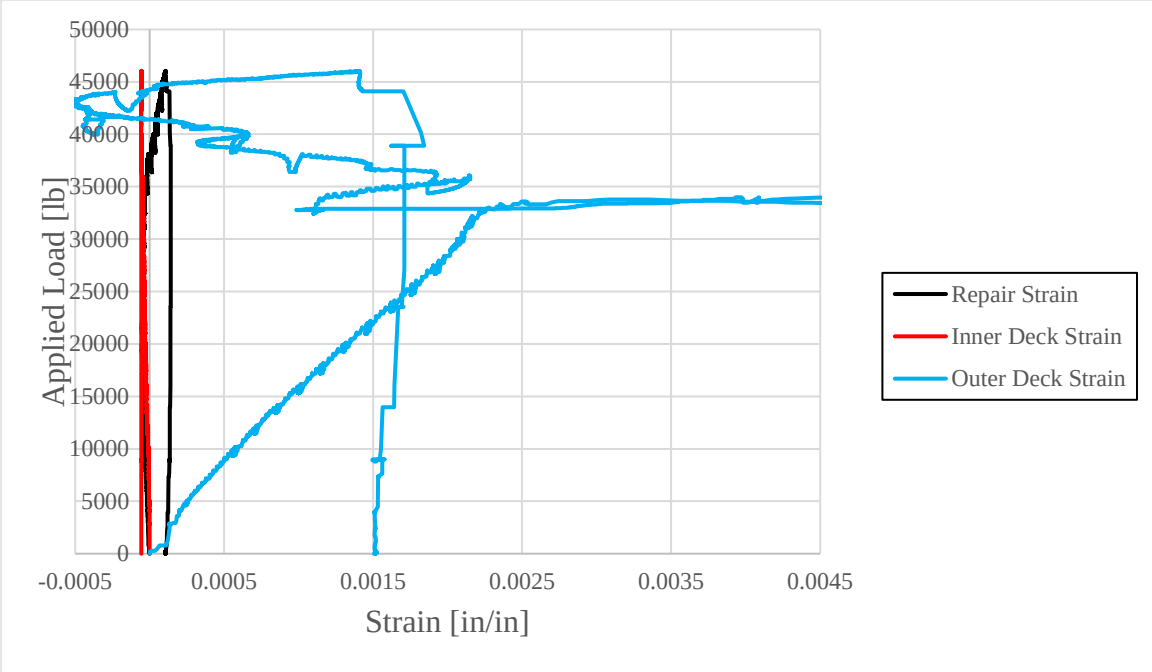

Figure 9-3:Specimen R2-J3 Full Load-Strain Curve

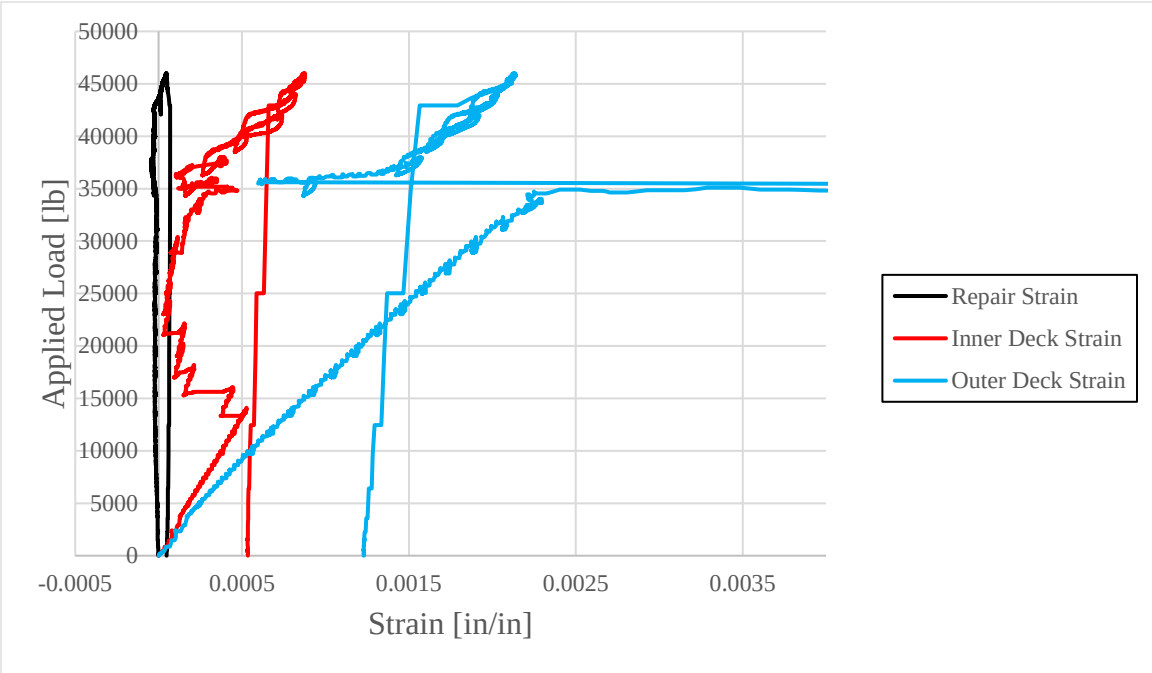

Figure 9-4:Specimen R3-J3 Full Load-Strain Curve

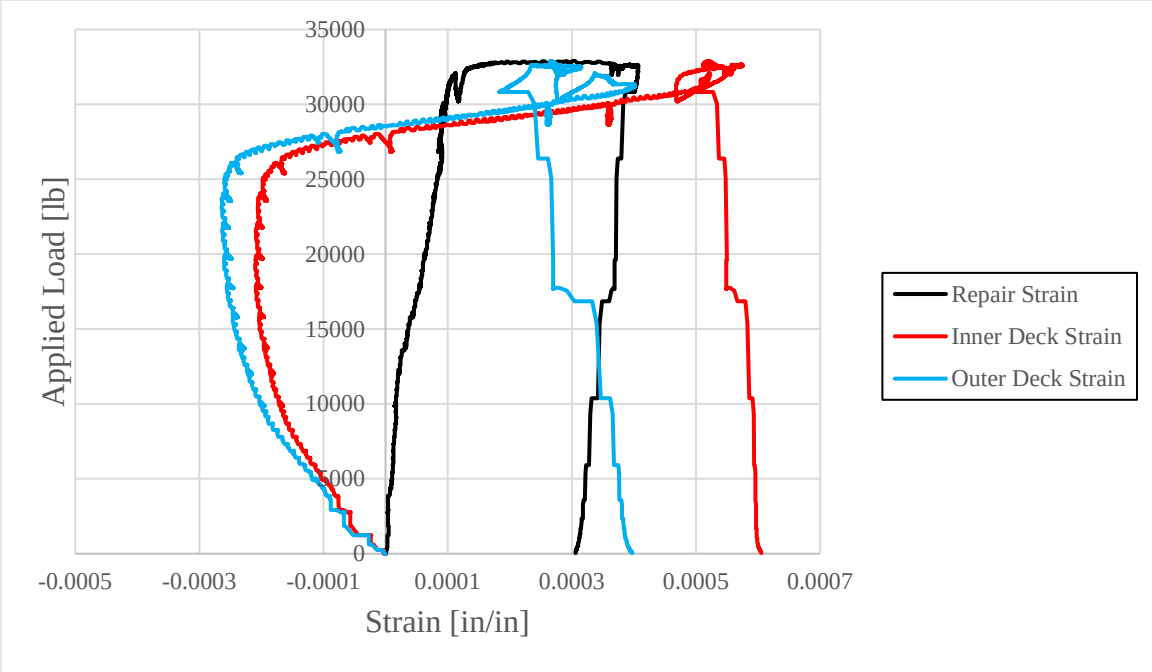

Figure 9-5:Specimen R1-FRSCC Full Load-Strain Curve

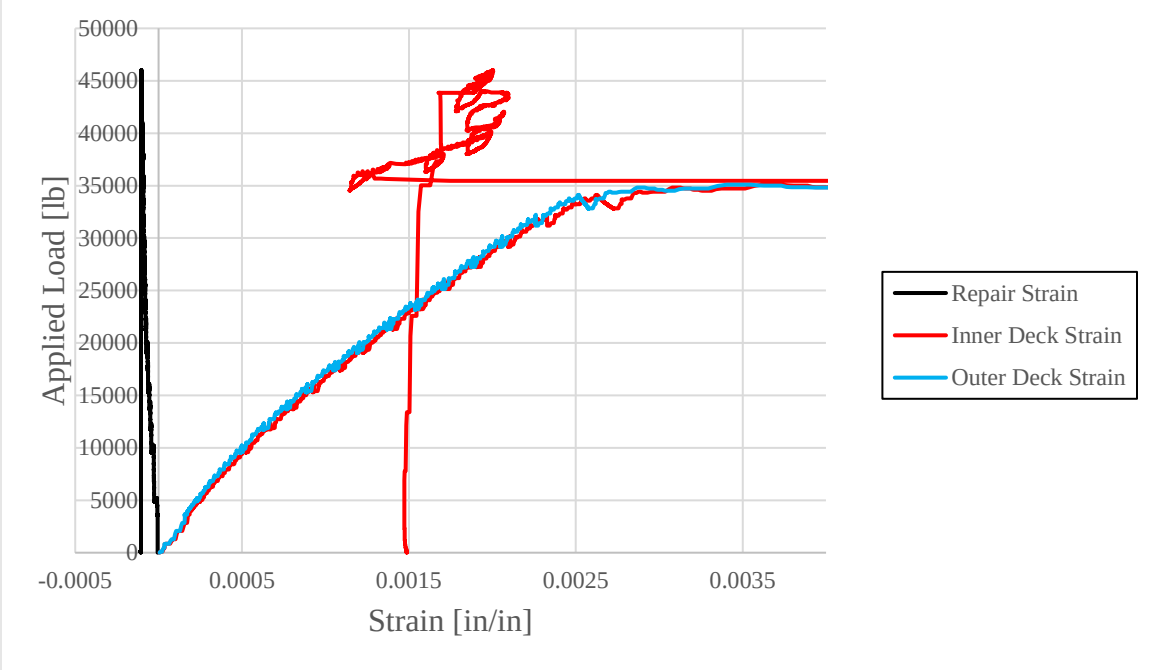

Figure 9-6:Specimen R2-FRSCC Full Load-Strain Curve

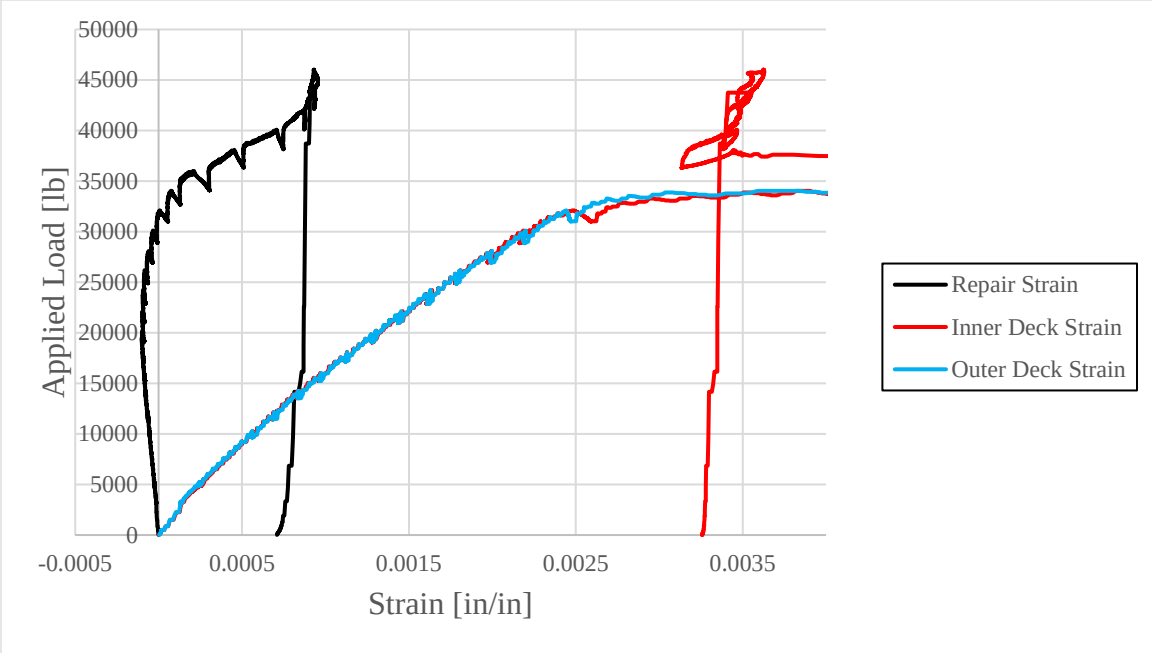

Figure 9-7:Specimen R3-FRSCC Full Load-Strain Curve

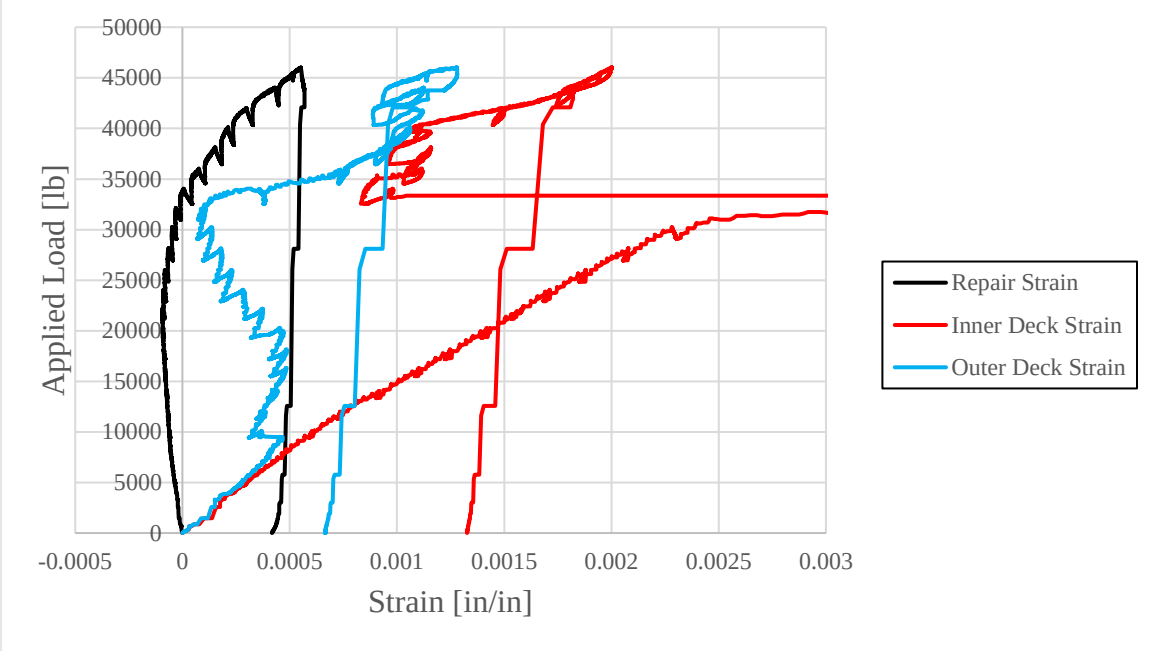

Figure 9-8:Specimen R2-PHOS Full Load-Strain Curve

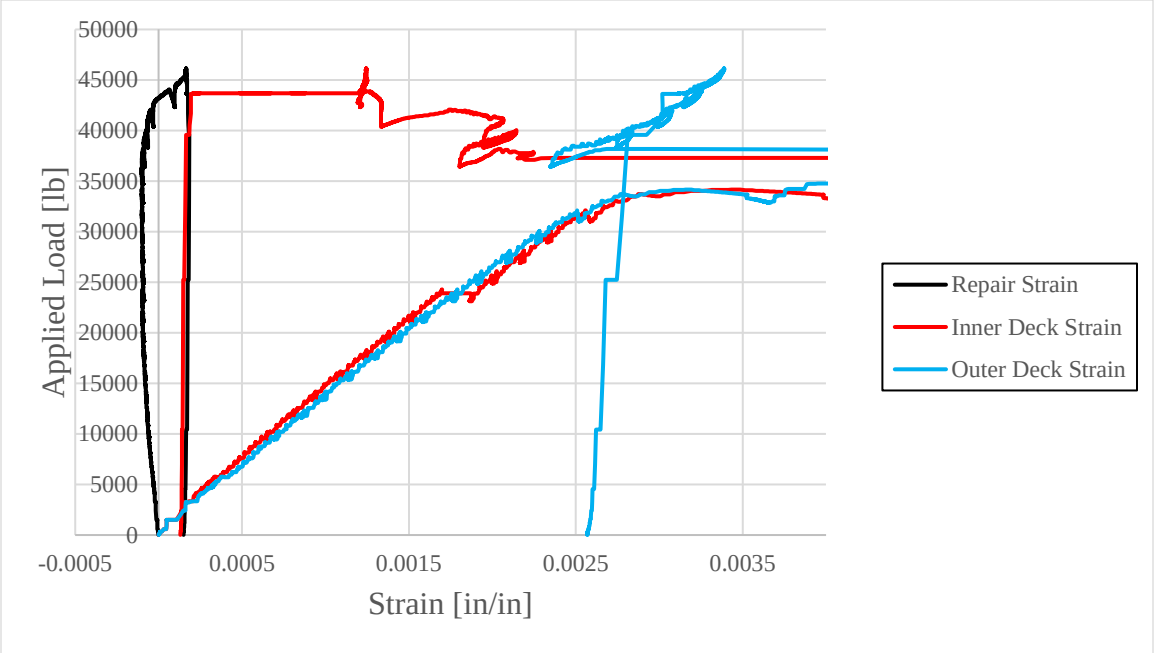

Figure 9-9:Specimen R3-PHOS Full Load-Strain Curve